Dissertation

The role of $CD8^+$ T cells in Nephrotoxic Serum Nephritis: Low-dose IL-15 as potential immunotherapy to treat Glomerulonephritis

submitted by

Agnes Anna MOOSLECHNER, MSc

for the Academic Degree of

Doctor of Philosophy

(PhD)

at the

Medical University of Graz

Clinical Division of Nephrology

Department of Internal Medicine

under the supervision of

Assoz. Prof.in Priv.-Doz.in Dr.in med.univ. Kathrin ELLER

2022

Statutory Declaration

I hereby declare that this thesis is my own original work and that I have fully acknowledged by name all of those individuals and organisations that have contributed to the research for this thesis. Due acknowledgement has been made in the text to all other material used throughout this thesis and in all related publications I followed the “Standards of Good Scientific Practice at the Medical University of Graz”.

Graz, December 2022

Disclosures

Parts of this thesis have been published as

Mooslechner AA[1], Schuller M[1], Artinger K[1], Kirsch AH[1], Schabhüttl C[1], Eller P[2], Rosenkranz AR[1], Eller K[1]. Low-Dose rIL-15 Protects from Nephrotoxic Serum Nephritis via CD8+ T Cells. Cells. 2022 Nov 18;11(22):3656. doi: 10.3390/cells11223656. PMID: 36429085.[1]

[1]Division of Nephrology, Department of Internal Medicine, Medical University of Graz, Austria

[2]Intensive Care Unit, Department of Internal Medicine, Medical University of Graz, Austria

This article belongs to the Special Issue ‘Immune Mechanisms in Glomerulonephritis’.

All co-authors have agreed to the use of the data in this thesis.

Acknowledgments

First and foremost, I would like to express my gratitude to my supervisor Assoz. Prof.in Priv.-Doz.in Dr.in med.univ. Kathrin Eller for her support and unwavering optimistic mindset through this incredible journey. Thank you for sharing your expertise, opening doors of opportunity, fostering my independence, and remaining open for countless discussions.

I would like to extend my gratitude to Prof. Dr. Alexander Rosenkranz, Assoz. Prof. Priv.-Doz. Dr.med.univ. Philipp Eller, and my thesis committee for valuable feedback and much-appreciated advice.

I had the pleasure of having many great colleagues in the lab to have fun with, who also offered support and motivation when needed. I want to thank Alexander Kirsch, Katharina Artinger, Ida Aringer, Corinna Schabhüttl, Máté Kétszeri, Foteini Moschovaki-Filippidou, Bianca Frauscher, Kerstin Schweighofer, John E. Mindur, Max Schuller, and Konstantin Klötzer.

This thesis project received funding from the Austrian Science Fund FWF (DK-MOLIN-FWF W1241) and the Medical University of Graz through the PhD program Molecular Inflammation (DK-MOLIN).

I am incredibly grateful to my husband, parents, siblings, extended family, and friends for their support and distractions. Having such a fantastic community puts everything else into perspective.

Table of Contents

Abbreviations

AB – Antibody
ACR – Albumin to creatinine ratio
AKI – Acute kidney injury
ANCA – Anti-neutrophil cytoplasmic antibodies
APC – Antigen presenting cell
BrdU – Bromdesoxyuridin
BUN – Blood urea nitrogen
CD – Cluster of differentiation
CFA – Complete Freund's Adjuvant
CKD – Chronic kidney disease
CTL – Cytotoxic T lymphocyte
CTLA – Cytotoxic T-lymphocyte-associated protein
CXCL – Chemokine ligand
CXCR – Chemokine receptor
DC – Dendritic cell
DM – Diabetes Mellitus
DN – Diabetic Nephropathy
EGFP – Enhanced green florescent protein
ELISA – Enzyme-linked immunosorbent assay
EMT – Epithelial–mesenchymal transition
ESRD – End stage renal disease
FCS – Fetal calf serum
GBM – Glomerular basement membrane
GFR – Glomerular filtration rate
GN – Glomerulonephritis
HLA – Human leukocyte antigen
Hpf – High power field
HSC – Haematopoietic stem cell
ICAM – Intracellular adhesion molecule
IFN – Interferon
Ig – Immunoglobulin
IL – Interleukin
ILC – Innate lymphoid cell
iNKT – Invariant natural killer T cell
KDIGO – Kidney Disease Improving Global Outcomes

KIR – Killer Ig-like receptors
KO – Knock out
LAG – Lymphocyte-activation gene
LFA – Lymphocyte function associated antigen
LN – Lupus Nephritis
LSK – Lineage-negative, Sca-1-positiv and c-kit-positive cells
MCP – Monocyte chemotactic protein
MHC – Major histocompatibility complex
MPO – Myeloperoxidase
NK – Natural killer cell
NKT – natural killer T cell
NTS – Nephrotoxic serum nephritis
PAS – Periodic-Acid-Schiff
PCR – Polymerase chain reaction
PD – Programmed cell death
RBC – Red blood cell
rh – recombinant human
ROR – Receptor-related orphan receptor
RPGN – Rapid progressive glomerulonephritis
RT – Room temperature
SCr – Serum creatinine level
SEM – Standard error of the mean
TAP – Transporter associated with antigen processing
TCM – central memory T cell
TCR – T cell receptor
TEC – Tubular epithelial cell
TEM – effector memory T cell
TGF – Transforming growth factor
TH – T helper cell
TIM – Innate memory T cell
TIM – T-cell immunoglobulin and mucin-domain
TIN – Tubulointerstitial Nephritis
TLR – Toll-like receptor
TNF – Tumor-necrosis factor
Treg – Regulatory T cell
TRM – Tissue-resident memory T cell
Tunel – Terminal transferase dUTP nick-ends

TVM – Virtual memory T cell
UUO – Unilateral ureteral obstruction
WKY – Wistar Kyoto
WT – Wild-type

List of Figures

List of Tables

Zusammenfassung

Einleitung: Glomerulonephritis (GN) führt häufig zu einem terminalen Nierenversagen, welches eine Nierenersatztherapie erforderlich macht und eine globale Gesundheitsbelastung darstellt. Die derzeitige Behandlung erfolgt häufig mit nicht-selektiven Immunsuppressiva, die das Risiko von Infektionen und bösartigen Erkrankungen erhöhen. Um neue gezielte interventionelle Therapien zu entwickeln, ist ein besseres Verständnis des zugrundeliegenden Pathomechanismus erforderlich. Die Beteiligung und die Funktion der $CD8^+$ T-Zellen bei der Entstehung und dem Fortschreiten der GN sind immer noch unklar, was unter anderem auch auf die vorhandene teils widersprüchliche Literatur zurückzuführen ist. In dieser Studie haben wir diese Frage in einem Mausmodell der nephrotoxischen Serumnephritis (NTS) untersucht, welches eine Form der nicht-autoimmunen GN nachahmt. IL-15 ist ein pleiotropes Zytokin, welches bereits mit der Nierengesundheit und dem Überleben von Tubulusepithelzellen (TEC) assoziiert wurde. Zusätzlich wurde es mit einer Verschiebung hin zu einem Gedächtniszellphenotyp innerhalb der $CD8^+$ T-Zellpopulation in Verbindung gebracht. Wir untersuchten das Potenzial von niedrig dosiertem IL-15 als Intervention in unserem NTS-Modell mit Fokus auf die Auswirkungen auf die $CD8^+$ T-Zellpopulation.

Methoden: Um die Beteiligung von $CD8^+$ T-Zellen zu untersuchen, injizierten wir NTS in *CD8α*$^{-/-}$-Mäusen und analysierten den Krankheitsverlauf über 21 Tage. Zusätzlich verwendeten wir einen CD8α-Antikörper-vermittelten Depletionsansatz bei C57Bl/6J-Wildtyp-Mäusen mit NTS. Wir identifizierten das Albumin-Kreatinin-Verhältnis im Urin (ACR), die Glomerulosklerose, die Infiltration der Niere mit myeloischen Zellen und den Harnstoff-Stickstoff-Spiegel im Blut als relevante Krankheitsresultate.

In unserer zweiten Versuchsreihe verabreichten wir C57Bl/6J-Mäusen am Tag 1 der NTS niedrig dosiertes IL-15 als Intervention. Nach 7 Tagen Krankheit analysierten wir die ACR, die Glomerulosklerose und die myeloische Zellinfiltration der Niere und konzentrierten uns auch auf die TEC-Schädigung. Wir untersuchten die IL-15-vermittelten Effekte auf $CD8^+$ T-Zellen im Detail. Wir verwendeten genetische Knockout-Mäuse des IL-15Rα und *CD8α*$^{-/-}$-Mäuse, um den Wirkort von IL-15 zu verstehen. Schließlich untersuchten wir die langfristigen Auswirkungen unserer Einmalgabe des niedrig dosierten IL-15 nach 21 Tagen NTS.

Ergebnisse: Bei genetischen Knockout-Mäusen und Wildtyp-Mäusen, die Depletion-Antikörper erhielten, fanden wir einen klaren Hinweis auf eine Verschlimmerung der Krankheit in Abwesenheit von CD8α. Glomerulosklerose und Makrophageninfiltration waren bei diesen Mäusen im Vergleich zu den entsprechenden Kontrollgruppen erhöht. Interessanterweise wiesen die *CD8α*$^{-/-}$-Mäuse höhere BUN-Werte auf.

Eine niedrig dosierte IL-15-Therapie verbesserte die ACR, die Glomerulosklerose und das TEC-Überleben am Tag 7 der NTS. Wir fanden keine Unterschiede in der Anzahl der iNKT- und CD4^{+} Treg-Zellen. Bei den CD8^{+} T-Zellen wurde jedoch eine Abnahme der relativen Genexpression von *Prf1*, *Gzmb* und *Ifnγ* festgestellt, während die Expression von *Ikzf2* erhöht war. Darüber hinaus wurden in der Behandlungsgruppe vermehrt CD8^{+} T-Zell-Gedächtniszellen, einschließlich Ly49^{+}CD8^{+} Gedächtnis-T-Zellen, gebildet. Bei *IL-15Rα*$^{-/-}$-Mäusen und *CD8α*$^{-/-}$-Mäusen zeigte die IL-15-Therapie keinen Nutzen für den Krankheitsverlauf. Nach 21 Tagen NTS waren die Vorteile einer einmaligen niedrig dosierten IL-15-Verabreichung nicht mehr so ausgeprägt wie an Tag 7.

Schlussfolgerung: Wir haben keine Hinweise darauf gefunden, dass eine generelle CD8-Depletion oder ein genetischer Knockout bei NTS von Vorteil ist. Im Gegenteil, wir fanden einen verschlimmerten Krankheitsphänotyp bei *CD8α*$^{-/-}$-Mäusen mit erhöhter Makrophageninfiltration und einer Assoziation mit einer auffälligen Verschlechterung der Nierenfunktion, was auf eine teilweise schützende Rolle von CD8^{+} T-Zellen schließen lässt. Wir konnten den NTS-Phänotyp bei Mäusen mit einer niedrig dosierten IL-15-Interventionstherapie verbessern. Dies erreichten wir teilweise durch den Schutz von TECs vor dem Zelltod in einer CD8-abhängigen Weise. Dank des verabreichten IL-15 zeigten CD8^{+} T-Zellen einen weniger zytotoxischen Phänotyp und die Hochregulierung des regulatorischen assoziierten Markers Helios. Darüber hinaus stellten wir eine deutliche Verschiebung der Population hin zu einer Zunahme der Gedächtniszellen fest, einschließlich der vermutlich regulatorischen Ly49^{+}CD8^{+} Gedächtnis-T-Zellen, die das murine Gegenstück zu den menschlichen KIR^{+}CD8^{+} T-Zellen darstellen. Zusammenfassend lässt sich sagen, dass, obwohl die Beteiligung von CD8^{+} T-Zellen an NTS komplex ist, wir IL-15 als potenziellen zytokinbasierten immuntherapeutischen Ansatz zur Behandlung von GN vorschlagen, wobei weiterführende translationale Studien erforderlich sind.

Abstract

Introduction: Rapid-progressive glomerulonephritis (GN) often progresses to end-stage renal disease, which poses a global health burden by creating the need for renal replacement therapy. Current treatments often involve non-selective immunosuppressants, which increase the risk of infections and malignancies. A better understanding of the underlying pathomechanism is needed to design new directed interventional therapies. The involvement and role of $CD8^+$ T cells in the onset and progression of GN are still not clear, partly due to conflicting literature published. In this study, we addressed this question in a mouse model of nephrotoxic serum nephritis (NTS), mimicking a form of non-autoimmune GN. IL-15 is a pleiotropic cytokine, which has previously been associated with kidney health and tubular epithelial cell (TEC) survival, but also with a memory shift in the $CD8^+$ T cell population. We investigated the potential of low-dose IL-15 as an intervention in our NTS model, focusing on the effects on the $CD8^+$ T cell population.

Methods: To investigate the involvement of $CD8^+$ T cells, we subjected *CD8α*$^{-/-}$ mice to NTS and analyzed disease outcomes after 21 days of disease. Additionally, we used a CD8α antibody-mediated depletion approach in C57Bl/6J wildtype mice subjected to NTS. We identified urinary albumin to creatinine ratio (ACR), glomerulosclerosis, myeloid cell infiltration of the kidney, and blood urea nitrogen levels as relevant disease outcomes.

In our second set of experiments, we administered low-dose IL-15 on day 1 of NTS as an intervention in C57Bl/6J mice. After 7 days of disease, we analyzed ACR, glomerulosclerosis, and myeloid cell infiltration of the kidney and focused on TEC injury. We investigated IL-15-mediated effects on $CD8^+$ T cells in detail. We used genetic knockout mice of the IL-15Rα and *CD8α*$^{-/-}$ mice to understand the point of activity of IL-15. Finally, we investigated the long-term effects of our single low-dose IL-15 therapy schedule in 21 days of NTS.

Results: Absence of CD8α in genetic knockout mice and wild-type mice that received depletion antibodies resulted in aggravated disease. Glomerulosclerosis and macrophage infiltration was increased in these mice compared to respective control groups. Interestingly, *CD8α*$^{-/-}$ mice presented with higher BUN levels.

Low-dose IL-15 therapy improved ACR, glomerulosclerosis, and TEC survival on day 7 of NTS. We found no differences in iNKT and $CD4^+$ Treg cell numbers. However, $CD8^+$ T cells showed a decrease in *Prf1*, *Gzmb,* and *Ifnγ* relative gene expression, while *Ikzf2* expression was increased. In addition, $CD8^+$ T cell memory subsets, including $Ly49^+CD8^+$ memory T cells, were increased in the treatment group. *IL-15Rα*$^{-/-}$ mice and *CD8α*$^{-/-}$ mice showed no benefit in disease outcomes by IL-15 therapy. After 21 days of NTS, the benefits of single low-dose IL-15 administration were not as pronounced as on day 7.

Conclusion: We found no evidence that overall CD8 depletion or genetic knockout is beneficial in NTS. On the contrary, *CD8α*$^{-/-}$ mice displayed an aggravated disease phenotype with increased macrophage influx and an association with a striking decline in kidney function, suggesting a partly protective role of $CD8^+$ T cells. We improved the NTS phenotype in mice with a low-dose IL-15 interventional therapy, partly by protecting TECs from cell death in a CD8-dependent manner. Due to administered IL-15, $CD8^+$ T cells presented with a less cytotoxic phenotype and the upregulation of the regulatory associated marker Helios. In addition, we noted a clear shift of the population to an increase in memory cells, including supposedly regulatory $Ly49^+CD8^+$ memory T cells, which are the murine counterpart to human KIR^+CD8^+ T cells. To summarize, although the involvement of $CD8^+$ T cells in NTS is complex, we propose IL-15 as a potential cytokine-based immunotherapeutic approach to treat GN, with a need for further translational studies.

1. Introduction

1.1 Immune Complex-mediated Glomerulonephritis

Chronic kidney disease (CKD) is a global health problem with a steady increase in prevalence. Worldwide over a million patients require renal replacement therapy, which is associated with poor outcomes and causes high costs[2]. Today, it is evident that early intervention in CKD directly determines the well-being and survival of patients on dialysis[3]. However, kidney disease is peculiar since it often presents with few and unspecific symptoms until late in the progression. Therefore, diagnosis relies on laboratory abnormalities to define clinical syndromes. Per standard, kidney disease is classified and graded by function, structure, and outcome independent of comorbidities. The function describes the decline in glomerular filtration rate (GFR) and increased serum creatinine level (SCr). The structure domain describes the damage seen in imaging, biopsies, or albuminuria. Therefore, the KDIGO guidelines propose an increase of SCr by 50% within 7 days or an increase of 0.3mg/dL within 2 days to characterize acute kidney injury (AKI). CKD is defined as a decrease in GFR under 60mL/min present for three months[4]. Risk factors for end-stage renal disease (ESRD) include but are not limited to obesity, diabetes mellitus, hypertension, old age, socioeconomic status, smoking, nephrotoxins, and ethnicity[5].

Up to a fifth of end-stage renal disease cases are attributed to glomerulonephritis (GN)[6,7]. The blood flow to the kidneys is about 20% of the cardiac output per minute, and the glomeruli filter about 120ml/min. Situated in the cortex, the outer part of the kidney, each glomerulus is surrounded by its' Bowman's capsule and, together with a tubule, builds up a unit called a nephron. The glomerulus is the blood filtration barrier and consists of a fenestrated endothelial layer, the glomerular basement membrane (GBM), and an epithelial cell layer characterized by foot processes sitting on the GBM. The primary function of the GBM is to restrict the movement of most cells and proteins from the blood into the urinary space of the tubular lumen[8].

Oversimplified glomerulonephritis describes a state of increased unphysiological cellularity within the glomerulus, representing inflammation and initiating fibrotic events, which can lead to sclerosis. The GBM (or antigens within) can be a target of the facilitated immune-mediated damage leading to proteinuria, hematuria, a decline in GFR, and urine sediment. In

2015, a standardized classification of GN into five groups based on etiology was defined[9]. The allocation is heavily based on immunofluorescence and electron microscopy of biopsies. The five groups are immune complex-mediated GN, ANCA-associated GN, anti-GBM GN, monoclonal Ig-GN, and C3 glomerulopathy. The purpose of defining these groups was to exclude other etiologies and guide toward diagnosing and managing the specific subtype of GN[10].

The presence of immunoglobulin seen in immunofluorescence microscopy characterizes immune complex-mediated GN. It includes IgA nephropathy, lupus nephritis, infection-related GN, and fibrillary GN. Specific light and electron microscopy findings are used to diagnose each subtype of immune complex-mediated GN. Our group's mouse model of NTS is best described as immune complex-mediated GN due to the exclusion of the other groups and since we cannot narrow it down to any subtype.

Additionally, the injury pattern is determined to indicate the activity and learn about lesions' severity, chronicity, and irreversibility (e.g., crescentic, necrotizing, membranoproliferative, mesangial proliferative, or sclerosing lesions)[10]. A secondary diagnosis like acute tubular necrosis or interstitial nephritis may also be necessary. In 2017, a scoring system was established to grade chronicity into four categories: minimal, mild, moderate, and severe[11]. The scores are the sum of individual scores for the manifestation of segmental glomerulosclerosis, tubular atrophy, interstitial fibrosis, and arteriosclerosis.

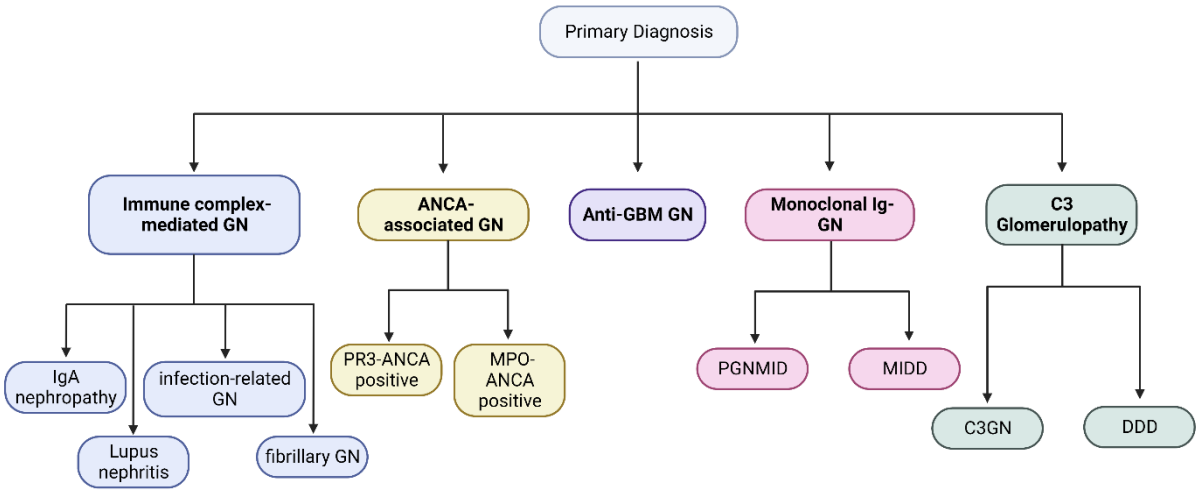

Figure 1. Standardized classification of GN based on etiology. Adopted and modified from Sethi et al.[10].

1.1.1 Experimental murine model of Nephrotoxic Serum Nephritis

To study human kidney disease's clinical and pathological features, rodent models are highly desirable and required to gain a deeper understanding of the underlying mechanisms and advance new therapy options. Nephrotoxic Serum Nephritis (NTS) presents an accessible and stably inducible mouse model of inflammatory kidney disease that enables the investigation of various hallmarks of rapid progressive glomerulonephritis.

In our group's model, we produce nephrotoxic serum by repeatedly injecting rabbits with isolated and disrupted murine glomeruli in adjuvant. We use male C57Bl/6J mice for the experiments, immunize them with rabbit IgG in adjuvant and then trigger disease by injecting the nephrotoxic rabbit serum[12]. As a result, immune complexes form and line the GBM. However, in our technique, the nephrotoxic serum is not exclusively directed against the GBM, and therefore we do not describe our model as anti-GBM glomerulonephritis. Further, the nature of disease induction does not classify our NTS model as autoimmune. Although our NTS model fulfills several criteria of CKD, such as albuminuria, mesangial expansion, renal inflammation, and injury[13], it does not show a decline in glomerular filtration rate in C57Bl/6J wild-type mice, therefore presenting a model of rather acute glomerulonephritis.

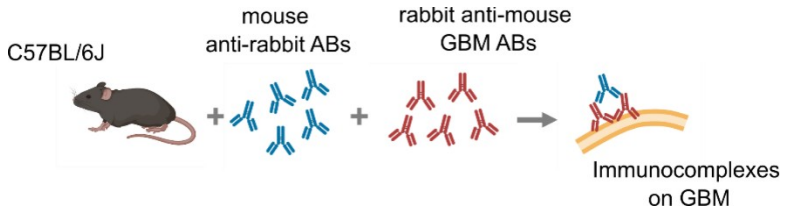

Figure 2. Immunocomplex formation in the mouse model of NTS. C57Bl/6J mice are immunized with rabbit IgG in incomplete FA substituted with *Mycobacterium Tuberculosis* and subsequently injected with rabbit anti-mouse antiserum.

Despite these limitations, the NTS model provides tremendous benefits compared to other supposedly CKD mouse models, e.g., systemic lupus erythematosus and diabetic nephropathy (DN). These models are based on gene mutations, and although they feature several disease characteristics, they are often mild and only develop spontaneously with age. The single largest cause of CKD is DN, with most incidence accounted for by type 2 diabetes. DN's

standard db/db mouse model is based on a leptin receptor mutation, rendering it dysfunctional. As a result, mice develop obesity, hyperglycemia, and glomerular sclerosis. However, to achieve a decline in glomerular filtration rate, additional surgeries must be performed to uni- or 5/6-nephrectomize the animals[14–16]. These two factors, spontaneous disease onset with age and additional surgery cause variations between study animals and successive rounds of experiments. In our NTS model, we can trigger disease with the same immunization mix and serum concentration in precisely 8-week-old mice. We refrain from nephrectomies and GFR decline for the advantage of reproducibility and preserving both kidneys for downstream processing and analysis.

Rodent models cannot reproduce all aspects of human pathophysiology. They are, however, good models for studying particular parts of the disease[14,17]. Although non-autoimmune and not per se chronic, NTS is an effective model to study immune mechanisms in rapid-progressive GN due to being easily inducible, reproducible, presenting with massive renal immune cell infiltration and renal tissue injury, while at the same time causing only minor to moderate discomfort in the animals' welfare.

1.1.2 T cell involvement in the pathophysiology of Nephrotoxic Serum Nephritis

Initially, B cell involvement was thought to be critical in the pathophysiology of GN due to the production of antibodies and their deposition in immune complexes with antigens on the GBM[18]. However, in 1984 Bolton et al. could show in an avian model that bursectomy, and therefore the lack of humoral response, did not ameliorate experimental GN. Antibodies could not transfer the disease, but it was transferred by primed T cells[19]. Since then, many studies have revealed a role for T cells in experimental GN and its underlying mechanism of T cell-mediated delayed-type hypersensitivity[19–23].

Under homeostatic conditions, the healthy kidney harbors resident immune cells like DCs, macrophages, and lymphocytes in the tubulointerstitium[24–27]. However, *in vivo* microscopy in mice confirmed that monocytes and neutrophils patrol the healthy glomeruli to sense danger, much like any other vessels throughout the body[28,29]. Therefore, these cell types are the first to respond after disease induction. In this early phase of the disease, γδ T cells recruit neutrophils via IL-17A gradients, facilitating undirected damage[30]. At the same

time, the antigen is trafficked to and presented in secondary lymphoid organs to generate an antigen-specific T cell response. The first players of this response are renal infiltrating Th17 cells, which cause a second wave of neutrophil infiltration and -mediated damage, this time in the interstitium[31]. Subsequently, renal mature DCs recruit Th17 cells via CXCL-9 into the periglomerular space[32,33]. From this point on, these cells produce IFN-γ and recruit macrophages, which produce pro-inflammatory mediators like nitric oxide and TNF[34]. The consequence is severe glomerular and tubular inflammation, which progresses to fibrosis. The absence of γδ T, Th1, or Th17 cells, either through knockout or depletion, has been shown to protect mice from injury or ameliorate NTS progression[34–36].

The immune system also takes countermeasures by trafficking regulatory cell types into the renal tissue. These also follow the same wave-like pattern as pro-inflammatory T cells. For example, early in pathophysiology, iNKT cells respond to immature DCs secreting CXCL16, resolving inflammation via IL-4 and IL-10 production[37]. Also, $STAT3^+$ Th17 regulatory T cells counteract Th17 cells via IL-10[38,39]. And later on, IL-10-producing $CD25^+FoxP3^+$ regulatory T cells can be found in lymph nodes alongside the inflammation-facilitating Th1 cells[40–43].

1.1.3 Proposed models of $CD8^+$ T cell involvement in Glomerulonephritis

Chen et al. elegantly showed that the Bowman's capsule protects the glomerulus, and $CD8^+$ T cells can only reach podocytes if that barrier is breached[44]. They used a mouse model with podocyte-specific expression of EGFP and transferred $CD8^+$ T cells directed against EGFP into the system. In healthy mice, no indices were found that $CD8^+$ T cells could reach podocytes. However, significant podocyte loss increased proteinuria and BUN levels in NTS. This study clearly shows the protective capacity of the Bowman's capsule. However, we would argue that it does not prove $CD8^+$ T cell involvement in podocyte injury because of the artificial nature of EGFP-directed $CD8^+$ T cells. Additionally, it does not rule out the possibility of a $CD8^+$ T cell subset involved in the breach of the Bowman's capsule in the disease state. Therefore, the contribution to further understanding the role of $CD8^+$ T cells in NTS is limited.

Tubulointerstitial nephritis (TIN) is seen in autoimmune- and non-autoimmune models of kidney disease. TIN was previously found to correlate best with the decline in kidney

function, proteinuria, and overall long-term outcome in patients with GN[45]. Macconi et al. show that proteinuria is harmful by itself, independent of immune responses in the glomerulus[46]. Albumin is reabsorbed by tubular epithelial cells and processed into peptides. In the interstitium, neighboring DCs sample these peptides and process the antigen further for cross-presentation. As a result, albumin-specific $CD8^+$ T cells get activated and produce IFN-γ. However, the authors do not address whether these cells contribute to general tissue damage [23,47]. While it was shown that proximal TECs themselves could present antigen via MHC II to $CD4^+$ T cells, it is not yet clear if they might also be able to activate via MHC I or are always dependent on DCs to activate $CD8^+$ T cells[48].

1.2. Classification of $CD8^+$ T cells

1.2.1 From naïve to cytotoxic effector $CD8^+$ T cells

$CD8^+$ T cells have three major functions: elimination of infected cells or tumor cells, establishing memory, and tolerance against self. Microbes and other antigens often enter the body through barrier tissues and get captured and transported to secondary lymphoid organs, where APCs display them. Naïve $CD8^+$ T cells are highly specific for any one antigen, leave the thymus and circulate through secondary lymphoid tissues. Activation of naïve $CD8^+$ T cells often requires cross-presentation via DCs and $CD4^+$ helper T cells. Since $CD8^+$ T cells only recognize peptides presented by MHC I, they depend on specialized APCs (often DCs) to ingest infected cells and process the antigen for cross-presentation. $CD4^+$ helper cells can stimulate DCs via CD40 ligand binding to make this process more efficient (APC licensing) [49].

Additionally, several cytokines are known to play a role in $CD8^+$ T cell activation, proliferation, and maintenance. IL-2 is produced by $CD4^+$ and $CD8^+$ T cells alike and stimulates proliferation. DCs produce IL-12 and type I interferons, stimulating the differentiation of $CD8^+$ T cells into effector cells. IL-15 is produced by many cell types and promotes survival and memory of $CD8^+$ T cells. Subsequently, $CD8^+$ T cells differentiate and clonally expand and migrate to the injury site. There they again recognize the same antigen presented at the site, effector functions are activated, and the antigen is eliminated[49,50].

Specific cytotoxicity is initiated by the binding of CD8 to the MHC molecule, the binding of the MHC-peptide complex to the T cell receptor, and the binding of integrins LFA-1 and ICAM-1 on the target cell. This structure is known as the immunological synapse and marks the confined space where $CD8^+$ T cells release granules by exocytosis aimed at the target cell to induce apoptosis[51]. The two most abundant proteins in granules of $CD8^+$ T cells are perforin and granzyme B. Perforin is homologous to the C9 complement protein. It triggers a process for endosomal uptake in the target cell. Perforin pierces the endosomal membrane and forms pores to deliver granzymes into the cytosol. Granzyme B is a serine protease that induces apoptosis by cleaving proteins and activating caspase cascades. A less abundant target cell killing pathway is mediated by FAS ligand-FAS receptor binding, which is also facilitated through the activation of caspases and independent of granules[52,53].

Like in chronic infections, prolonged or repeated activation gradually leads to exhaustion, meaning effector function decreases, proliferation is halted, and inhibitory receptors (CTLA-4, PD-1, TIM-3, LAG-3, and others) are upregulated on the cell surface. However, studies show this process is reversible, which offers great potential in anti-tumor therapies[54–56].

1.2.2 Memory $CD8^+$ T cells

Memory is a key component of the adaptive immune system. After effector $CD8^+$ T cells successfully fight the first encounter of a microbe or tumor cell, they diminish in numbers, and memory $CD8^+$ T cells ensure that a second encounter with the same antigen gets cleared faster[57,58]. Previously, it was unclear whether effector and memory $CD8^+$ T cells have unique specific precursor cells. However, today we have detailed studies that do not support the separate-precursor model but support the hypothesis that memory cells are formed from a subset of effector $CD8^+$ cells[59–61]. Moreover, while memory cells were already shown to be divided into two subsets in 1999, today, we know of even more memory populations with distinct functions[62].

1.2.2.1 Central vs. effector Memory T cells

Upon activation, T cells upregulate the expression of CD44, which allows the distinction of naïve from memory T cells[63]. Sallusto et al. further defined two subpopulations within the memory T cell pool via the expression of CD62L and CCR7. Central memory T cells (T_{CM}) express CD62L to roll on endothelial venules and facilitate lymph node entry via CCR7 expression. T_{CM} cells represent a long-living population of antigen-specific memory cells with an enormous proliferation potential. On the other hand, effector memory T cells (T_{EM}) do not express CD62L or CCR7, allowing them to circulate the periphery and home to tissues[64]. While T_{EM} cells display moderate proliferation potential, they represent a readily available pool of antigen-specific effector cells. Only $CCR7^-$ cells were able to produce IFN-γ and IL-4 and show cytotoxicity in response to antigen encounter[62]. In humans, the defining phenotypic markers are CD27 and CD45RA, with only T_{CM} cells expressing CD27[65,66].

1.2.2.2 Tissue-resident Memory T cells

T_{EM} cells were considered solely responsible for peripheral tissue surveillance and defense. However, studies revealed that memory T cells could not enter specific non-lymphoid tissues like the small intestine or brain. Indicating that effector T cells seeded these tissues and reside within the organ long after the initial infection is cleared[67,68]. Further studies suggest that the phenotype of tissue-resident memory T cells (T_{RM}) is shaped by the environment, with daughter cells being able to adapt after relocation[69,70]. This non-circulating population of memory T cells is found in most organs[71,72]. T_{RM} cells are defined by their expression of integrin CD103 and CD69, which facilitates retention in the tissue[73,74]. In addition, T_{RM} cells build a local defense mechanism, sense threat, and are highly effective in recruiting innate and adaptive immune cells to their location[75,76].

1.2.2.4 Virtual and innate $CD8^+$ Memory T cells

While T_{CM}, $T_{EM,}$ and T_{RM} are described in $CD4^+$ and $CD8^+$ T cells, several other populations have been primarily described in $CD8^+$ T cells[77]. One of the most striking of these memory subsets is the virtual memory T cell (T_{VM}) population. T_{VM} cells defy the very logic of memory created due to antigen encounters.

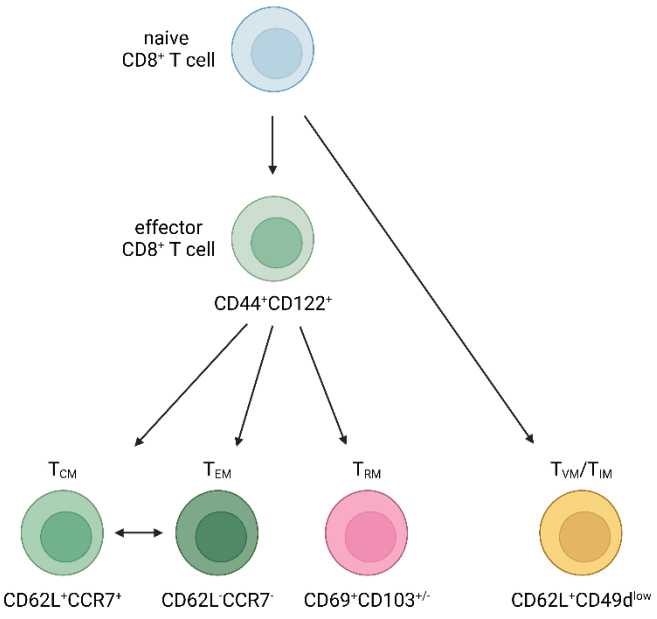

Figure 3. Origin of T_{CM}, T_{EM}, T_{RM} and T_{VM}/T_{IM} in $CD8^+$ T cell development.

In unimmunized and unmanipulated mice, most T cells are naïve. However, up to 20% of these circulating cells display a memory phenotype[78]. Virtual and innate memory T cells (T_{IM}) are antigen-inexperienced T cells with a memory phenotype of $CD44^{+}CD122^{+}CD62L^{+}CD49d^{low}$, making it hard to distinguish between these two types.

However, it is known that CD57Bl/6 mice harbor a vast majority of T_{VM} cells rather than T_{IM} cells, which have yet to be found outside the thymus in wild-type C57Bl/6 mice[79]. Both subsets show regular TCR arrangement and thymic selection but differentiate into memory cells upon cytokine stimuli, not antigens.

T_{IM} cells depend on IL-4 for their development in the thymus. On the contrary, T_{VM} cells show a strong avidity for self-peptide in the thymus and depend on IL-15 presented in *trans* by DCs in the periphery. T_{VM} cells are also found in IL-4-deficient mice but not in IL-15-deficient hosts [80]. Both types, however, are maintained by IL-15 in the periphery, which facilitates their expansion and likely converses T_{IM} cells into T_{VM} cells explaining the identical phenotypes[81,82].

Although undistinguishable by surface marker phenotype, the origin and gene expression of T_{IM} and T_{VM} cells differ. T_{IM} cells develop in the thymus in the presence of IL-4 and are $NKG2D^{-}T\text{-}bet^{-}EOMES^{+}$. T_{VM} cells develop in the periphery with the trans-presentation of IL-15 and are $NKG2D^{+}T\text{-}bet^{+}EOMES^{+}$[79].

In humans, the innate-like memory $CD8^{+}$ T cells form a subset most comparable to T_{VM} cells. They develop in the periphery with IL-15 presence and are $CD45RO^{-}CD27^{-}$ $CD45RA^{+}NUR77^{+}KIR^{+}T\text{-}bet^{+}EOMES^{+}$[81,83–85].

However, functionally they all have the same properties. T_{IM}, $T_{VM,}$ and innate-like human memory $CD8^{+}$ T cells produce IFN-γ in response to foreign antigens and can clear infections rapidly and successfully[79,86,87]. These cells are found mainly in the early stages of life when the adaptive immune system is not yet experienced. But T_{VM} cells increase with age when the adaptive immune response is known to decline. Therefore, these non-specific but effective $CD8^{+}$ T cell populations present a bridge between the innate and adaptive immune systems, representing a distinct population from ILCs and NKT cells.

Table 1. The distinguishing characteristics of memory CD8$^+$ T cell subsets. Reproduced and further developed from Martin et al.[66] and White et al.[79].

	Phenotype		Responds to	Location	Function
	Mouse	Human			
CTL	CD44$^+$	CD44$^+$CD45RO$^+$	MHC I	Lymph and periphery	fight primary Ag encounter, cytotoxicity
T_{CM}	CD44$^+$CD127$^+$ CD62L$^+$CCR7$^+$	CD27$^+$CD45RA$^-$	MHC I	sec. lymph tissues	proliferation, low circulation potential
T_{EM}	CD44$^+$CD127$^+$ CD62L$^-$CCR7$^-$	CD27$^-$CD45RA$^-$	MHC I	circulation of peripheral tissues	fight secondary Ag encounter, cytotoxicity, moderate proliferation potential
T_{RM}	CD44$^+$ CD69$^+$CD103$^{+/-}$	CD69$^+$CD103$^{+/-}$	MHC I	tissue resident	local defense, IFN-γ production, recruitment of immune cells
T_{VM}/T_{IM}	CD44$^+$CD122$^+$ CD62L$^+$CD49d^{low}	CD45RO$^-$CD27$^-$ CD45RA$^+$	IL-15 /IL-4+IL-15	periphery	Ag inexperienced cell for immediate defense

1.2.3 CD8$^+$ regulatory T cells

Regulatory T cells (Treg) play a critical protective role by maintaining immunological homeostasis and self-tolerance. Although early work highlighted the immunosuppressive functions of CD4$^+$ and CD8$^+$ T cells, only the concept of CD4$^+$ Tregs became widely popular[88]. CD4$^+$ Tregs, in humans and mice, are universally characterized as CD25$^{hi/+}$Foxp3$^+$[89,90]. Based on this, today, we have decades of studies on CD4$^+$ Tregs, their origin and function, and even ongoing clinical trials in which they are used as a therapy against various autoimmune diseases. Research on defining a regulatory arm of CD8$^+$ T cells is subject to more recent and ongoing studies. Although in the last decade the evidence of the importance of CD8$^+$ regulatory T cells accumulates, their sheer existence is still debated and not accepted by all. This seems to be mostly due to the lack of clear definition of one CD8$^+$ Treg subset. Contrary to CD4$^+$ Tregs, CD8$^+$ Tregs seem to be a heterogenous group, with different origins, and distinct modes of action.

In the beginning, phenotyping was based on the markers known of $CD4^+$ Tregs. Indeed, there is a subset of $CD8^+$ T cells expressing Foxp3 and a subset of those is also $CD25^+$. However, there are also $CD8^+CD25^-Foxp3^+$ Tregs which facilitate suppressive activities and express either GITR, CTLA-4, ICOS or CD73 in mice and GITR, TNFR-2 or CD39 in human[91]. Additionally, these subsets are associated with uniquely secreted molecules and partly different mechanisms of function. However, $CD8^+Foxp3^+$ Tregs are only one of several currently discussed populations, making the topic of $CD8^+$ Treg research complex. Niederlova et al. proposed six distinct subsets of $CD8^+$ Tregs based on their markers, maintenance of self-tolerance, and their known mechanism of immunosuppression: $CD8^+CD122^+$, $CD8\alpha\alpha^+$, $CD8^+$ Qa-1-restricted, $CD8^+Foxp3^+$, $CD8^+CD28^-$, and $CD8^+CD45RC^{low}$[91].

In mice, $CD8^+CD122^+$ Tregs have been proven to be critical for homeostasis. Genetic knockout studies revealed a predisposition for autoimmune diseases, which was reverted by the adoptive transfer of these cells[92,93]. Modern technologies enabled a more thorough characterization of the surface marker profile of these cells. Today, they are defined as $CD8^+CD44^+CD122^+Ly49^+$, with the F receptor of Ly49 seemingly being the most impactful[94]. They show a pronounced phenotypically overlap with $CD8^+$ Qa-1-restricted Tregs and antigen-inexperienced virtual or innate memory T cells[91]. The gene expression profile seems to be shaped by Helios, Eomes, and TGF-β receptor 2 expression[94–97]. Most recently, an equivalent of these cells was found in humans, characterized as $CD8^+KIR^+$ T cells, proven to be active in autoimmune disease and infection, and capable of suppressing pathogenic T cells[98].

1.3. Current state of research

1.3.1 $CD8^+$ T cells in experimental non-autoimmune GN rodent models

Non-autoimmune GN models are not uniform in their disease induction. Although several studies are dedicated to the role of $CD8^+$ T cells in experimental non-autoimmune GN, they often vastly differ in their findings. In the following section, three early studies on the role of CD8 in non-autoimmune GN are discussed, which build the stepping stones of this thesis.

Early work from Kawasaki et al. in Wistar Kyoto rats revealed that $CD8^+$ T cells contribute to rabbit anti-rat NTS pathophysiology[99]. CD8-positive cells were found in the glomeruli and the interstitium as early as four hours after NTS injection. Immunohistochemistry revealed the highest numbers of $CD8^+$ cells on day 3, and numbers declined after that. In comparison, macrophage numbers peaked with a significant delay on days 6 and 11, surpassing 3-fold the number of $CD8^+$ T cells. Interestingly, this study reported only minimal numbers of intraglomerular $CD4^+$ T cells from the beginning throughout day 11 of NTS. Regarding the location within the renal tissue, this early study placed $CD8^+$ T or NK cells in the interstitium and not in glomeruli after day 1 of NTS.

Depletion of $CD8^+$ T cells prevented proteinuria, and glomeruli crescent formation was reduced. Blocking the infiltration of $CD8^+$ T cells resulted in limited infiltration of macrophages in the later days of the disease. These results were independent of circulating anti-rabbit IgG and rat C3 since levels were comparable to controls. These results show a role for CD8 in the development of proteinuria, crescent formation, and macrophage recruitment to the kidney. All of these GN hallmarks are eased in the absence of CD8.

Tipping et al. showed an overall aggravated GN phenotype in *CD8*$^{-/-}$ mice with sheep anti-mouse GBM GN[100]. Histology revealed exacerbated crescent formation compared to WT mice, ascites, and signs of nephrotic syndrome on day 14. On day 21, *CD8*$^{-/-}$ mice showed more PAS-positive material and crescent formation. In line with these results, glomerular deposition of mouse IgG and C3 was more prominent in *CD8*$^{-/-}$ mice than in controls. *CD8*$^{-/-}$ mice showed comparable $CD4^+$ cell numbers in renal tissue to controls. Glomerular cell counts for macrophages were higher on days 7 and 14 and similar to WT cell numbers on day 21 of the disease.

Of note, this study found similar $CD8^+$ cell numbers infiltrating the kidney tissue in *CD4*$^{-/-}$ mice compared to controls, but fewer macrophages on days 7, 14, and 21. Proteinuria was comparable in WT, *CD4*$^{-/-}$, *CD8*$^{-/-}$ and *CD4*$^{-/-}$*CD8*$^{-/-}$ mice. However, BUN levels were strikingly different. While *CD4*$^{-/-}$ and *CD4*$^{-/-}$*CD8*$^{-/-}$ mice failed to develop elevated BUN levels throughout the disease, *CD8*$^{-/-}$ mice showed even higher levels than WT mice on day 14. These results clearly show the role of $CD8^+$ cells is independent of proteinuria development, but macrophage recruitment, renal tissue injury, and BUN levels are aggravated in the absence of CD8[100].

Li et al. also used a model based on sheep anti-mouse GBM globulin in *TAP-1*$^{-/-}$ mice and WT mice with CD8 depletion. *TAP-1*$^{-/-}$ mice are defective in their MHC I antigen presentation and have reduced numbers of $CD8^+$ T cells. *TAP-1*$^{-/-}$ mice developed severe histological features of GN. Proteinuria and creatinine clearance reduction were comparable to control *TAP-1*$^{+/-}$ mice. Glomerular infiltration of $CD4^+$ T cells and macrophages was similar in both groups, while $CD8^+$ cell infiltration was markedly reduced in *TAP-1*$^{-/-}$ mice. The systemic immune response was not altered in *TAP-1*$^{-/-}$ mice, represented in comparable levels of anti-sheep antibody titers and GBM-deposition of immunoglobulin to controls[101].

Anti-mouse CD8 antibody was administered 2 hours before GN induction in WT mice and again 7 days later. CD8 depletion did not change anti-sheep antibody levels or glomerular deposition of immunoglobulin compared to isotype-controlled mice. Both groups showed severe crescentic GN, with no difference in creatinine clearance reduction. However, proteinuria was markedly reduced, and the same was true for glomerular infiltration of $CD4^+$ T cells and macrophages. All results represent day 14 of disease.

Results in *TAP-1*$^{-/-}$ mice show that MHC I-dependent antigen presentation is not necessary for the development of crescentic GN in this model, which is mediated by exogenous antigen. Also, MHC I-restricted $CD8^+$ T cell-dependent cytotoxicity is likely not the cause of renal injury. Different results with the necessity of MHC I presentation were shown in an autoantibody-mediated murine MRL/lpr lupus-prone model, highlighting a major difference[102]. Interestingly, however, this model was also independent of CD8 cells. Depletion of CD8 cells in the effector phase of anti-GBM GN did not halt tissue injury, but reduced cell infiltration and proteinuria[101].

Table 2. An overview of the literature on the role of $CD8^+$ T cells in rodent non-autoimmune GN models.

Study	Disease	Model	Histology	Proteinuria	Kidney function	cell infiltration
Kawasaki et al., *Kidney Int*. 1992	rabbit anti-rat GBM NTS	CD8 depletion in WKY rats	↓ crescent formation	↓	---	↓ macrophages
Tipping et al., *Am J Pathol*. 1998	Sheep anti-mouse GBM GN	$CD8^{-/-}$ mice	↑ crescent formation ↑ PAS-positive	=	↑ BUN	= CD4 ↑ macrophages
Li et al., *Clin Exp Immunol*. 2000	Sheep anti-mouse GBM GN	CD8 depletion in C57Bl/6 mice	= crescent formation	↓	= creatinine clearance	↓ CD4 ↓ macrophages

1.3.2 $CD8^+$ T cells in experimental autoimmune GN rodent models

The role of CD8 T cells has also been studied in models of experimental autoimmune GN models. For example, WKY rats were immunized with collagenase-solubilized normal rat GBM in adjuvant. Two groups with CD8 depletion were studied against a control group. The prevention group was depleted of CD8 at the time of immunization. The treatment group was depleted of CD8 at week 2 of 4. The prevention group showed no detectable albuminuria, while the treatment group had reduced albuminuria compared to controls. The measured creatinine clearance in both groups was comparable to a healthy control group. Both groups' histological analysis showed no fibrin deposits at week 4. The prevention group, in general, showed no histological signs of disease. The treatment group showed mild glomerular and minimal interstitial injury. Positive control animals showed crescent formation, interstitial damage, and signs of necrotizing glomerulonephritis. The prevention group showed no CD8 cells, macrophages, or neutrophils in the glomeruli. The treatment group had marked reductions in all mentioned cell populations compared to controls. While the prevention group had no circulating anti-GBM antibody titers, the treatment group showed similar levels of circulating antibodies compared to controls.[103]

In another study, experimental anti-myeloperoxidase GN was used as a model for ANCA-associated vasculitis. C57Bl/6 WT mice were injected twice with murine MPO (day 0 in CFA, day 7 in IFA). Controls received OVA as antigen. The disease was triggered with sheep anti-mouse GBM globulin (days 16 and 17), and injury was assessed on day 20. CD8b cells were depleted (YTS169.4) on day 15 and analyzed against controls receiving an isotype control antibody. Mice depleted of CD8b cells showed reduced albuminuria and segmental necrosis. Glomerular cell infiltration of $CD4^+$ T cells and macrophages was reduced, while no change in neutrophil numbers was shown. mRNA expression profiles of kidney tissue showed a reduction in IFN-γ, TNF, CXCL9, and CXCL10 in mice depleted of CD8b cells compared to controls[104].

Although the two chosen studies only reflect a fraction of experimental autoimmune studies dedicated to CD8, in general, the results seem to be more in line with showing a benefit of CD8 depletion in disease.

1.4 Interleukin-15

IL-15 belongs to the α-helix bundle family of cytokines, as do IL-2, IL-3, IL-6, IL-7, G-CSF, and GM-CSF[105]. IL-15 and IL-2 share the Rβ-chain (CD122) and use the same Rγ-chain (CD132, common γ, γ_c); however, both receptors have unique α-chains. Since signaling is possible via the Rβγ-heterodimer, IL-15 and IL-2 show overlapping functions, which might have been overestimated from *in vitro* studies[106–108]. *In vivo*, however, through signaling via the IL-15Rαβγ-heterotrimer, which seems to be favored, IL-15 facilitates essential and different functions from IL-2[109,110]. While IL-15Rα alone was sufficient for high-affinity IL-15 binding, it does not facilitate signal transduction. IL-15Rα, and its 8 isoforms, were found widespread in tissues, PBMCs, and cell lines[105,111]. Therefore, APCs expressing IL-15Rα can present bound IL-15 in *trans* to other cell types. After IL-15 binding, Rβ activates Jak1/STAT3, Rγ signals via Jak3/STAT5[112,113], and src-related tyrosine kinases induce Bcl-2 and stimulate the Ras/Raf/MAPK pathway[114].

IL-15 is expressed in various tissues, e.g., muscle, heart, and kidney. Different cell types have been found to produce IL-15 mRNA: monocytes, macrophages, dendritic cells, bone marrow stromal cells, epithelial cells in various organs, fibroblasts[115–118] as well as T cells[105,119]. As early as 1998, IL-15 expression was also found in kidney epithelial cells[120].

IL-15 signaling plays a major role in NK, NKT, and $CD8^+$ T cell differentiation, proliferation, survival, and cytotoxicity[105]. The major phenotypes of both *IL-15*$^{-/-}$ and *IL-15Rα*$^{-/-}$ mice are the absence of NK cells and deficiencies of NKT and memory $CD8^+$ T cells[109,110]. IL-15 was found to mediate antibody-dependent cellular cytotoxicity in NK cells participating in innate defense against viral infections[121,122]. It was also identified as a growth factor and a chemoattractant for T cells. *IL-15Rα*$^{-/-}$ mice have defects in T cell homing to peripheral tissues[109,123]. Stimulation with IL-15 leads to the proliferation of memory CD4 and CD8 and naïve CD8 T cells. It does not affect naïve CD4 T cells, which do not express the Rβ-chain[124]. The most affected cell type is $CD44^{hi}CD8^+$ memory T cells, which are absent in *IL-15Rα*$^{-/-}$ mice[125]. *IL-15*$^{-/-}$ mice have reduced numbers of $CD8^+$ memory cells in secondary lymphoid organs, which was shown to be reversible upon doses of exogenous IL-15. However, IL-15 does not seem to affect $CD8^+$ T cell development but is critical for their proliferation and survival[110].

Monocytes and macrophages have been shown to express all three chains of the IL-15R[105]. IL-15 was shown to regulate macrophage cytokine production in a dose-dependent manner. Higher levels of IL-15 enhanced the production of TNFα, IL-1, and IL-6[126]. Human monocytes stimulated with IL-15 produced MCP-1 and IL-8, which are autocrine chemotactic[127].

IL-15 provides the potential for therapeutic uses. So far, the most effort has been put into using IL-15 to expand cytotoxic lymphocyte subsets in patients with tumors or potentially immunodeficiencies. Immunotherapies using IL-2, G-CSF, and GM-CSF of the same cytokine family have been used successfully to activate and expand immune cells *in vivo*. As of 2020, phase I clinical trials were already conducted studying the administration of rhIL-15 in combination immunotherapies to treat cancer[128]. Pre-clinical studies have also shown benefits when blocking IL-15 in collagen-induced arthritis[129]. However, with IL-15 and IL-15Rα being produced in a wide range of tissues and cell types and its pleiotropic characteristics, which might be dose- and affinity-dependent, the complete and complex potential for its use in immunotherapy is likely far from understood.

1.4.1 IL-15 in kidney health and disease

Transcriptome datasets revealed that healthy kidney biopsies showed overall higher IL-15 expression levels than patients with different nephropathies, including diabetic nephropathy, minimal change disease, segmental glomerulosclerosis, IgA nephropathy, and membranous glomerulonephritis[130]. Immunohistochemistry confirmed these findings on a protein level, showing IL-15 regulation in acute interstitial nephritis, IgA nephropathy, and diabetic nephropathy.

Tejman-Yarden et al. used western blotting and flow cytometry methods to show that TECs express the functioning full-length α-chain of the IL-15R in mice and humans[131]. Stimulation with IFN-γ upregulated the expression of the α-chain, but IL-2 or IL-15 did not. Years later, Giron-Michel et al. proved that renal proximal TECs actually express all three chains of the IL-15R[132]. Stimulation with rhIL-15 led to increased survival of TECs and inhibited epithelial-mesenchymal transition (EMT). Interestingly, in renal cell carcinoma (RCC), they found a defect in the signaling pathway via the γ-chain, resulting in increased

signaling via a heterodimer of the α- and β- chains, causing downregulation of tumor suppressor genes (e.g., E-cadherin) and increased EMT. In a further study, they could show that even paratumoral primary renal epithelial cells show elevated signaling via the abnormal IL-15Rαβ heterodimer, favoring the development of the tumor microenvironment[133].

IL-15 is also tested in the context of increased cytotoxicity of T cells against tumors. Zhang et al. investigated that concept in RCC[134]. IL-15 stimulated γδ T cells showed higher cytotoxic activity and better survival *in vitro*, and these results correlated with higher expression of NKG2D. Furthermore, upon adoptive transfer of IL-15-stimulated cells into an RCC-PDX mouse model, transferred γδ T cells significantly suppressed tumor growth compared to the transfer of γδ T cells stimulated with IL-2 as control.

Devocelle et al. compared mRNA datasets of renal transplant biopsies of recipients with good renal function versus recipients with renal dysfunction[130]. The analysis revealed significantly lower IL-15 levels in transplants not functioning well. Interestingly, TGF-β1 was inversely expressed. Previous studies could show that TGF-β drives spontaneous EMT in an *in vitro* model using primary renal epithelial cells. rhIL-15 treatment and TGF-β1 neutralization protected cells from spontaneous EMT caused by growth factor starvation via inhibition of TGF-β1-induced collagen IV synthesis. This study highlighted the IL-15 to TGF-β ratio as a marker for kidney dysfunction.

In contrast, Weiler et al. investigated elevated IL-15 mRNA levels expressed in kidney allograft rejections and found human tubular epithelial cells to be the source[120]. They found that upon stimulation with IFN-γ, mRNA and protein levels were increased. Vice versa, the supernatant of human TECs induced proliferation in a T cell line *in vitro*, which was blocked by anti-IL-15 antibodies. In a later study, Weiler et al. could narrow down the stimulation of IL-15 production of TECs to be an effect of CD40-CD40L binding of supposedly Th1 cells to TECs[135].

The effect of IL-15 in murine models of acute kidney injury was studied by Eini et al.[136]. They investigated a sepsis model, an ischemia-reperfusion (IRI) model, and a model of cisplatin nephrotoxicity. After 24 hours, sepsis-induced and IRI mice showed a multiple-fold decline of renal IL-15 and the renal IL-15Rα detected by qPCR and western blot compared to respective controls. In steady-state, *IL-15Rα*$^{-/-}$ mice showed less *Bcl-2* and higher *Bax* expression patterns, which could be reversed *in vitro* by adding rIL-15. In cisplatin-induced

nephrotoxicity, this study was also able to show renoprotective effects of IL-15 *in vivo* and *in vitro* cultures of primary tubular cells. In a mouse model of cisplatin nephrotoxicity, IL-15 levels dropped lower than baseline after 24 hours. Additionally, a correlation between the decline in kidney function measured by BUN and low IL-15 mRNA was observed.

In a CKD model of unilateral ureteral obstruction (UUO), IL-15 was shown to have renoprotective function by inhibiting fibrosis[137]. Administration of IL-15 or IL-15-IL-15Rα complexes led to reduced collagen and fibronectin deposition. Additionally, in this model, IL-15 reduced the expression of *Mcp-1* and, in hand with this finding, reduced macrophage infiltration.

Shinozaki et al. used *IL-15*$^{-/-}$ mice to study the role of IL-15 in NTS[138]. With their experiments, they were able to show that also in autoimmune-like disease, IL-15 protects TECs from apoptosis by reduced anti-Fas or actinomycin D induction. *IL-15*$^{-/-}$ mice presented with more tubular injury, higher BUN levels, accumulation of cells in glomeruli, and increased numbers of interstitial CD4^{+} T cells and macrophages. The abundance of macrophages might be explainable by higher MCP-1 levels in these mice. However, interestingly, *IL-15*$^{-/-}$ mice showed reduced numbers of CD8^{+} cells in glomeruli from the beginning continuously through the end of the experiment on day 14. Also, this study showed that IL-15 transcription is downregulated in wild-type NTS mice kidney tissue compared to healthy controls.

1.5 Aims

IL-15 is a proliferation and survival factor for CD8^{+} T cells. While IL-15 has been observed and proven critical in several contexts of kidney health and disease, the role of CD8^{+} T cells in these findings has not been discussed.

Therefore, in this thesis, we used our murine model of NTS and aimed to investigate the role of CD8^{+} T cells in disease progression and to explore the potential of low-dose rIL-15 to treat GN.

2. Material and Methods

2.1 Animal Studies

All animal studies were approved by local authorities, namely the Federal Ministry of Education, Science, and Research of the Republic of Austria (BMBWF-66.010-0103-V-3b-2018 and 2020-0.078.387 with amendment 2020-0.827-357. All mice were housed and maintained in a pathogen-free environment at the Medical University of Graz, Austria.

New Zealand White Rabbits and C57Bl/6J mice were purchased from Charles River, Germany. Breeding pairs of B6.129S2-Cd8a^{tm1Mak}/J2 102 (*CD8α*$^{-/-}$) and B6.129X1-Il15ra^{tm1Ama}/J2 (*IL-15Rα*$^{-/-}$) were purchased from The Jackson Laboratory, USA through Charles River, Germany.

All experiments were performed on mice aged 8-14 weeks old, using littermate- where possible, or age- and sex-matched controls.

2.2 Mouse model of Nephrotoxic Serum Nephritis

Production of rabbit anti-mouse antigen: New Zealand White Rabbits were purchased to produce anti-mouse Nephrotoxic Serum to induce the NTS model in mice. Therefore 1.5 canonical Falcon tubes (50ml each) of mouse kidneys (approx. 600 kidneys for 3 rabbits) from various mouse strains were collected and frozen at -20°C until further use. According to the 3Rs, mouse kidneys were collected from mice used in other experiments or for breeding purposes only. Mice were not bred or purchased solely for this purpose. Frozen mouse kidneys were kept on ice and decapsulated, cut longitudinally, renal pelvis and medulla were separated from the cortices and discarded. A razor blade was used to mince the cortices and spread them on the top of three stainless steel sieves. Tissue was pushed through three thieves (150-90-45 nm) with precooled PBS applied in a stream. The glomerular fraction was gently washed from the lowest sieve (45 nm), microscopically checked for purity, centrifuged, and diluted in 5 ml 1M NaCl. Isolated glomerular fractions were sonicated until the disruption of the glomeruli was achieved (assessed by microscopy). Murine antigen fraction was centrifuged, dissolved in 500 µl PBS, and stored at -20°C until use. The protocol was adapted and modified from Assmann et al. [139].

Male New Zealand White Rabbits were kept until a body weight of 2.5-3kg was reached. In week 0, rabbits were intradermally injected at 5-8 sites on the rabbit's neck with 500 µl of complete Freund's Adjuvant (purchased as incomplete FA from Sigma Aldrich, USA and substituted with *Mycobacterium Tuberculosis*, BD, USA) emulsified with 500 µl isolated murine antigen. In weeks 4, 8, and 12, booster injections were administered containing 500 µl isolated murine antigen emulsified with 500 µl of incomplete Freund's Adjuvant. After 16 weeks, rabbits were anesthetized and terminally exsanguinated via cardiac puncture executed by a veterinarian. Harvested blood was centrifuged, and serum was collected, heat-inactivated (45 mins at 56°C), aliquoted, and stored at -20°C until use.

NTS induction in mice: Male mice between 8 and 14 weeks of age were used to induce NTS. The mouse strain used is indicated in the results section of each experiment. Mice were s.c. injected in the footpad with an emulsion of rabbit IgG in complete Freund's Adjuvant. Depending on the experiment setup, this immunization step was carried out 3 or 5 days before NTS was induced (indicated as day -3 or day -5). On day 0 of NTS, mice were injected with a 1:2 dilution in PBS of rabbit anti-mouse antiserum via the tail vein. Mice were kept for 7, 14, or 21 days of NTS, depending on the experiment setup. Throughout this time period, spot-urine and plasma were sampled. Plasma was taken retro-orbitally under isoflurane anesthesia.

All experiments in this study were performed with rabbit anti-mouse serum indexed as "#12" in the Eller lab.

2.4 In vivo interventions

CD8α Depletion: For CD8α depletion studies, anti-CD8α (Clone YTS 169.4, BioXCell, USA) antibody was injected i.p. in a concentration of 0.1 µg/g bodyweight twice per week. Control animals were injected with isotype control (Clone LTF-2, BioXcell, USA) antibody in the same concentration and interval as the intervention group.

rIL-15 treatment: For IL-15 intervention, recombinant IL-15 was administered i.p. in a single dose of 2 µg/20 g bodyweight. This dose was termed "low-dose" and is reflected as a dose that is still a sub-proliferation dose for $CD8^+$ and NK cells *in vivo* [125,140,141].

BrdU incorporation: Mice were injected with 2 mg/20 g bodyweight of BrdU for cell proliferation studies. *In vivo* incorporation period was 48 hrs, and mice were sacrificed after that.

Adoptive transfer of enriched $CD8^+$ cells: Negatively sorted enriched $CD8^+$ cells were checked for purity >95%. Enriched cells from five donor mice were pooled, and $2.5x10^6$ cells per mouse were adoptively transferred into recipient mice via the tail vein.

2.5 Assessment of Renal Injury

Urinary Albumin concentration: Urinary albumin was assessed by double-sandwich ELISA (Bethyl Laboratories, USA). The plate was coated with goat anti-mouse albumin antibody (1 µg/ml overnight at 4°C. On the next day, wells were blocked with PBS/Tween/0.5 % BSA for 30 mins at RT. Spot-urine samples were diluted in PBS/Tween/0.5 % BSA in serial concentrations ranging from 1:100 to 1:1.000.000. A standard curve was created with mouse albumin stock of 2 mg/ml and applied in 6 dilutions with the concentrations 1 µg/ml, 0.1 µg/ml, 0.03 µg/ml, 0.01 µg/ml, and 0.001 µg/ml. A blank control was used. Samples, standard, and blank were incubated for 2 hrs at RT. Goat anti-mouse albumin HRP conjugate in a concentration of 0.02 µg/ml was used as the second antibody. After two hours of incubation, enzymatic substrate (TMB Buffer) was applied until a visual color change to dark blue, and the reaction was stopped with 2 M H_2SO_4. The plate was read at 450 nm in a microplate spectrophotometer.

Urinary Creatinine concentration: Three methods were used to measure urinary creatinine levels in this study. Initially, creatinine was measured using a commercial picric acid-based method (Sigma Aldrich, USA). Then, all samples were remeasured using liquid chromatography-tandem mass spectrometry in a corporation with the Clinical Institute of Medical and Chemical Laboratory Diagnostics at the Medical University of Graz, Austria. Finally, samples were measured using a commercially available enzymatic assay kit (Crystal Chem, USA). This kit is based on the enzymatic conversion of creatinine to creatine, which is converted to sarcosine. Sarcosine gets oxidated to produce hydrogen peroxide, which can be quantified at 550 nm in the presence of peroxidase. Random samples have been remeasured to ensure comparable concentrations.

Albuminuria is expressed as urinary albumin to urinary creatinine ratio in mg/mg.

Plasma creatinine concentration: Creatinine levels were measured, as described before, with the enzymatic assay kit (Crystal Chem, USA) according to standard protocol.

Blood urea nitrogen concentration: BUN was measured via colorimetric detection assay (Invitrogen, Carlsbad, USA) according to the manufacturer's protocol. Plasma samples were diluted 1:50 in PBS to lie on the nitrogen standard curve, ranging from 0.156 mg/dl to 10 mg/dl. The reactions colored product was read at 450 nm in a microplate spectrophotometer.

PAS Score: Glomerulosclerosis was analyzed on formalin-fixed 4 µm thick sections of renal tissue embedded in paraffin. After deparaffinization and hydration with Xylene and Ethanol, samples were stained with Periodic Acid-Schiff solution and Schiff's reagent (PAS staining kit, Merck KGaA, Darmstadt, Germany). After washing steps, samples were counterstained with Gill's III Hematoxylin and developed under running tap water. Slides were dehydrated and mounted with an anhydrous mounting medium (Roti-Histokitt II, Roth, Karlsruhe, Germany). Exactly 50 equatorial glomerular cross-sections were evaluated and semiquantitatively scored according to the presence of PAS-positive material within the glomerulus. If no PAS-positive material was present in the area, the glomerulus scored a 0. It scored 1 if $\leq$ 1/3 of the area was PAS-positive, 2 if = 1/3 up to 2/3 of the area was PAS-positive, and 3 if > 2/3 of the area was PAS-positive. The evaluation was adapted from Kitching et al.[142].

Tubular cast formation: Tubular injury was assessed in PAS-stained kidney tissue sections. Tubular cast formation was defined as the presence of acellular PAS-positive cylindrical casts within proximal and distal tubuli. Six or 12 hpf were counted, as indicated in the results section of each experiment. Results were expressed in absolute numbers per respective hpf counted.

Cell death staining: $TUNEL^+$ cells were detected by FITC-labeling of terminal transferase dUTP nick-ends with the In Situ Death Detection Kit (Merck, Germany), according to the manufacturer's standard protocol on 4 µm kidney cryosections.

Crescent formation: PAS-stained kidney tissue sections were also used to assess crescent formation, defined as the presence of a minimum of 3 cellular layers in the Bowman's space. The identical 50 equatorial glomerular cross-sections used for the PAS score were evaluated.

Results were expressed in the percent of incidence in evaluated glomeruli. The evaluation was adapted from Kitching et al.[142].

2.6 Autologous antibody response

Circulating autologous antibody response was detected by ELISA for the serum response to rabbit IgG antibody (Jackson ImmunoResearch Laboratories). Plates were coated with rabbit IgG overnight and blocked with PBS/0.05 % Tween/0.05 % BSA. After that, serial dilutions of serum samples were incubated for 2 hrs, followed by incubation with HRP-conjugated goat anti-rabbit IgG (Jackson ImmunoResearch Laboratories) to detect circulating rabbit immunoglobulin. TMB Buffer was used as a substrate, and the enzymatic reaction was stopped with 2 M H_2SO_4. Autologous antibody response in each mouse was measured in all experiments to guarantee equal activation levels of the immune system and exclude B cell responses as possible causes for different outcomes. Kidney cryosections were used to stain for autologous IgG deposition by serial dilutions of FITC-labeled goat anti-mouse IgG (Jackson ImmunoResearch Laboratories).

2.7 Immunohistochemistry

Myeloid cell infiltration was evaluated by immunohistochemistry. Therefore, kidney tissue was embedded in OCT medium (Tissue-Tek O.C.T, Sakura Finetek, USA) and flash-frozen in liquid nitrogen. Samples were stored at -80°C until processed. Tissue was cryo-cut at -16°C in 4 µm thick sections. Slides were stained at RT in a moist chamber to prevent dehydration. Samples were fixed with Acetone and blocked with fetal bovine serum, goat serum, and 200 µl/ml Avidin (Vector Laboratories, CA, USA). After the washing steps, the primary antibody was applied in PBS and 200 µl/ml Biotin (Vector Laboratories, CA, USA). An antibody against CD68 (Biorad, USA) was used to stain macrophages. An antibody against Ly6G (Abcam, USA) was used to stain neutrophils. Both primary antibodies were rat-derived anti-mouse. After an hour of incubation and subsequent washing, a secondary biotinylated goat anti-rat IgG antibody (Jackson ImmunoResearch Laboratories, USA) was applied for 45 min. After washing in PBS and 0.1 M Sodium-acetate buffer, stains were developed in 3-amino-9-ethylcarbazole substrate chromogen. Slides were also counterstained with Gill's III hematoxylin (Sigma Aldrich, USA) and developed under running tap water. Slides were

mounted in Aquatex mounting medium (Merck KGaA, Germany). Cell infiltration was quantified as total cell numbers per 6 hpf in each renal cortex and medulla.

2.8 Multicolor flow cytometry analysis

Lymph nodes were passed through a 70µm cell strainer to obtain single cell suspensions, washed, and kept in MACS buffer (PBS, 0.5% BSA, 2mM EDTA) for subsequent staining.

For kidney flow cytometry, the left kidney of the mouse was mechanically homogenized and digested with RPMI media supplemented with FBS, β-Mercaptoethanol, HEPES-Buffer, Collagenase D, and DNase I. Tissue was passed through a 70µm cell strainer with magnesium- and calcium-free HBSS, and subsequently through a 50µm cell strainer with HBSS. After centrifugation, the cell pellet was dissolved in 37,5% osmo-adjusted Percoll solution (Sigma-Aldrich, USA) and centrifuged for 15 mins at 500g with the breaks off. Percoll and debris were removed, and the cell pellet was incubated for 4 mins with 1xRBC lysis buffer (eBioscience, USA). The reaction was stopped with PBS, and cells were washed and transferred into MACS Buffer for cell surface staining.

All samples were stained with a fixable viability dye eF780 (ThermoFisher Scientific, USA) in PBS for 15mins at 4°C and washed before cell surface staining.

After cell surface staining for 30mins at 4°C, cells were washed with MACS and fixed with Cytofix (BD Biosciences, USA) for 30mins. After that, cells were washed and kept in MACS Buffer until samples were acquired on Cytoflex LX (Beckman Coulter, USA) flow cytometer.

Intracellular staining for Foxp3 was achieved with the eBioscience FOXP3/Transcription Factor Staining Buffer Set (Invitrogen, Carlsbad, CA, USA) according to protocol.

Intracellular staining for IFNγ was achieved with the eBioscience™ Intracellular Fixation & Permeabilization Buffer Set (ThermoFisher Scientific, USA).

Table 3. Antibody panel for flow cytometric analysis of Ly49 on $CD8^+$ T cells.

Antibody	Clone	Company
FVD		ThermoFisher Scientific
CD45	30-F11	BD Biosciences
CD3	17A2	ThermoFisher Scientific
CD25	PC61	Biolegend
CD8α	53-6.7	ThermoFisher Scientific
CD122	TM-b1	ThermoFisher Scientific
Ly49 C/F/H/I	14B11	ThermoFisher Scientific
CD4	RM4-5	ThermoFisher Scientific
CD44	IM7	ThermoFisher Scientific

Table 4. Antibody panel for flow cytometric analysis of NK, NKT and iNKT cells.

Antibody	Clone	Company
FVD		ThermoFisher Scientific
CD45	30-F11	BD Biosciences
CD19	1D3	ThermoFisher Scientific
CD3	17A2	ThermoFisher Scientific
NK1.1	PK136	ThermoFisher Scientific
CD1d-tet	PBS-57	NIH tetramer core facility at the Emory University, Atlanta, GA, USA

Table 5. Antibody panel for flow cytometric analysis of exhaustion phenotype on $CD4^+$ and $CD8^+$ T cells.

Antibody	Clone	Company
FVD		ThermoFisher Scientific
CD45	30-F11	BD Biosciences
CD3	17A2	ThermoFisher Scientific
CD4	RM4-5	ThermoFisher Scientific
CD8α	53-6.7	ThermoFisher Scientific
CTLA-4	UC10-4B9	Biolegend
LAG-3	eBioC9B7W	ThermoFisher Scientific
PD-1	RRMP1-30	ThermoFisher Scientific
TIM-3	RMT3-23	ThermoFisher Scientific

Table 6. Antibody panel for flow cytometric analysis of proliferation studies in $CD8^+$ memory T cells.

Antibody	Clone	Company
FVD		ThermoFisher Scientific
CD45	30-F11	BD Biosciences
CD3	17A2	ThermoFisher Scientific
CD8α	53-6.7	ThermoFisher Scientific
CD122	TM-b1	ThermoFisher Scientific
Ly49 C/F/H/I	14B11	ThermoFisher Scientific
CD44	IM7	ThermoFisher Scientific
aBrdU	BU20A	ThermoFisher Scientific

Table 7. Antibody panel for flow cytometric analysis of tissue-resident markers on Ly49$^+$CD8$^+$ memory T cells.

Antibody	Clone	Company
FVD		ThermoFisher Scientific
CD45	30-F11	BD Biosciences
CD3	17A2	ThermoFisher Scientific
CD8α	53-6.7	ThermoFisher Scientific
CD122	TM-b1	ThermoFisher Scientific
Ly49 C/F/H/I	14B11	ThermoFisher Scientific
CD103	2E7	ThermoFisher Scientific
CD69	H1.2F3	ThermoFisher Scientific
CD62L	MEL-14	ThermoFisher Scientific

Table 8. Antibody panel for flow cytometric analysis CD4$^+$ regulatory T cells.

Antibody	Clone	Company
FVD		ThermoFisher Scientific
CD45	30-F11	BD Biosciences
CD3	17A2	ThermoFisher Scientific
CD4	RM4-5	ThermoFisher Scientific
CD25	PC61	Biolegend
FoxP3	150D	ThermoFisher Scientific

Table 9. Antibody panel for flow cytometric analysis of IFNγ-production of CD4$^+$ and CD8$^+$ T cells.

Antibody	Clone	Company
FVD		ThermoFisher Scientific
CD45	30-F11	BD Biosciences
CD3	17A2	ThermoFisher Scientific
CD4	RM4-5	ThermoFisher Scientific
CD8α	53-6.7	Biolegend
IFNγ	XMG1.2	ThermoFisher Scientific

2.9 TEC isolation

TECs were isolated from fresh kidney cortex tissue, separated from the medulla and renal pelvis. The material was minced with a razor blade and spread on three stainless steel sieves (150-90-45 nm). Tissue was flushed through the sieves with a stream of cold PBS. TECs were gently washed from the middle sieve (90 nm) and checked for purity under the microscope. Cells were frozen and kept at -80°C in TRIzol Reagent (Sigma Aldrich, USA) until processed further.

2.10 RNA isolation, Transcription, and qPCR in kidney cortex and isolated TECs

Total RNA was extracted from flash-frozen kidney cortices, homogenized through 18 G needles and 1 ml syringes in cold TRIzol Reagent (Sigma Aldrich, USA). One-fifth of the volume was added in Chloroform, incubated, and centrifuged at 12.000g. The supernatant was transferred, incubated with Isopropanol, and again centrifuged. Samples were washed with cold 70 % Ethanol, centrifuged, and washed with absolute Ethanol. Pellets were dried and diluted in RNase-free dH_2O.

cDNA from kidney cortices was synthesized with the Superscript III Transcription kit (Invitrogen, CA, USA).

Total RNA was extracted from pre-isolated TECs with the RNeasy Mini Kit (Qiagen, USA) according to the manufacturer's protocol. Samples were lysed, homogenized, and mixed with Ethanol. The lysate was loaded onto the filter of an RNeasy column which binds RNA to a silica membrane. All contaminants were washed away in several washing steps. In the final step, RNA is eluted from the membrane in RNase-free dH_2O.

cDNA from pre-isolated TECs was synthesized with the High-Capacity cDNA Reverse Transcription kit (Applied Biosystems, USA).

The real-time polymerase chain reaction was performed using TaqMan gene expression assays (Applied Biosystems, USA) and SYBR green (BioRad, USA).

Relative gene expression in kidney cortices was measured using *Hprt* (SYBR Green Assay, Invitrogen) as a reference gene with the forward primer 5´GCT TCC TCC TCA GAC CGG TTT TTG C 3´ and the reverse primer 5´ATC GCT AAT CAC GAC GCT GGG ACT G 3´.

TaqMan gene expression assay (Applied Biosystems, USA) was used to measure *Tbx21* (Mm00450960_m1), *Rorc* (Mm012611022_m1), *Gata3* (Mm00484683_m1), and *Foxp3* (Mm00475162_m1).

Isolated TECs were analyzed for gene expression with reference gene *Actb* (Mm00607939_s1) for *Il-15ra* (Mm04336046_m1) and *Bcl2* (SYBR Green Assay, Invitrogen) expression. Chemokine and Nlrp3 expression were analyzed with TaqMan probes for *Mcp1* (Mm00441242_m1), *Cxcl1* (Mm00433859_m1), *Cxcl5* (Mm00436451_g1), and *Nlrp3* (Mm00840904_m1).

2.11 Magnetic-activated cell sorting and adoptive cell transfer

Lymph node single-cell suspensions were stained with APC-labelled antibodies and subsequently incubated with anti-APC magnetic microbeads (Miltenyi Biotec, Germany). Cell suspensions were transferred onto LD columns (Milentyi Biotec, Germany), and flow-through containing enriched and unstained $CD8^+$ cells was collected. Flow through was checked for purity >95%. All other cells were restrained in the column due to magnetic beads binding to APC-stained cells. Enriched $CD8^+$ cells were either used for cell culture experiments or adoptive cell transfer into *CD8*$^{-/-}$ mice. Therefore, enriched cells from five mice were pooled, and $2.5x10^6$ cells per mouse were adoptively transferred into recipient mice.

Table 10. Antibody panel for negative magnetic-activated cell sorting of $CD8^+$ T cells.

Antibody	Clone	Company
CD4	RM4-5	ThermoFisher Scientific
CD11b	M1/70	
CD19	1D3	
TER119	TER-119	
B220	RA3-682	

2.12 Cell Culture

Splenocytes were cultured in media (RPMI, 10% FCS, 1% Pen/Strep) at a concentration of $1x10^6$ cells per ml, in 2.5ml, and duplicates at 37,5°C and 5% CO_2. Duplicates were pooled for subsequent intracellular flow cytometry analysis.

To assess IFNγ-production in $CD4^+$ T cells, splenocytes were stimulated with eBioscience Cell Stimulation Cocktail Plus Protein Transport Inhibitor (Invitrogen, USA) for 5 hours.

To assess IFNγ-production in $CD8^+$ T cells, splenocytes were stimulated with Dynabeads® Mouse T-Activator CD3/CD28 (Gibco by LifeTechnologies, USA) in a ratio of 1:1 for 4 days. Then, cells were restimulated with eBioscience Cell Stimulation Cocktail Plus Protein Transport Inhibitor (Invitrogen, USA) for 5 hours.

2.13 Cell Culture and relative gene expression of isolated $CD8^+$ T cells

$CD8^+$ T cells were negatively MACS sorted from lymph nodes and cultured in media (RPMI, 10% FCS, 1% Pen/Strep). Cells were stimulated with Dynabeads® Mouse T-Activator CD3/CD28 (Gibco by LifeTechnologies, USA) in a ratio of 1:1 for 4 days. Thereafter, cells were transcribed into cDNA with TaqMan® Gene Expression Cells-to-CT™ Kit (Thermo Fisher Scientific, USA) according to standard protocol. Dynabeads® were removed according to the standard protocol for downstream analysis. Relative gene expression was analyzed with TaqMan probes for *Prf1* (Mm00812512_m1), *Gzmb* (Mm00442834_m1), *Ifnγ* (Mm00801778_m1), *Ikzf2* (Mm00496108_m1), *Tgfb1* (Mm01178820_m1) and *Foxp3* (Mm00475162_m1).

2.14 Statistical Analysis

All statistical analyses were performed with GraphPad Prism version 9.4.1 for Windows, GraphPad Software, San Diego, California, USA, www.graphpad.com. Normal distribution testing was done using the Kolmogorov-Smirnov test and the Shapiro-Wilk normality test. Depending on the data distribution, Student's t-test or nonparametric Mann-Whitney test was used for statistical analysis. All data are shown as mean ± SEM. Statistical significance was indicated by *$p \leq 0.05$, **$p \leq 0.01$, ***$p \leq 0.001$, ****$p \leq 0.0001$.

2.15 Figure Design

Graphs were created with GraphPad Prism version 9.4.1 for Windows, GraphPad Software, San Diego, California USA, www.graphpad.com. The colors of the bars were modified, and figure composition was done with Inkscape version 1.1 (c68e22c387, 2021-05-23), Inkscape Project 2020. Illustrations were created with BioRender.com.

3. Results

3.1 Involvement of CD8α in NTS

To investigate the involvement of $CD8^+$ T cells in the pathophysiology of NTS C57Bl6/J WT mice versus *CD8α*$^{-/-}$ mice were subjected to NTS for 21 days. As indicated in the following figures, these results are represented by white and red bar graphs.

In a second independent set of experiments, we used antibody-mediated CD8α-depletion to study the role of CD8 in NTS. Therefore, WT mice were treated with an isotype control antibody or an anti-CD8α depletion antibody. These data are represented by light grey and dark grey bar graphs.

To easily compare these two approaches, we opted to show these separately conducted experiments in the same figures. However, each set of experiments has its own control group. Therefore, statistical analysis was performed independently between each set of experiments. For clarification, the experimental timeline of the two sets of experiments is shown in Figure 4.

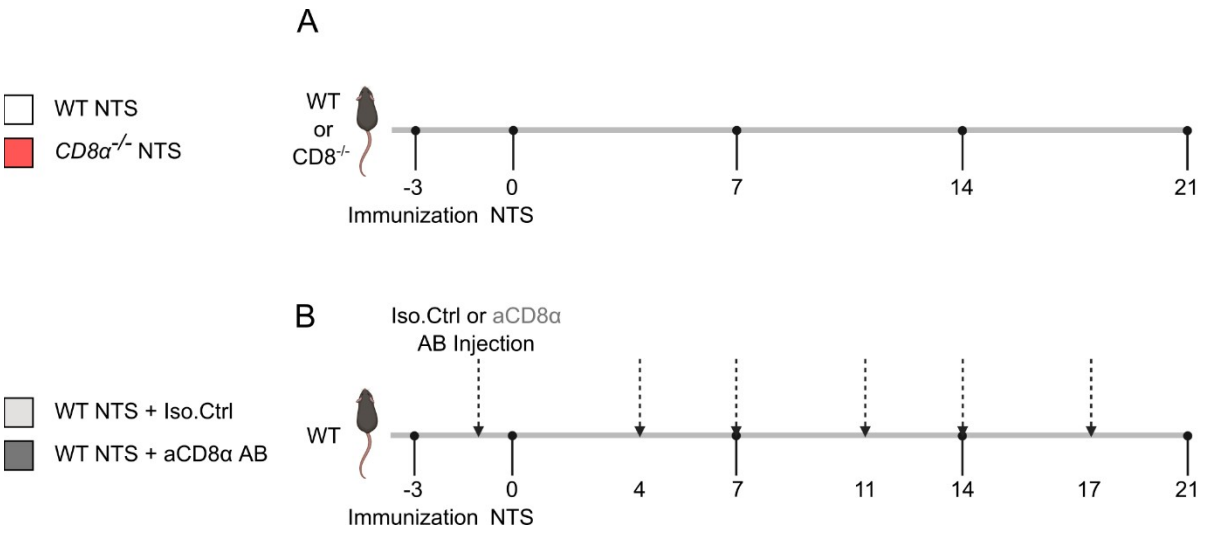

Figure 4. Experimental timeline to study the role of $CD8^+$ T cell involvement in NTS. (**A**) C57Bl/6J WT mice versus *CD8α*$^{-/-}$ mice were subjected to NTS and followed up for 21 days. (**B**) Two groups of WT mice were subjected to NTS. Mice received 6 injections with either anti-CD8α antibodies or respective isotype control antibodies.

We studied $CD8^+$ T cell involvement in NTS using homozygous *CD8α*$^{-/-}$ mice. We used C57Bl/6J WT mice as controls, as recommended by The Jackson Laboratories. After immunization on day -3, we injected rabbit anti-mouse antiserum on day 0. The experimental timeline is shown in Figure 4A.

In the second approach, we used an anti-CD8α depletion antibody. The first administration of the isotype control or depletion antibodies was performed on day -1 of NTS and repeated on days 4, 7, 11, 14, and 17 - amounting to 6 times in total. The timeline of the experimental setup is shown in Fig. 4B. Successful depletion was assessed once per mouse by flow cytometry staining and analysis for CD8α in peripheral blood in the first two days of NTS.

We periodically sampled plasma and urine in both experiments and sacrificed animals on day 21 of NTS.

On day 21, flow cytometry data showed that the kidneys of WT mice harbor more $CD45^+$ cells than knockout mice (Figure 5A). This trend was also seen in absolute $CD3^+$ cell numbers (Figure 5B). However, gating on $CD3^+$ T cells for $CD4^+$ cells revealed that both mice strains showed comparable $CD4^+$ T cell numbers (Figure 5C). Gating for $CD8^+$ T cells revealed that WT mice presented with $CD8^+$ T cells in the kidney on day 21 of NTS. As expected, these cells were absent in the kidneys of *CD8α*$^{-/-}$ mice (Figure 5D and representative flow cytometry plots Figure 5E).

Mice treated with anti-CD8α depletion AB showed a trend for lower numbers of $CD45^+$ cells (Figure 5A) and $CD3^+$ T cells (Figure 5B) in the kidney compared to controls. However, absolute $CD4^+$ cell numbers were comparable in control mice and CD8α-depleted WT mice on day 21 of NTS (Figure 5C). In addition, representative flow cytometry plots in Figure 5E and the graph in Figure 5D show that depletion of CD8α led to a lack of $CD8^+$ T cells in the kidney of treated mice. In contrast, WT mice treated with a control AB revealed the presence of $CD8^+$ T cells in kidney tissue on day 21 of NTS.

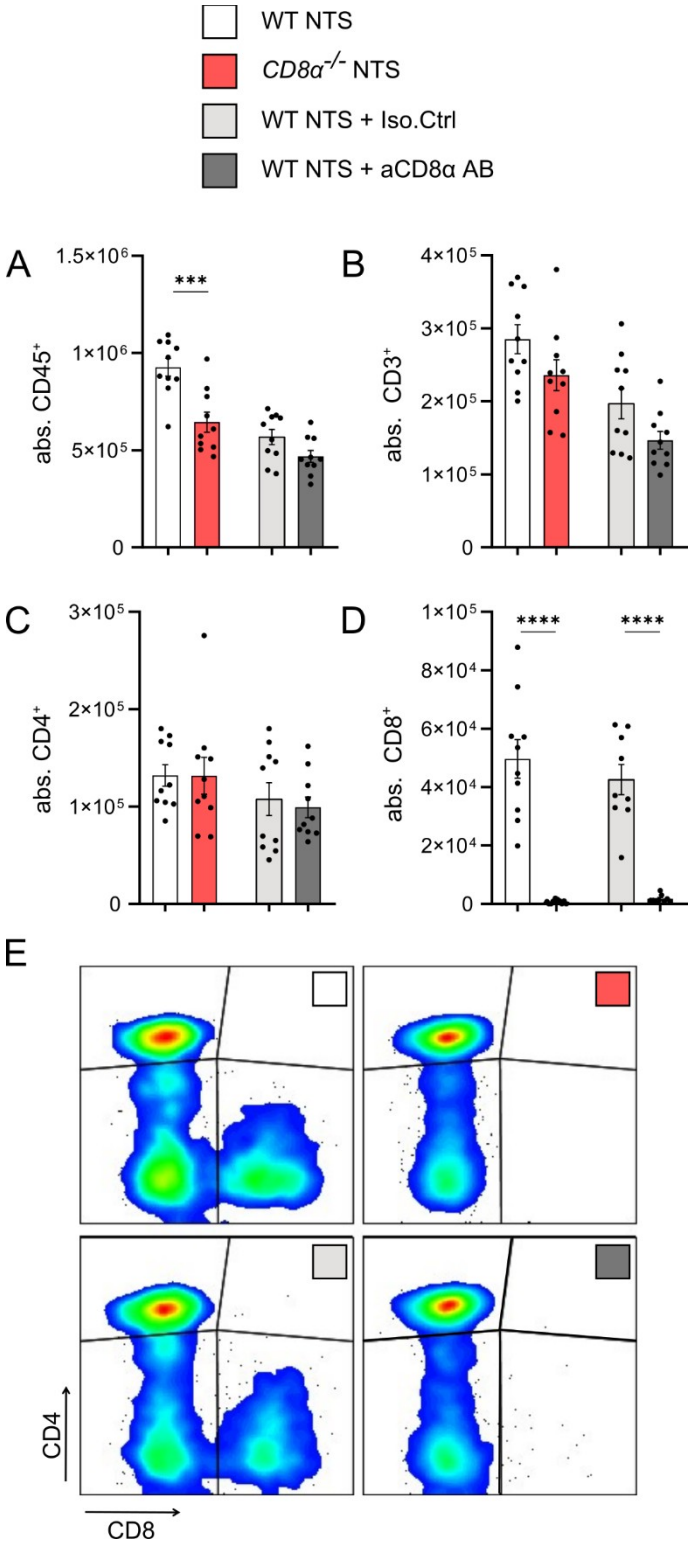
WT NTS
CD8α-/- NTS
WT NTS + Iso.Ctrl
WT NTS + aCD8α AB
A
abs. CD45+
1.5×10^6
1×10^6
5×10^5
0
***
B
abs. CD3+
4×10^5
3×10^5
2×10^5
1×10^5
0
C
abs. CD4+
3×10^5
2×10^5
1×10^5
0
D
abs. CD8+
1×10^5
8×10^4
6×10^4
4×10^4
2×10^4
0
****
****
E
CD4
CD8

Figure 5. Flow cytometry analysis of the T cell subsets in the kidneys of WT mice, *CD8α*$^{-/-}$ mice, WT mice treated with isotype control antibody, and WT mice treated with anti-CD8α depletion antibody. Data represent day 21 of disease. (**A**) Absolute numbers of CD45^{+} cells gated on viability dye negative cells, (**B**) absolute numbers of CD3^{+} T cells gated on CD45^{+} cells, and (**C**) absolute numbers of CD4^{+} T cells gated on CD3^{+}CD8^{-} cells per kidney are shown. (**D**) Absolute CD8^{+} T cell numbers of CD3^{+}CD4^{-} cells per mouse kidney on day 21 of NTS. (**E**) Representative flow cytometry plots of CD4^{+} and CD8^{+} cells gated on CD3^{+}CD45^{+} cells of all four groups. ***p≤0.001, ****p≤0.0001. Data were tested for normal distribution, and Student's *t*-test or Mann-Whitney test was used for statistical analysis. All data are represented as mean ± SEM.

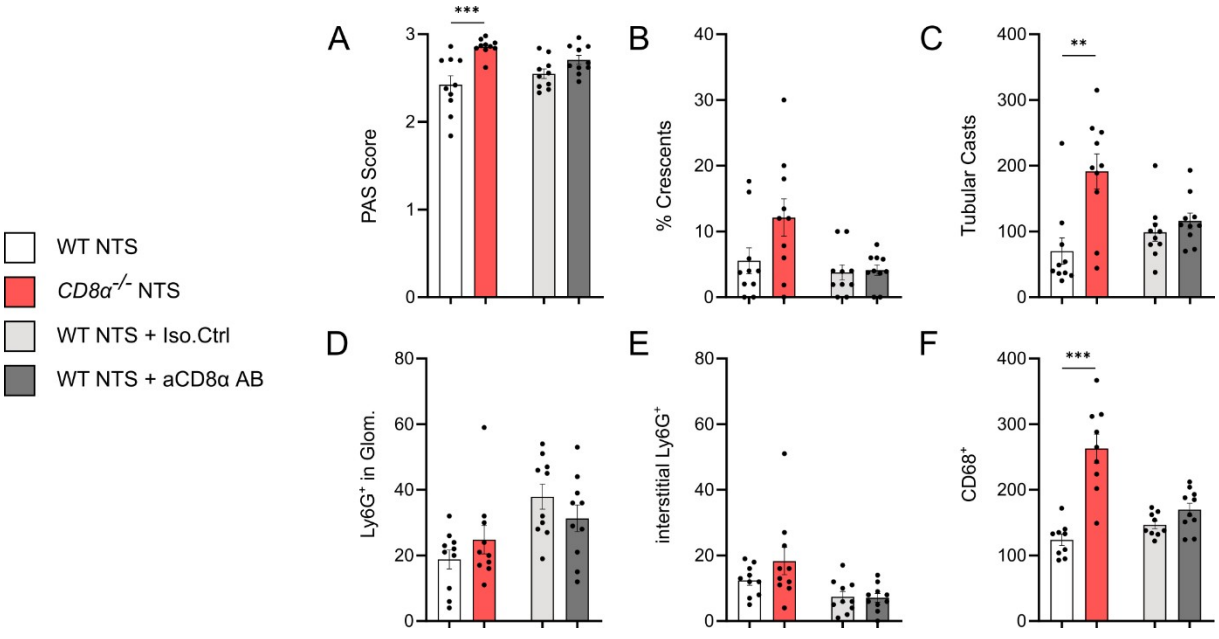

Figure 6. Histological analysis of kidney tissue of WT mice, *CD8α*$^{-/-}$ mice, WT mice treated with isotype control antibody, and WT mice treated with anti-CD8α depletion antibody. Data represent day 21 of disease. (**A**) PAS Score and (**B**) percent of crescents counted per 50 glomeruli per sample. (**C**) Tubular casts were counted in 12 hpf. (**D**) Absolute numbers of Ly6G^{+} cells per 50 glomeruli and (**E**) in interstitial tissue counted in 6 hpf. (**F**) Absolute numbers of CD68^{+} cells counted in 6 hpf. **p≤0.01, ***p≤0.001. Data were tested for normal distribution, and Student's *t*-test or Mann-Whitney test was used for statistical analysis. All data are represented as mean ± SEM.

Histological analysis of kidney tissue revealed a higher PAS score in *CD8α*$^{-/-}$ mice compared to WT mice (Figure 6A). Along with this finding, *CD8α*$^{-/-}$ mice showed a trend to more glomerular crescents (Figure 6B) and, at the same time, presented with an increase in tubular injury (Figure 6C), indicated by tubular cast formation, compared to controls. In addition, while no increase in absolute Ly6G^{+} cell numbers was detected in glomeruli (Figure 6D) and interstitial regions (Figure 6E), CD8α$^{-/-}$ mice showed a 2-fold increase of overall CD68^{+} cell infiltration in the kidney tissue (Figure 6F) compared to WT mice.

PAS staining of the kidneys from mice treated with anti-CD8α antibody revealed no differences in glomerulosclerosis as assessed by scoring PAS-positive material in 50 glomeruli (Figure 6A). Percentages of glomerular crescents (Figure 6B) and tubular cast formation (Figure 6C) were comparable to control mice. Also, absolute myeloid cell infiltration of kidney tissue was similar in both groups on day 21, as seen in glomerular Ly6G^{+} cell numbers (Figure 6D), interstitial Ly6G^{+} cell numbers (Figure 6E), and CD68^{+} cell numbers counted in 6 hpf (Figure 6F).

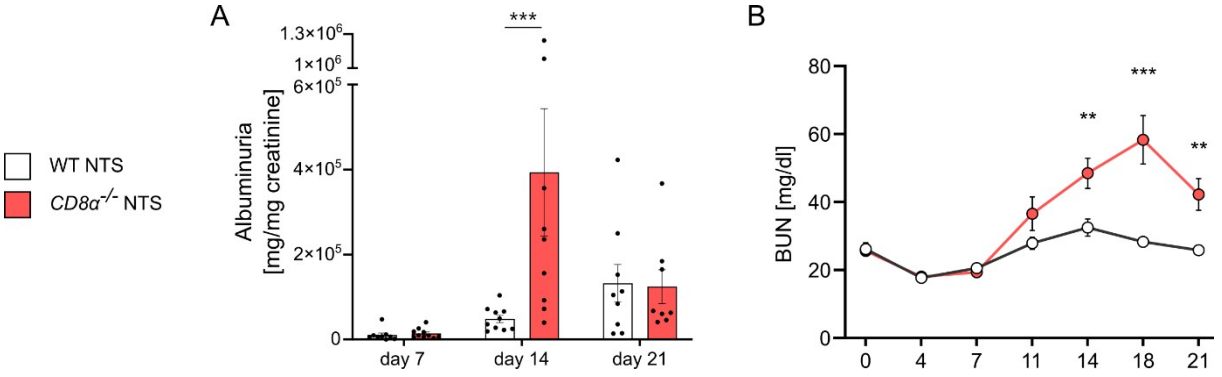

Figure 7. Analysis of albuminuria and kidney function in WT versus *CD8α*$^{-/-}$ mice after 21 days of NTS. Pooled data from two independent experiments are shown (n=9 and 10 per group). (**A**) Urinary albumin to creatinine ratio on day 7, day 14, and day 21. (**B**) Time course of blood urea nitrogen levels from day 0 to day 21 of NTS. **p≤0.01, ***p≤0.001. Data were tested for normal distribution, and Student's *t*-test or Mann-Whitney test was used for statistical analysis. All data are represented as mean ± SEM.

As an indicator of disease severity, the urinary albumin to creatinine ratio was assessed on day 7, day 14, and day 21 of NTS (Figure 7A). On day 7 and day 21, no difference in ACR

was shown in WT vs. *CD8α*$^{-/-}$ mice. However, on day 14 of NTS, *CD8α*$^{-/-}$ mice showed a significantly higher ratio than WT mice. Also, while the ACR ratio of WT mice increased from day 7 through day 14 to day 21, *CD8α*$^{-/-}$ mice showed a more than 2-fold higher ratio on day 14 than on day 21.

The kidney function of WT vs. *CD8α*$^{-/-}$ mice was assessed by a time course of BUN levels (Figure 7B). While WT mice with NTS did not show a high fluctuation in BUN levels through the progression of the disease, *CD8α*$^{-/-}$ mice showed an increase from day 7 on, reaching a peak on day 18. On day 21 of NTS, *CD8α*$^{-/-}$ mice still showed significantly higher BUN levels than controls.

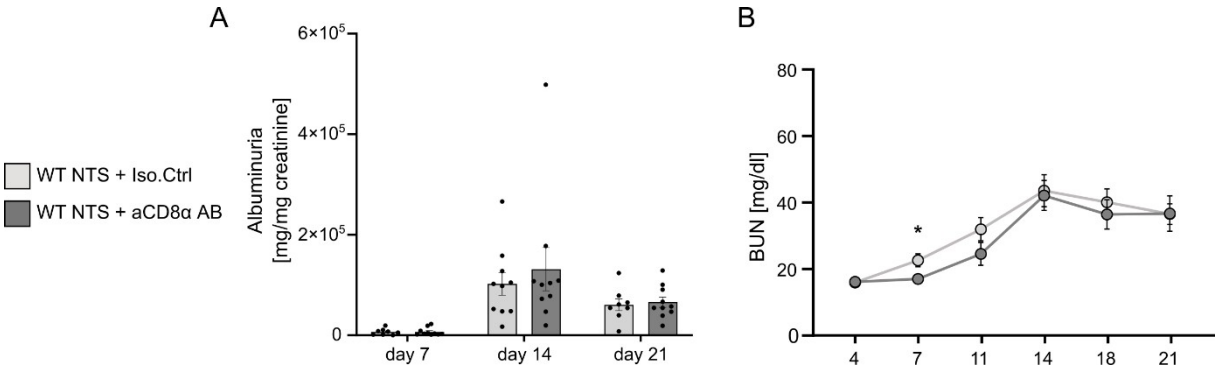

Figure 8. Analysis of albuminuria and kidney function in WT mice treated with anti-CD8α depletion antibody and controls after 21 days of NTS. Pooled data from two independent experiments are shown (n=10 per group). (**A**) Urinary albumin to creatinine ratio on day 7, day 14, and day 21. (**B**) Time course of blood urea nitrogen levels from day 4 to day 21 of NTS. *p≤0.05. Data were tested for normal distribution, and Student's *t*-test or Mann-Whitney test was used for statistical analysis. All data are represented as mean ± SEM.

No marked difference in ACR could be seen in WT controls versus WT mice depleted of CD8α on days 7, 14, and 21 of NTS (Figure 8A).

Blood urea nitrogen levels from day 4 through day 21 were also measured. Depletion of CD8α led to an attenuated increase of BUN levels, with significantly lower levels on day 7. However, in the later days of the disease, the benefit of CD8α depletion on BUN levels was not significant (Figure 8B).

3.2 Low-dose rIL-15 as a therapeutic intervention in NTS

3.2.1 Administration of low-dose rIL-15 ameliorates NTS disease outcomes, protects TECs from cell death, and promotes a Ly49^{+}CD8^{+} memory T cell phenotype

The role of overall CD8^{+} T cells in NTS seems rather complex. IL-15 is, on the one hand, known to be essential for CD8^{+} and NK cell proliferation and maintenance, while on the other hand has been shown to benefit TEC survival. In this study, we further focused on the potential of low-dose rIL-15 to treat GN and its effects on the CD8^{+} T cell population. Therefore, we treated mice on day 1 of NTS with a sub-proliferation dose of rIL-15, previously established by other groups[125,140,141], and investigated its effects on disease outcomes.

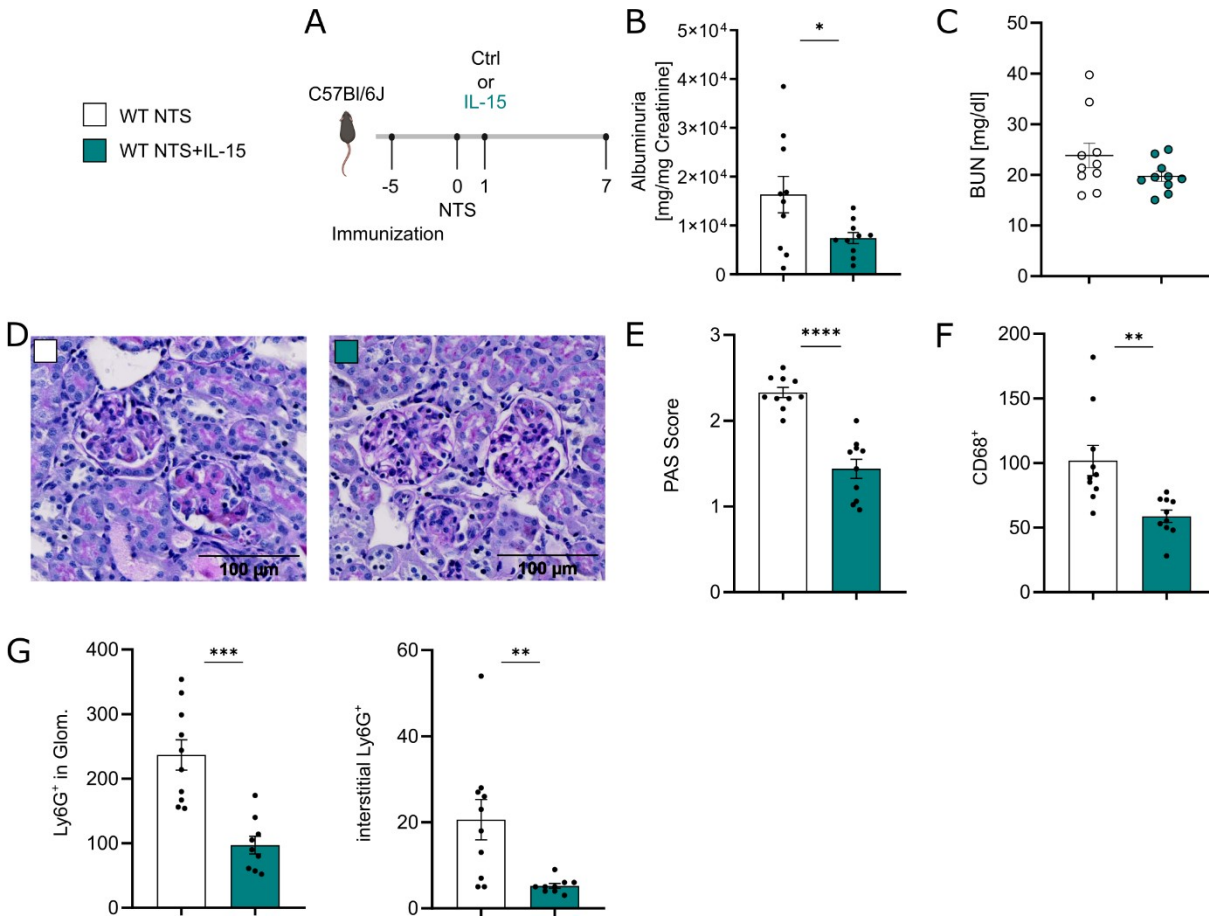

Figure 9. Low-dose rIL-15 intervention in NTS ameliorates disease outcomes and reduces myeloid cell infiltration. Data represent day 7 of disease. Pooled data from two independent experiments are shown (n=10 per group). (**A**) Experimental timeline of 7 days with intervention on day 1 of NTS. (**B**) Urinary albumin to creatinine ratio and (**C**) BUN levels. (**D**) Representative histological stainings and (**E**) scoring of PAS-positive material in kidney sections. Quantification of immunohistochemical stainings of (**G**) $Ly6G^+$ cells in glomeruli and interstitial tissue and (**H**) $CD68^+$ cells counted in 6 hpf. *p≤0.05, **p≤0.01, ***p≤0.001, ****p≤0.0001. Data were tested for normal distribution, and Student's *t*-test or Mann-Whitney test was used for statistical analysis. All data are represented as mean ± SEM. Reproduced with modifications from Mooslechner et al. [1] with permission through the MDPI Open Access Policy.

We chose a 7-day NTS protocol with low-dose rIL-15 administration on day 1 of the disease. Control mice were treated with PBS. A schematic experimental timeline is provided (Figure 9A). The low-dose rIL-15 intervention showed a 50% reduction of urinary albumin to creatinine ratio (Figure 9B), but no effect was seen in BUN levels on day 7 (Figure 9C).

Histological analysis of PAS stainings (representative photos Figure 9D) revealed a marked reduction of PAS-positive material in glomeruli, represented by a lower PAS score (Figure 9E).

Immunohistochemistry with antibodies against Ly6G and CD68 revealed a reduction of $CD68^+$ cells in the kidney interstitium (Figure 9F) and lower $Ly6G^+$ cell numbers in glomeruli and interstitial tissue (Figure 9G).

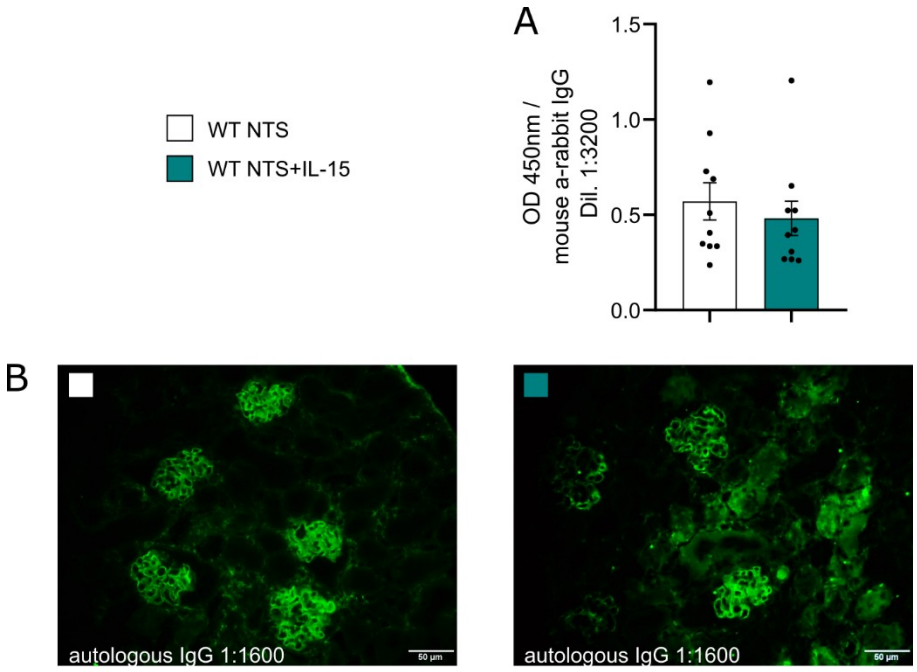

Figure 10. Low-dose rIL-15 administration does not influence circulating IgG levels and autologous IgG deposition on the GBM. Data represent day 7 of disease. Pooled data from two independent experiments are shown (n=10 per group). (**A**) Optical density of circulating mouse anti-rabbit IgG and (**B**) representative immunofluorescent stainings of deposited autologous IgG on the GBM. Data were tested for normal distribution, and Student's *t*-test or Mann-Whitney test was used for statistical analysis. All data are represented as mean ± SEM. Reproduced with modifications from Mooslechner et al. [1] with permission through the MDPI Open Access Policy.

IL-15 has been shown to influence B cells[143,144]. Therefore, to exclude a potential change in the humoral immune response, which would explain a better disease outcome, we analyzed circulating mouse anti-rabbit IgG levels but found no difference between groups (Figure 10A). Additionally, we found a comparable amount of autologous and heterologous IgG deposits on the GBM in both groups (Figure 10B).

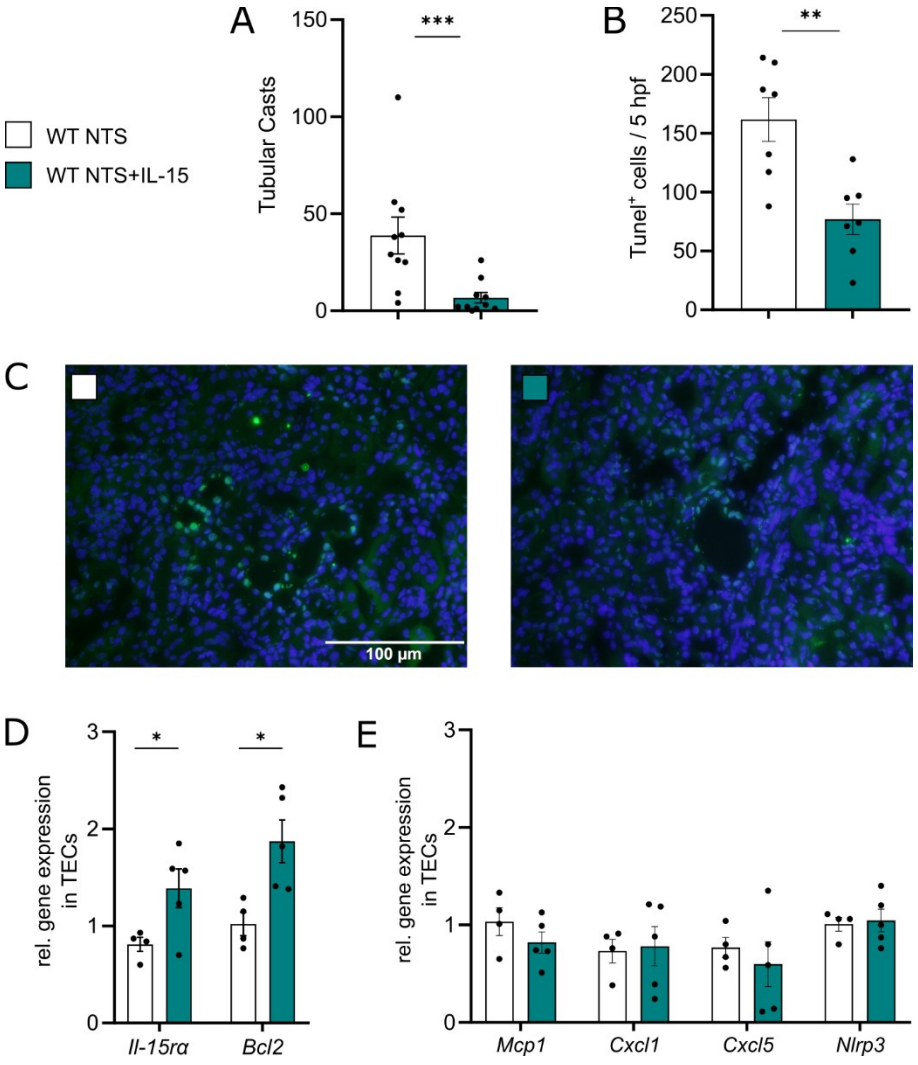

Figure 11. Low-dose rIL-15 treatment in NTS mediates TEC survival. Data represent day 7 of disease. (**A**) Numbers of tubular casts in 12 hpf as seen on PAS-stained kidney sections. (**B**) Numbers of Tunel^{+} cells in 5 hpf and (**C**) representative micrographs of fluorescent Tunel-staining. (**D**) Relative *Il-15ra* and *Bcl2* and (**E**) *Mcp1*, *Cxcl1*, *Cxcl5*, and *Nlrp3* gene expression in renal TECs. *p≤0.05, **p≤0.01, ***p≤0.001. Data were tested for normal distribution, and Student's *t*-test or Mann-Whitney test was used for statistical analysis. All data are represented as mean ± SEM. Reproduced from Mooslechner et al. [1] with permission through the MDPI Open Access Policy.

It is already known that IL-15 has beneficial effects on TEC survival[138]. We found less tubular cast formation in PAS-stained kidney sections (Figure 11A), which indicates less tubular injury. In line with these findings, we also saw a reduction of Tunel^{+} cells, mainly found in the tubuli (Figure 11B and Figure 11C) in the rIL-15 treated group.

To investigate the engagement of TECs with rIL-15, we isolated TECs on day 7 of NTS. Gene expression analysis revealed that in the presence of rIL-15, TECs upregulate the IL-15Rα-chain and simultaneously show a higher relative gene expression of *Bcl2*, indicating better survival of the cells (Figure 11D). However, we found no difference in the expression pattern of *Mcp1*, *Cxcl1*, *Cxcl5*, and *Nlrp3* with rIL-15 intervention (Figure 11E).

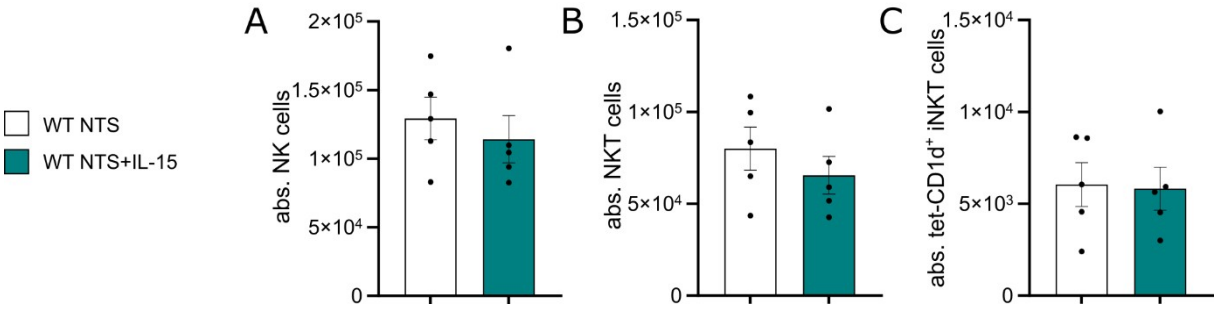

Figure 12. Low-dose rIL-15 intervention does not alter NK, NKT, and iNKT cell numbers in the NTS kidney. Data represent day 7 of disease. Absolute numbers of (**A**) $CD3^-NK1.1^+$ NK cells, (**B**) $CD3^+NK1.1^+$ NKT cells, and (**C**) $CD3^-$tet-$CD1d^+$ iNKT cells per kidney. Data were tested for normal distribution, and Student's *t*-test or Mann-Whitney test was used for statistical analysis. All data are represented as mean ± SEM. Reproduced with modifications from Mooslechner et al. [1] with permission through the MDPI Open Access Policy.

IL-15 is a pleiotropic cytokine previously shown to affect TECs directly[138], but it also has several targets among immune cell populations. Therefore, we analyzed the most known target cell types. NK cells are highly responsive to IL-15, which mainly stimulates their proliferation. Consequently, we analyzed NK cell subsets in the NTS kidney on day 7 of the disease. We found no difference in absolute numbers of NK (Figure 12A), NKT (Figure 12B), and the regulatory iNKT subset (Figure 12C) due to rIL-15 treatment.

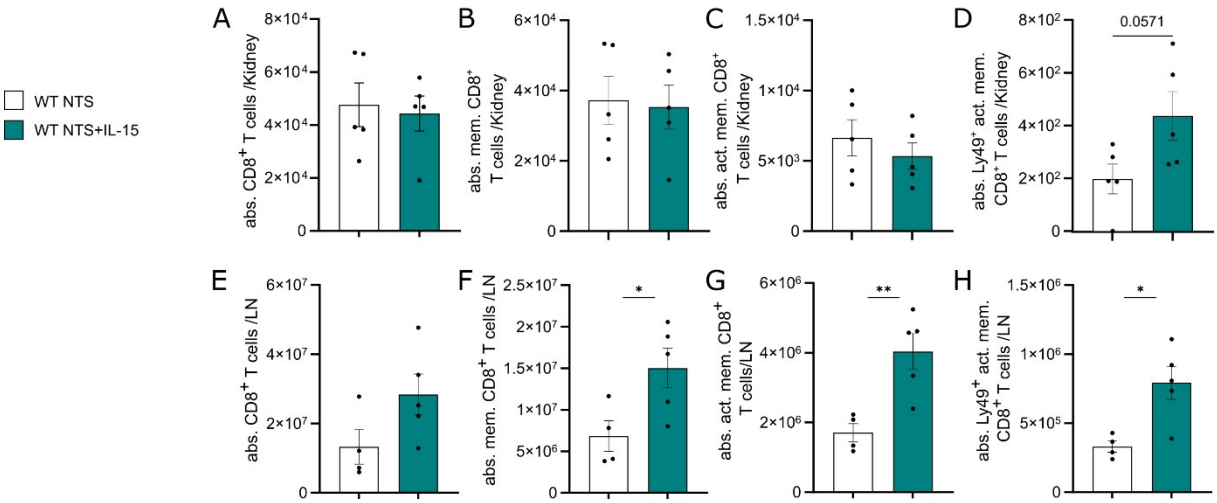

Figure 13. Low-dose rIL-15 intervention in NTS mediates a memory shift in CD8$^+$ T cells. Data represent day 7 of disease. Quantification of (**A**) CD8$^+$ T cells, (**B**) CD8$^+$CD44$^+$ memory T cells, (**C**) CD8$^+$CD44$^+$CD122$^+$ activated memory T cells, and (**D**) Ly49$^+$ activated memory T cells per kidney. Quantification of respective subsets per lymph node (**E-H**). *p≤0.05, **p≤0.01. Data were tested for normal distribution, and Student's *t*-test or Mann-Whitney test was used for statistical analysis. All data are represented as mean ± SEM. Reproduced with modifications from Mooslechner et al. [1] with permission through the MDPI Open Access Policy.

Next to NK cells, CD8$^+$ T cells are the most responsive to IL-15. We analyzed overall CD8$^+$ T cells and three memory subsets in the NTS kidney and lymph node and compared absolute cell numbers to NTS mice treated with rIL-15. On day 7 of NTS, we found no difference in the numbers of CD8$^+$ T cells (Figure 13A), CD8$^+$CD44$^+$ memory T cells (Figure 13B), and CD8$^+$CD44$^+$CD122$^+$ activated memory T cells (Figure 13C) in the kidney between groups. However, Ly49$^+$ activated memory CD8$^+$ T cells were increased without reaching significance (Figure 13D). In the periphery, absolute CD8$^+$ T cells showed a trend of increased numbers (Figure 13E). Significantly more memory CD8$^+$ T cells (Figure 13F), activated memory CD8$^+$ T cells (Figure 13G), and Ly49$^+$ activated memory CD8$^+$ T cells (Figure 13H) were found in the lymph nodes of the treatment group compared to the control group.

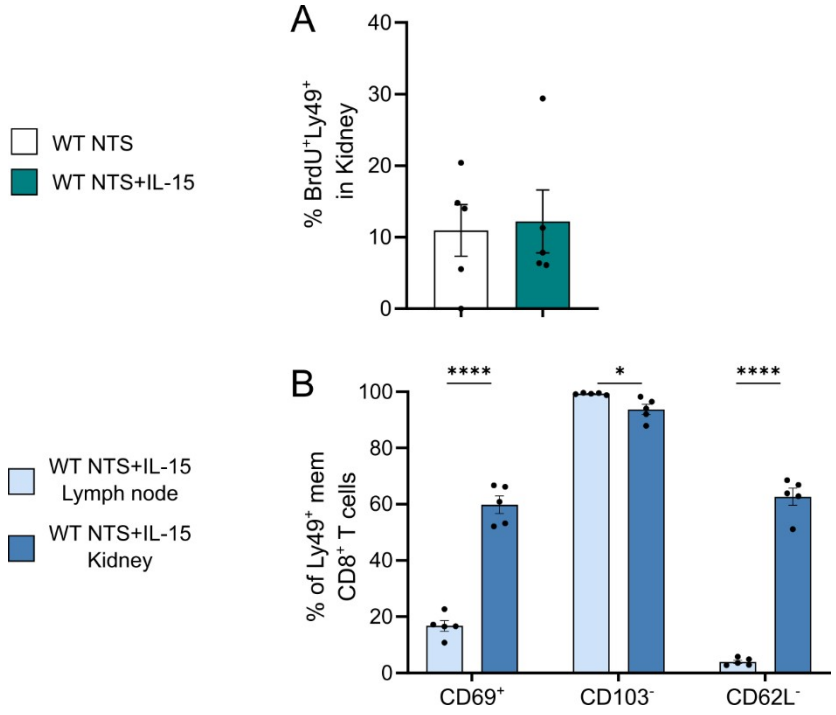

Figure 14. Kidney Ly49$^+$CD8$^+$ T cells show no difference in BrdU incorporation but have a distinct phenotype. Data represent day 7 of disease. (**A**) Frequencies of BrdU$^+$Ly49$^+$CD8$^+$ T cells in the kidney. (**B**) Frequencies of CD69$^+$, CD103$^-$, and CD62L$^-$ Ly49$^+$CD8$^+$ T cells in lymph nodes and kidney. ****p≤0.0001. Data were tested for normal distribution, and Student's *t*-test or Mann-Whitney test was used for statistical analysis. All data are represented as mean ± SEM. Reproduced with modifications from Mooslechner et al. [1] with permission through the MDPI Open Access Policy.

Next, we were interested if the increase of Ly49$^+$CD8$^+$ memory T cells in the kidney is explained by local proliferation. We administered BrdU to mice on day 5 of NTS and sacrificed them on day 7. Flow cytometry analysis revealed comparable frequencies of BrdU incorporation in kidney Ly49$^+$CD8$^+$ memory T cells (Figure 14A) in control NTS mice and NTS mice treated with rIL-15.

To further characterize Ly49$^+$CD8$^+$ memory T cells, we stained lymph node- and kidney-derived cells for CD69, CD103, and CD62L of NTS mice treated with rIL-15. On day 7 of NTS, flow cytometry analysis revealed that most Ly49$^+$CD8$^+$ memory T cells in kidney tissue have a CD69$^+$CD103$^-$CD62L$^-$ phenotype, while the same cells found in lymph nodes show a CD69$^+$CD103$^-$CD62L$^+$ phenotype (Figure 14B).

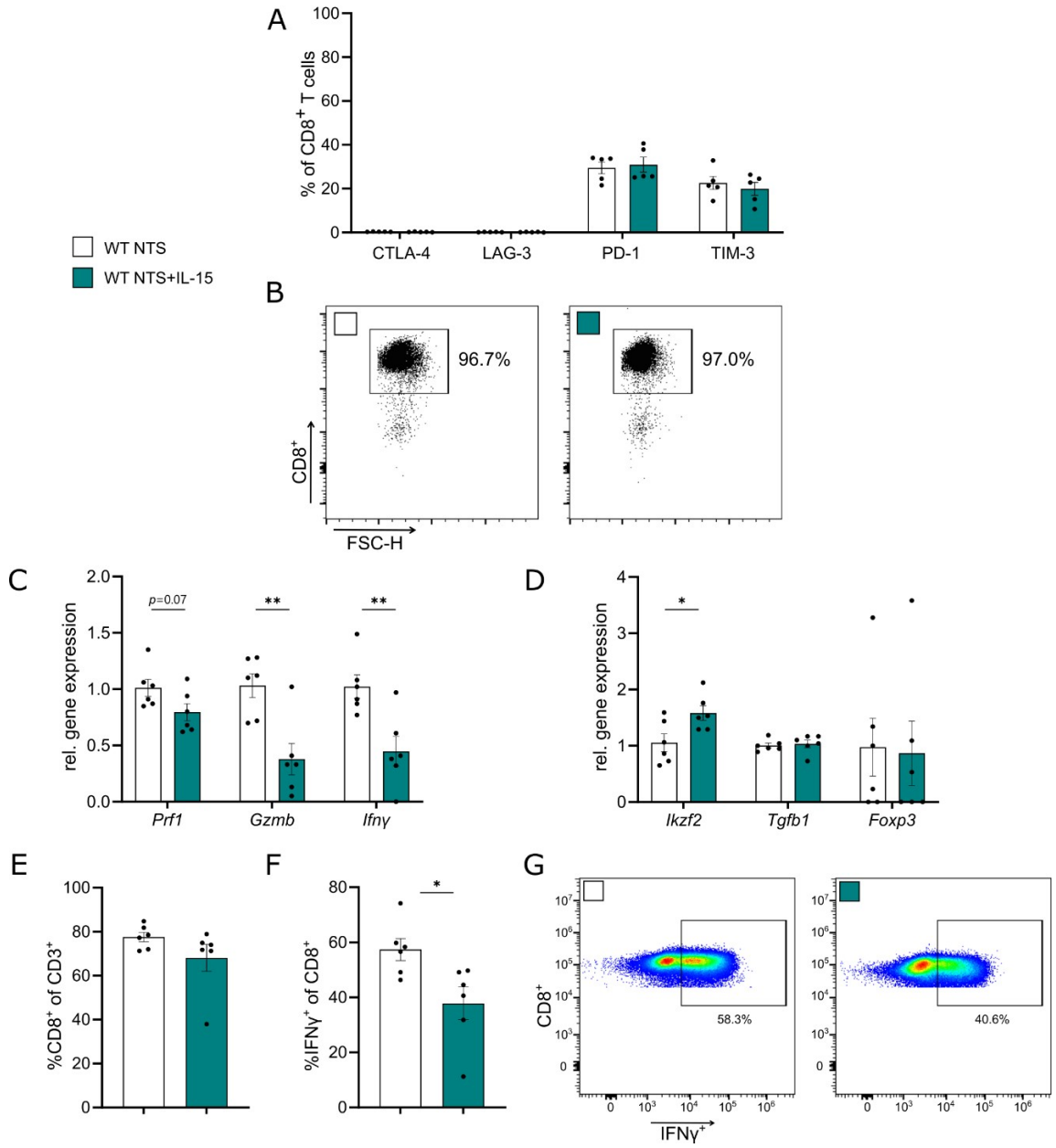

Figure 15. rIL-15 treatment does not alter the exhaustion phenotype but mediates a less cytotoxic phenotype of CD8$^+$ T cells. Data represent day 7 of disease. (**A**) Frequencies of exhaustion markers CTLA-4, LAG-3, PD-1, and TIM-3 of CD8$^+$ T cells in the kidney. (**B**) Flow plots of negatively magnetic bead sorted CD8$^+$ lymphocytes. Groups represent concatenated data of all samples used. Relative gene expression of (**C**) *Prf1*, *Gzmb*, *Ifnγ* and (**D**) *Ikzf2*, *Tgfb1*, and *Foxp3* in CD8$^+$ lymphocytes. Frequencies of (**E**) CD8$^+$ T cells and (**F**) IFNγ$^+$ CD8$^+$ T cells from spleen after culture. (**G**) Representative flow plots of IFNγ production in CD8$^+$ splenocytes. *p≤0.05, **p≤0.01. Data were tested for normal distribution, and Student's *t*-test or Mann-Whitney test was used for statistical analysis. All data are represented as mean ± SEM. Reproduced with modifications from Mooslechner et al. [1] with permission through the MDPI Open Access Policy.

Ly49 has been associated with T cell inhibition and exhaustion. To rule out general T cell exhaustion in our group of NTS mice treated with rIL-15, we stained kidney $CD8^+$ T cells for the exhaustion markers CTLA-4, LAG-3, PD-1, and TIM-3. Flow cytometry analysis revealed no difference in the expression of either of these exhaustion markers on $CD8^+$ T cells (Figure 15A) found in the kidney.

To investigate the gene expression profile of $CD8^+$ T cells in NTS with rIL-15 treatment, we negatively isolated $CD8\alpha^+$ cells with magnetic beads from the lymph nodes of NTS control mice and NTS mice treated with rIL-15. We measured the relative gene expression of genes associated with cytotoxicity and regulatory functions. Figure 15B shows flow cytometry plots of concatenated data from samples after magnetic bead isolation. Both groups show a purity of over 96.5% of $CD8\alpha^+$ cells. After 4 days of culture with anti-CD3/anti-CD28 stimulation beads, relative gene expression analysis revealed that rIL-15 treatment reduced the expression of *Prf1* (not significant), *Gzmb*, and *IFNγ* (Figure 15C). On the other hand, the relative expression of *Ikzf2* was significantly increased (Figure 15D). The relative expression of *Tgfb1* and *Foxp3* was not changed (Figure 15D).

To confirm part of these results on protein level, we cultured splenocytes from mice subjected to NTS and treated with vehicle or rIL-15 under the previously described conditions. Flow cytometric analysis revealed comparable frequencies of $CD8^+$ T cells gated on $CD3^+$ T cells (Figure 15E). However, $IFN\gamma^+CD8^+$ T cells were significantly reduced in cells derived from NTS mice with rIL-15 intervention (Figure 15F and representative flow plots Figure 15G).

$CD4^+$ T cells do not express the IL-15Rα, but the β- and γ-chain of the receptor, which are shared with the IL-2R. Since $CD4^+$ T cells have a major role in the pathomechanism of NTS, we analyzed their numbers in the kidney and the periphery and indicators of subsets and function in NTS with rIL-15 treatment.

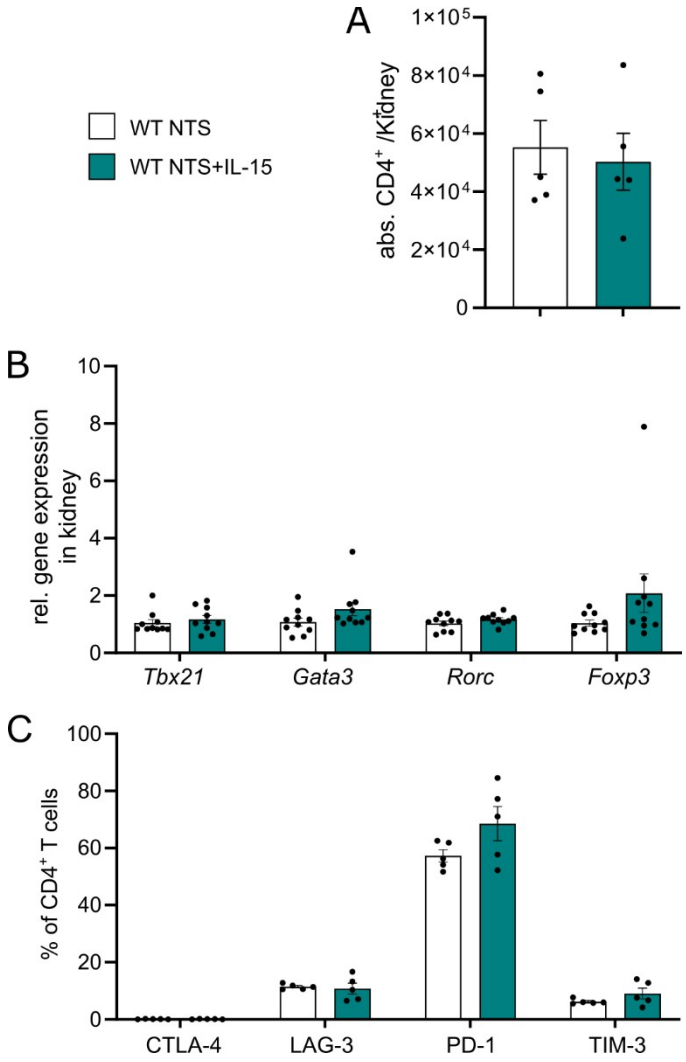

Figure 16. Absolute numbers, expression of major transcription factors of subpopulations, and exhaustion phenotype were not altered in kidney CD4$^+$ T cells after rIL-15 administration. Data represent day 7 of disease. Absolute numbers of (**A**) Quantification of CD4$^+$ T cells per kidney. (**B**) Relative gene expression of master transcription factors *Tbx21*, *Gata3*, *Rorc*, and *Foxp3* in whole kidney tissue. (**C**) Frequencies of exhaustion markers CTLA-4, LAG-3, PD-1, and TIM-3 on kidney CD4$^+$ T cells. Data were tested for normal distribution, and Student's *t*-test or Mann-Whitney test was used for statistical analysis. All data are represented as mean ± SEM. Reproduced with modifications from Mooslechner et al. [1] with permission through the MDPI Open Access Policy.

Absolute numbers of CD4$^+$ T cells in the kidney were comparable in both groups (Figure 16A). To exclude a shift in CD4$^+$ T cell populations as a cause for the amelioration of NTS, we analyzed the expression of master transcription factors associated with Th1, Th2, Th17,

and Treg subsets in the kidney cortex. Gene expression data showed no difference in the relative expression of *Tbx21*, *Gata3*, *Rorc,* and *Foxp3* in control WT NTS mice and NTS mice treated with rIL-15 (Figure 16B).

Since IL-15 utilizes the same β- and γ-chains as IL-2 and could potentially harm T cells' activation status, we analyzed frequencies of markers associated with exhaustion. On day 7 of NTS, mice treated with rIL-15 showed a trend towards higher PD-1 frequencies on $CD4^+$ T cells but no differences in CTLA-4, LAG-3, and TIM-3 frequencies (Figure 16C).

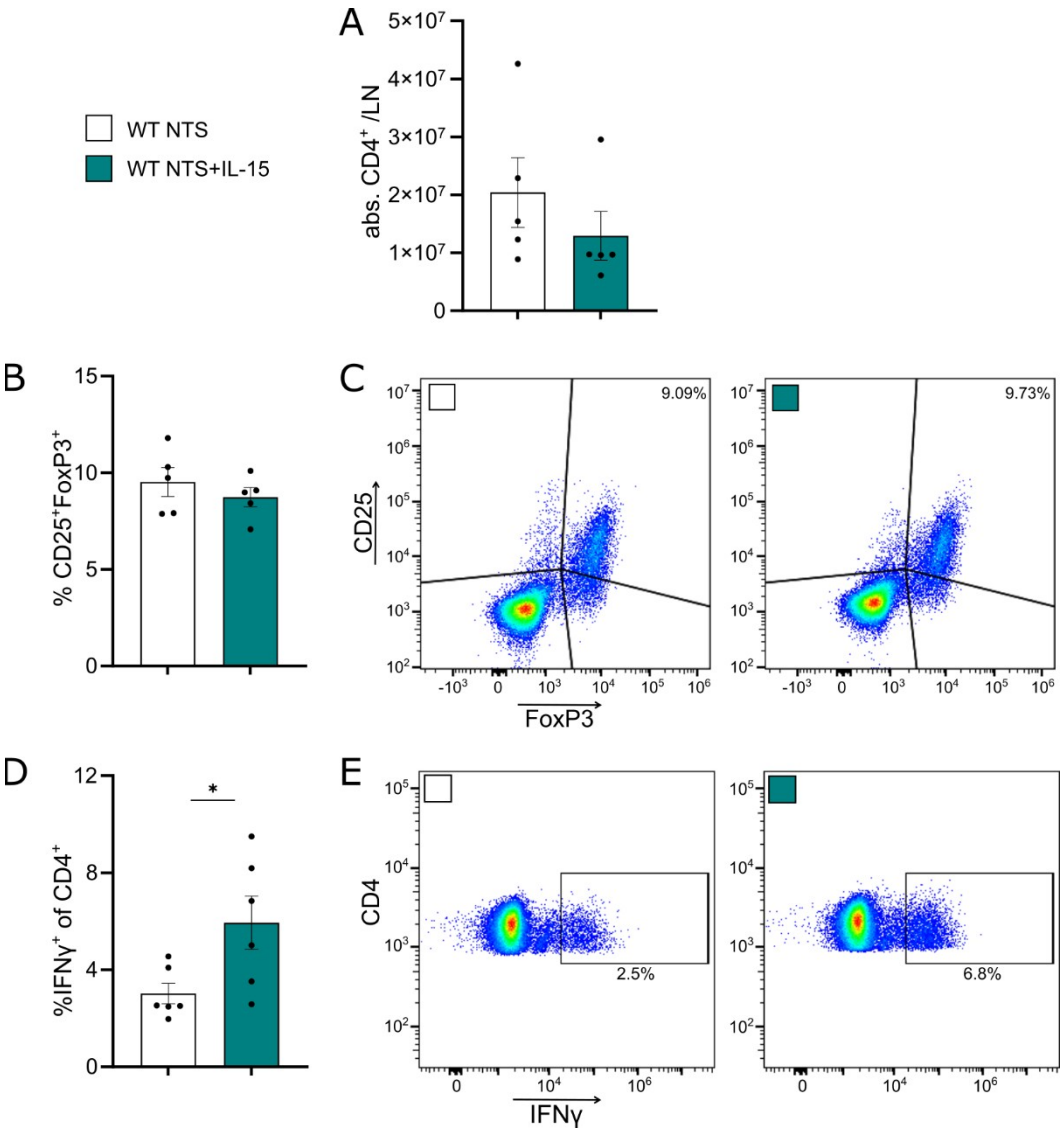

Figure 17. Low-dose rIL-15 increases IFNγ-production of peripheral CD4$^+$ T cells in NTS. Data represent day 7 of disease. Absolute numbers of (**A**) Quantification of CD4$^+$ T cells per lymph node. (**B**) Frequencies and (**C**) representative flow plots of CD25$^+$FoxP3$^+$ CD4$^+$ T cells. (**D**) Frequencies and (**E**) representative flow plots of IFNγ$^+$CD4$^+$ splenocytes. *p≤0.05. Data were tested for normal distribution, and Student's *t*-test or Mann-Whitney test was used for statistical analysis. All data are represented as mean ± SEM. Reproduced with modifications from Mooslechner et al. [1] with permission through the MDPI Open Access Policy.

Also, absolute numbers of CD4$^+$ T cells in the periphery (lymph node) were comparable in both groups (Figure 17A). Ex vivo stained lymphocytes also revealed the same frequencies of CD25$^+$FoxP3$^+$ regulatory CD4$^+$ T cells in both groups independent of rIL-15 treatment (Figure 17B and representative flow cytometry plots Figure 17C). However, splenocytes revealed that CD4$^+$ T cells from NTS mice injected with rIL-15 have a more pronounced Th1-phenotype, measured by IFNγ production (Figure 17D and representative flow cytometry plots Figure 17E).

3.2.2 rIL-15-mediated protection from NTS and improved TEC survival is dependent on $CD8^+$ T cells

The IL-15 receptor consists of three chains. IL-15 can be presented in *trans* to $CD8^+$ T cells expressing the β- and γ- chains, which are also part of the IL-2 receptor. We already showed that upon administration of rIL-15, TECs of WT mice upregulate *Il-15rα* in NTS. To investigate the importance of this upregulation and the engagement with TECs, we repeated the rIL-15 administration experiments in *IL-15Rα*$^{-/-}$ and *CD8α*$^{-/-}$ mice with NTS.

Administration of low-dose rIL-15 in *IL-15Rα*$^{-/-}$ mice revealed no difference in frequencies of $Ly49^+CD8^+$ memory T cells (Figure 18A), urinary albumin to creatinine ratio (Figure 18B), BUN levels (Figure 18C), PAS Score (Figure 18E), tubular cast formation (Figure 18F), and myeloid cell infiltration (Figure 18G-I) compared to control *IL-15Rα*$^{-/-}$ mice on day 7 of NTS.

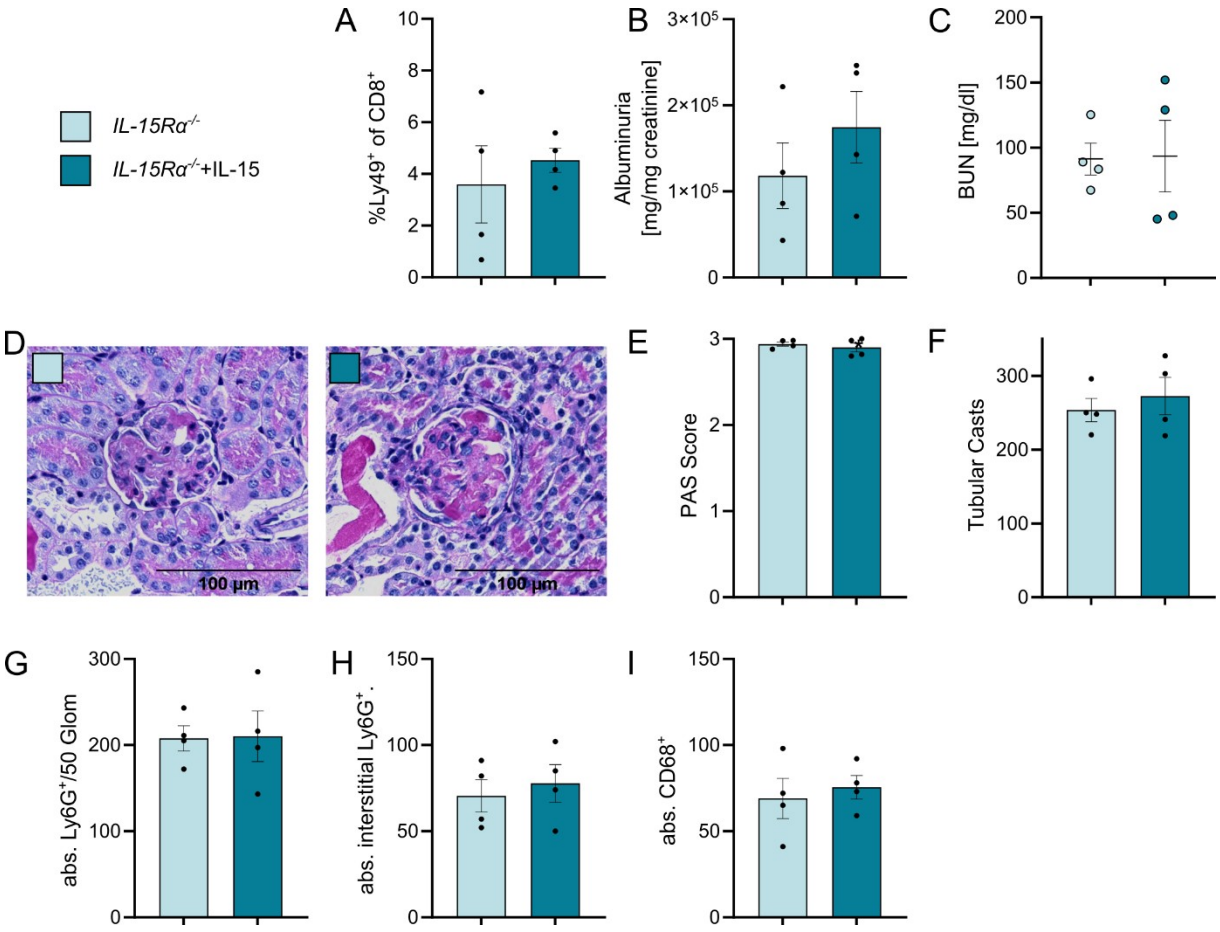

Figure 18. rIL-15 treatment does not alter disease outcomes in *IL-15Rα*$^{-/-}$ mice in NTS. Data represent day 7 of disease. (**A**) Frequencies of kidney Ly49^{+}CD8^{+} memory T cells, (**B**) urinary albumin to creatinine ratio, and (**C**) BUN levels. (**D**) Representative PAS stainings of kidney tissue used to analyze (**E**) PAS Score and (**F**) tubular cast formation counted in 12 hpf. Quantification of immunohistochemistry stainings of (**G**) absolute glomerular and (**H**) interstitial Ly6G^{+} cells and (**I**) absolute CD68^{+} cell numbers in 6 hpf. Data were tested for normal distribution, and Student's *t*-test or Mann-Whitney test was used for statistical analysis. All data are represented as mean ± SEM.

However, administration of low-dose rIL-15 in *CD8α*$^{-/-}$ mice revealed several differences compared to control *CD8α*$^{-/-}$ mice on day 7 of NTS. The urinary albumin to creatinine ratio was increased in the group treated with rIL-15 (Figure 19B). Histology revealed a higher PAS Score (Figure 19C and representative micrographs of staining Figure 19D) in the group treated with rIL-15. Circulating mouse anti-rabbit IgG levels were comparable in both groups (Figure 19E). As expected, we could not detect Ly49^{+}CD8^{+} memory T cells in the kidney of *CD8α*$^{-/-}$ mice NTS mice (Figure 19F). Interestingly, there was a slight trend for an increase in absolute numbers of kidney iNKT cells (Figure 19G).

Additionally, cryosections of kidney tissue were stained immunohistochemically for myeloid cell infiltration. There was a trend for more glomerular Ly6G^{+} cells (Figure 19H) and interstitial CD68^{+} cells (Figure 19J). However, only interstitial Ly6G^{+} cells were significantly increased in rIL-15 treated *CD8α*$^{-/-}$ mice compared to control *CD8α*$^{-/-}$ mice (Figure 19I).

Analysis of TEC cell health revealed a trend for more tubular casts (Figure 19K) but no difference in Tunel^{+} cells (Figure 19L). Subsequently, we isolated TECs to see the effects on *Il-15rα* and *Bcl2* expression in control *CD8α*$^{-/-}$ NTS mice and *CD8α*$^{-/-}$ NTS mice treated with rIL-15. Relative gene expression data of isolated TECs revealed no difference in the expression of these two genes (Figure 19M).

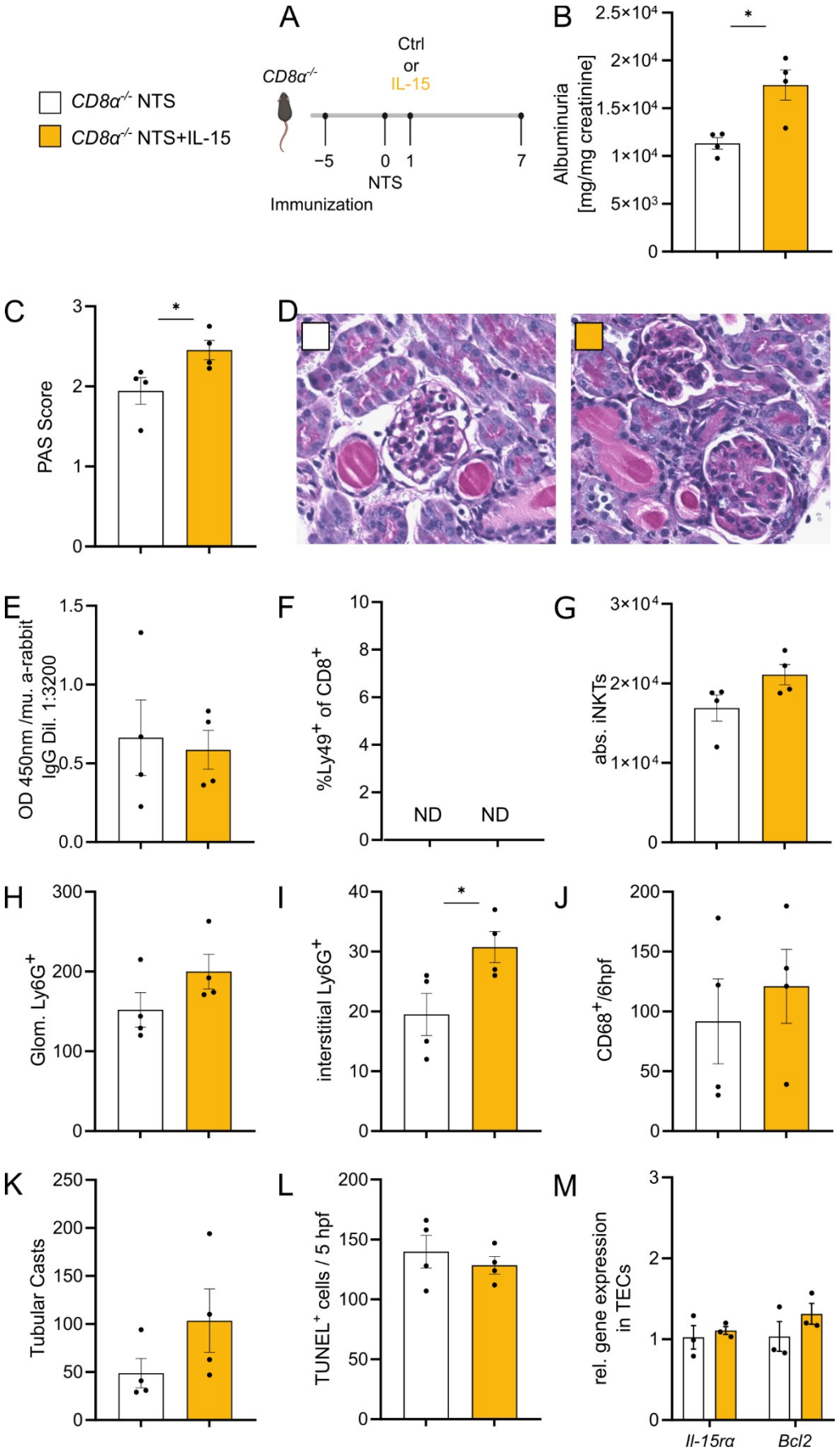
A
CD8α-/- NTS
CD8α-/- NTS+IL-15
CD8α-/-
Ctrl
or
IL-15
−5
0
1
7
NTS
Immunization
B
Albuminuria [mg/mg creatinine]
2.5×10⁴
2×10⁴
1.5×10⁴
1×10⁴
5×10³
0
*
C
PAS Score
3
2
1
0
*
D
E
OD 450nm /mu. a-rabbit IgG Dil. 1:3200
1.5
1.0
0.5
0.0
F
%Ly49+ of CD8+
10
8
6
4
2
0
ND
ND
G
abs. iNKTs
3×10⁴
2×10⁴
1×10⁴
0
H
Glom. Ly6G+
300
200
100
0
I
interstitial Ly6G+
40
30
20
10
0
*
J
CD68+/6hpf
200
150
100
50
0
K
Tubular Casts
250
200
150
100
50
0
L
TUNEL+ cells / 5 hpf
200
150
100
50
0
M
rel. gene expression in TECs
3
2
1
0
Il-15rα
Bcl2

Figure 19. rIL-15 treatment aggravates the NTS phenotype in *CD8α*$^{-/-}$ mice. Data represent day 7 of disease. (**A**) Experimental timeline of 7 days NTS with rIL-15 treatment on day 1. (**B**) Urinary albumin to creatinine ratio. (**C**) PAS-Score and (**D**) representative micrographs of PAS-stained kidney sections. (**E**) Optical density of circulating mouse anti-rabbit IgG. (**F**) Frequencies of kidney Ly49^{+}CD8^{+} memory T cells and (**G**) absolute numbers of kidney iNKT cells. Quantification of immunohistochemistry stainings of absolute (**H**) glomerular and (**I**) interstitial Ly6G^{+} cells and (**J**) absolute CD68^{+} cells in 6 hpf. Quantification of (**K**) tubular cast formation in 12 hpf and (**L**) Tunel^{+} cells in 5 hpf. (**M**) Relative gene expression data of *Il-15rα* and *Bcl2* in isolated TECs. *p≤0.05. Data were tested for normal distribution, and Student's *t*-test or Mann-Whitney test was used for statistical analysis. All data are represented as mean ± SEM. Reproduced with modifications from Mooslechner et al. [1] with permission through the MDPI Open Access Policy.

To further investigate the association of rIL-15-mediated benefits with CD8^{+} T cells in NTS, we induced NTS in WT mice, treated two groups with rIL-15, and on the following day additionally administered an isotype control AB or an anti-CD8α depletion AB.

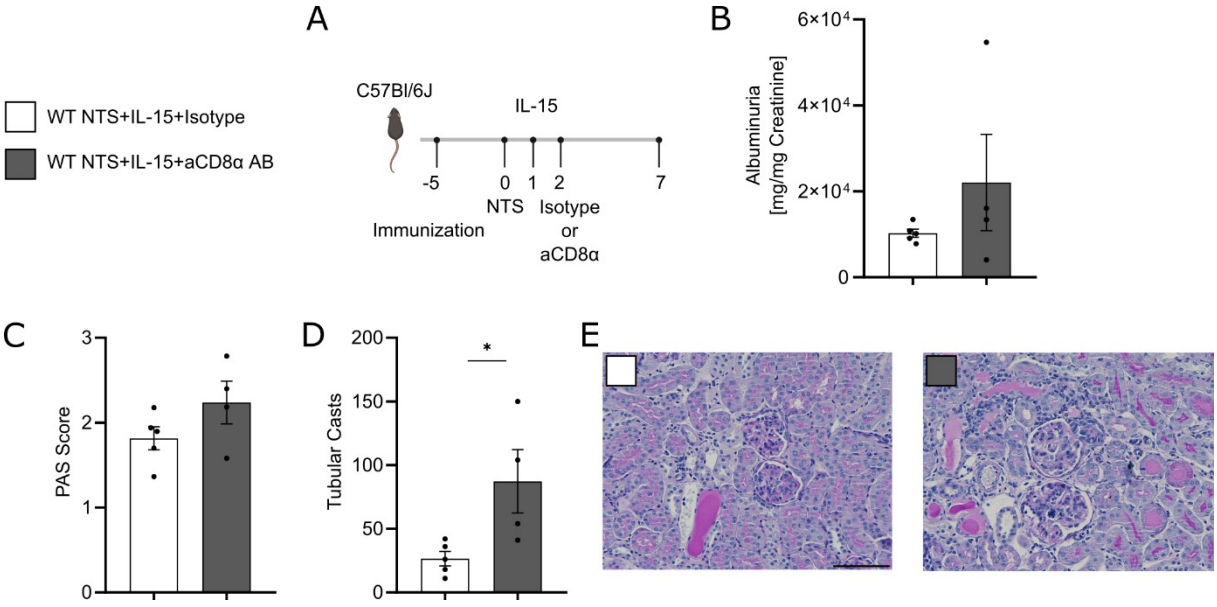

Figure 20. WT mice treated with rIL-15 and subsequently depleted of CD8α show an increase in tubular cast formation. Data represent day 7 of disease. (**A**) Experimental timeline of 7 days NTS with rIL-15 treatment on day 1 and CD8α-depletion on day 2 of NTS. (**B**) Urinary albumin to creatinine ratio. (**C**) PAS Score and (**D**) tubular cast formation counted in 12 hpf. (**E**) Representative micrographs of PAS staining used to analyze PAS Score and tubular casts (x20 magnification, scale bar bottom right 100µm). *p≤0.05. Data were tested for normal distribution, and Student's *t*-test or Mann-Whitney test was used for statistical analysis. All data are represented as mean ± SEM. Reproduced with modifications from Mooslechner et al. [1] with permission through the MDPI Open Access Policy.

Depletion of CD8α after the administration of rIL-15 in NTS revealed a trend for higher urinary albumin to creatinine ratio (Figure 20B) than controls. Histological analysis showed the same trend in PAS Score (Figure 20C). In addition, a significant increase in the formation of tubular casts (Figure 20D) was seen in WT NTS mice with rIL-15 and depleted of CD8α compared to WT NTS mice treated with rIL-15 receiving a control AB. Figure 20E shows representative PAS-stained kidney sections.

Another experimental setup to test the association of rIL-15-mediated benefits in NTS with $CD8^+$ cells can be seen in Figure 21A. *CD8α*$^{-/-}$ mice received adoptively transferred $CD8^+$ cells on day -1 isolated from WT mice. The control group was built of *CD8α*$^{-/-}$ mice receiving only transfer solution without any cells on day -1. On day 1 of NTS, both groups were administered low-dose rIL-15. Figure 21B shows the flow cytometry analysis done as purification control of a sample taken of the adoptively transferred $CD8^+$ cells. The dot plot shows that 97.2% of the cells in the sample stained positive for CD8α.

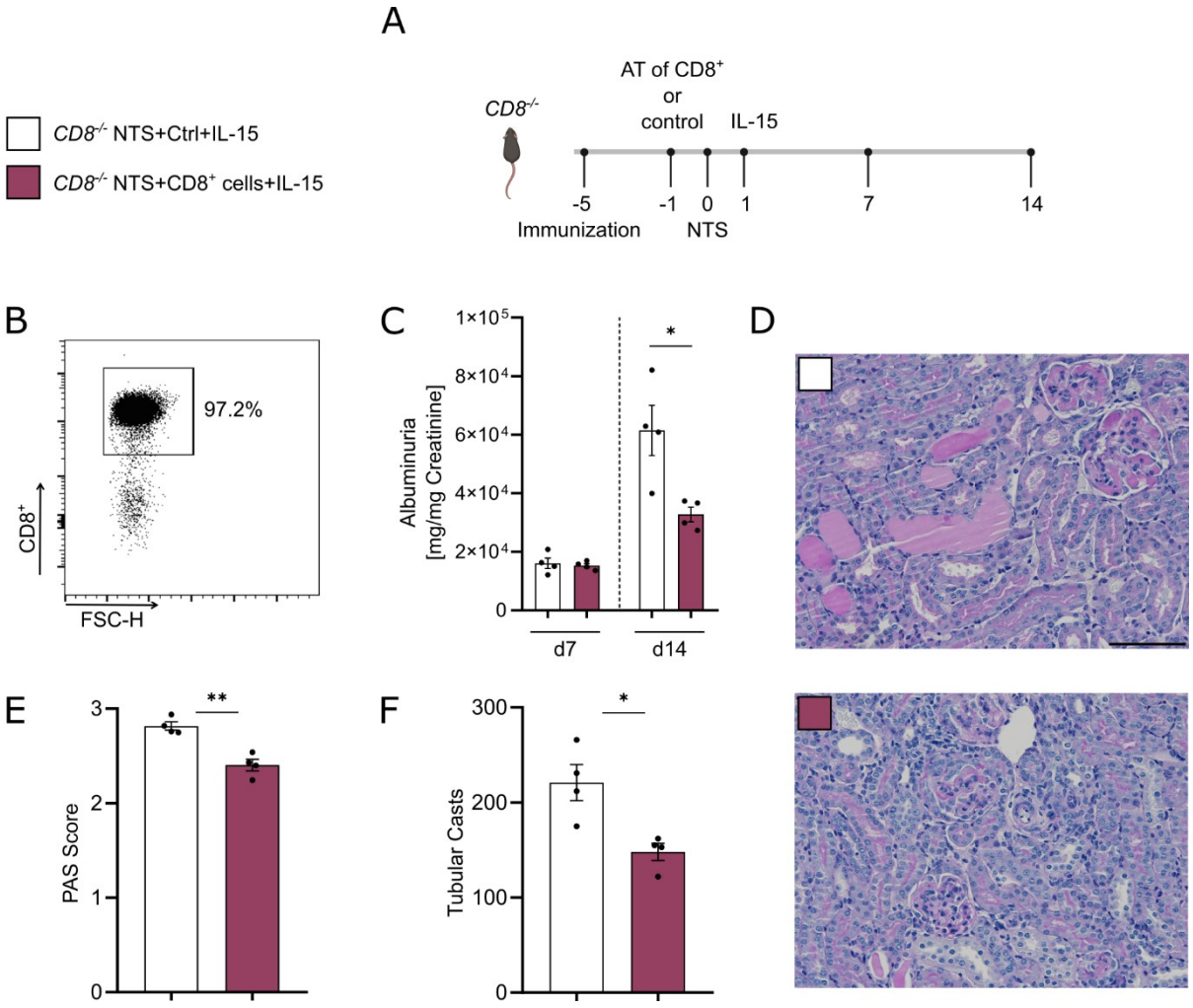

Figure 21. Adoptive transfer of CD8α$^+$ cells into *CD8α$^{-/-}$* mice shows delayed amelioration of disease outcomes in NTS. Data represent day 14 of disease or as indicated. (**A**) Experimental timeline of 7 days of NTS with adoptive transfer of CD8α$^+$ cells on day -1 and rIL-15 treatment on day 1. (**B**) Flow cytometry dot-plot of isolated and stained CD8α$^+$ cells from pooled lymph nodes of WT mice used for adoptive transfer into *CD8α$^{-/-}$* mice. (**C**) Urinary albumin to creatinine ratio on day 7 and day 14 of NTS. (**D**) Representative micrographs of PAS-staining used to analyze (**E**) PAS Score and (**F**) tubular cast formation counted in 12 hpf (x20 magnification, scale bar bottom right 100µm). *p≤0.05, **p≤0.01. Data were tested for normal distribution, and Student's *t*-test or Mann-Whitney test was used for statistical analysis. All data are represented as mean ± SEM. Reproduced with modifications from Mooslechner et al. [1] with permission through the MDPI Open Access Policy.

Urinary albumin to creatinine ratio on day 7 of NTS showed no difference between *CD8α*$^{-/-}$ mice transferred with CD8^{+} cells compared to *CD8α*$^{-/-}$ mice without CD8^{+} cells (Figure 21C). Therefore, the experiment was prolonged for a week. On day 14 of NTS, the group with transferred CD8^{+} cells showed lower urinary albumin to creatinine ratio than control mice.

Histological analysis, as seen in representative stainings in Figure 21D, showed less PAS-positive material per 50 glomeruli (Figure 21E) and less tubular cast formation (Figure 21F) in the group of *CD8α*$^{-/-}$ mice with transferred CD8^{+} cells than control *CD8α*$^{-/-}$ mice without transferred cells.

3.2.3 Long-term impact of low-dose rIL-15 treatment in NTS

Low-dose rIL-15 mediated significant benefits in the pathology of NTS. To test if these effects are sustainable for longer, we performed an experiment with the same treatment regimen but an extended follow-up period of 21 days.

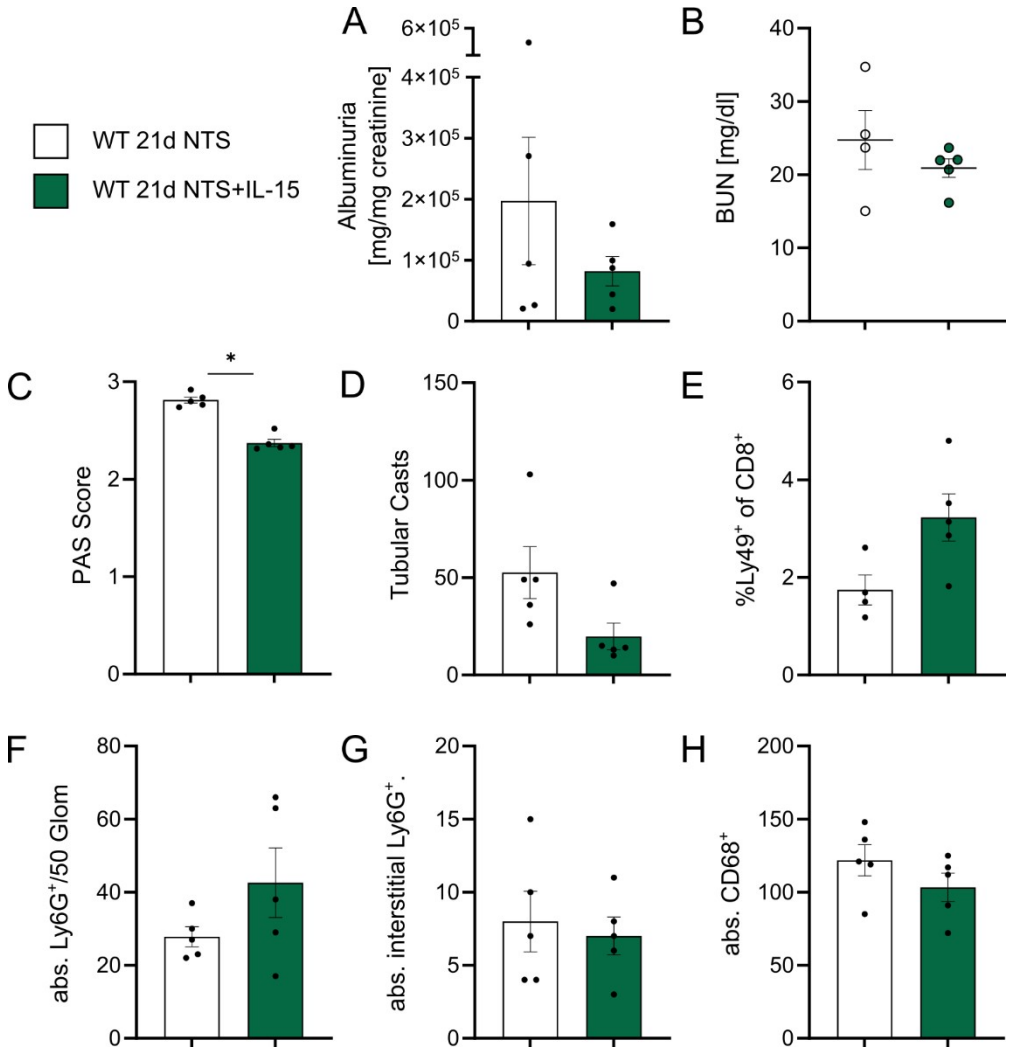

Figure 22. The benefits of a single low-dose of rIL-15 are not pronounced on day 21 of NTS. Data represent day 21 of disease. (**A**) Frequencies of kidney Ly49$^+$CD8$^+$ memory T cells, (**B**) urinary albumin to creatinine ratio, and (**C**) BUN levels on day 21 of NTS. (**D**) Representative PAS stainings of kidney tissue used to analyze (**E**) PAS Score and (**F**) tubular cast formation counted in 12 hpf. Quantification of immunohistochemistry stainings of (**G**) absolute glomerular and (**H**) interstitial Ly6G$^+$ cells and (**I**) absolute CD68$^+$ cells in 6 hpf on day 21 of NTS. *p≤0.05. Data were tested for normal distribution, and Student's *t*-test or Mann-Whitney test was used for statistical analysis. All data are represented as mean ± SEM.

Urinary albumin to creatinine ratio showed a trend to lower albuminuria in rIL-15 treated mice (Figure 22A), and BUN levels were comparable in both groups (Figure 22B). In addition, histological analysis revealed significantly less PAS-positive material per 50 glomeruli, represented by a lower PAS Score (Figure 22C) in rIL-15-treated mice. The same trend was shown in reduced tubular cast formation (Figure 22D).

Flow cytometry analysis showed a trend but not significantly increased frequencies of kidney $Ly49^{+}CD8^{+}$ memory T cells in WT mice treated with rIL-15 on day 21 of NTS (Figure 22E).

Interestingly, immunohistochemical staining of $Ly6G^{+}$ cells showed a trend of more cells in glomeruli in mice with NTS and rIL-15 (Figure 22F). However, absolute $Ly6G^{+}$ cells found in the kidney interstitium were comparable in both groups (Figure 22G). Also, rIL-15 treatment did not change absolute $CD68^{+}$ cell numbers in the kidney interstitium on day 21 of NTS (Figure 22H).

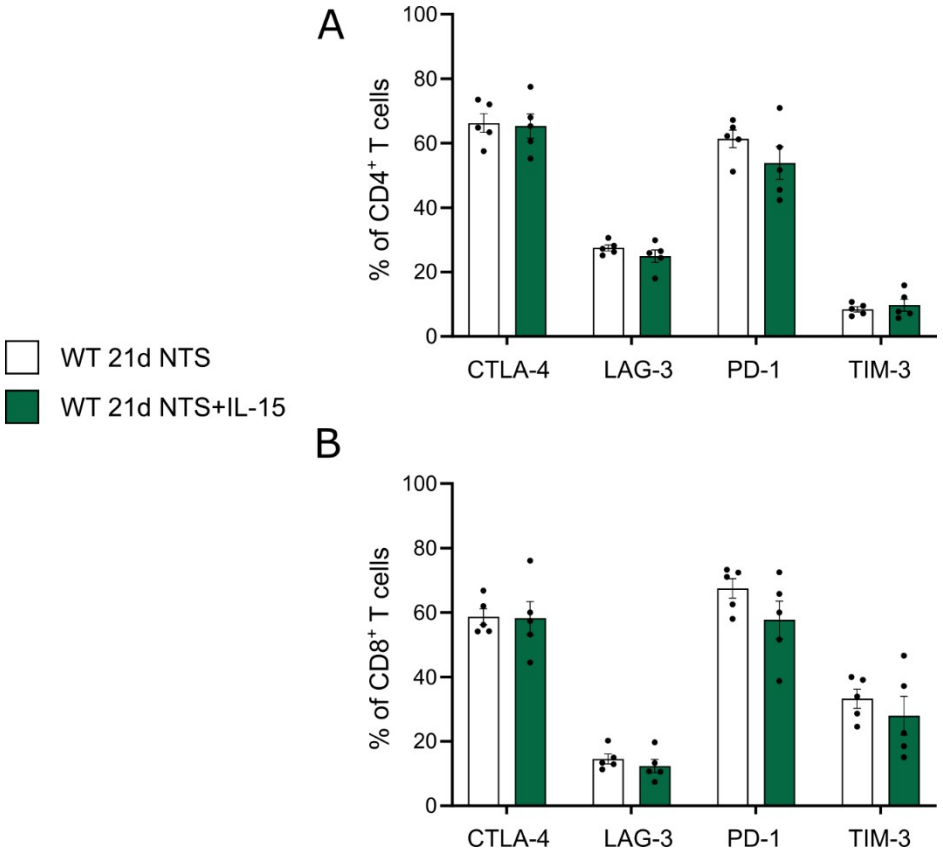

Figure 23. T cell exhaustion profile on day 21 of NTS is not changed due to rIL-15 treatment. Data represent day 21 of disease. Frequencies of exhaustion markers CTLA-4, LAG-3, PD-1, and TIM-3 are shown on (**A**) $CD4^+$ and (**B**) $CD8^+$ T cells in the kidney. Data were tested for normal distribution, and Student's *t*-test or Mann-Whitney test was used for statistical analysis. All data are represented as mean ± SEM.

The T cell exhaustion pattern was not altered on day 7 of NTS. However, the frequencies of the specific markers were not very pronounced at this early time point. Therefore, to see whether T cell activation status is impacted on day 21 of NTS, we again measured CTLA-4, LAG-3, PD-1, and TIM-3 frequencies via flow cytometry. However, like on day 7, between the groups no significant changes in frequencies of these exhaustion-associated markers were found on kidney $CD4^+$ (Figure 23A) and $CD8^+$ T cells (Figure 23B).

4. Discussion

Current treatments for autoimmune disease often include broad and non-specific immunosuppression. However, this form of intervention comes with potentially serious side effects, such as susceptibility to infections and cancers. More directed approaches are urgently needed. One way to achieve this could be the downregulation of harmful immune responses while simultaneously harnessing the intrinsic protective effects of the immune system. $CD8^+$ T cells contribute to the initiation and progression of pathogenic immune responses in several autoimmune diseases. Simplified, they facilitate cytotoxicity by recognizing MHC I-peptide complexes on target cells or attracting other immune cells via chemokines aggravating inflammation. Only recently, evidence has been accumulating that $CD8^+$ T cells also play an essential role in immune regulation[91], making them a potential target for new therapeutic options to shift the balance from pathogenic to regulatory immune responses within a cell population. Although $CD8^+$ T cells infiltrate kidney tissue during GN, their degree of involvement in the onset and progression of the disease is unclear. The literature excludes the contribution of $CD8^+$ T cells in the breach of the Bowman's capsule and suggests a possible role in podocyte injury[44] and TIN[23].

This study aims to investigate the contribution of $CD8^+$ T cells to NTS pathology, a murine model of non-autoimmune GN. We identified albuminuria, glomerulosclerosis, and myeloid cell infiltration of the kidney as disease outcomes of interest. Additionally, we investigated the potential of IL-15, a pleiotropic cytokine that is both associated with kidney health and a $CD8^+$ memory T cell shift, to treat GN.

The role of $CD8^+$ T cells in the pathogenesis and disease progression of NTS and other rodent models of GN is still disputed. This fact is partly attributed to different and somewhat conflicting findings in previous studies. One explanation could be that the rodent models of choice vary in several factors. First, it has to be mentioned that most of the earlier studies were conducted over 20 years ago, and there is a somewhat looseness in what the rodent model of non-autoimmune experimental GN is called. Some studies call it anti-GBM GN. However, their methods section does not specify an isolation or purification step, which would justify the assumption that only murine GBM was used to produce anti-mouse antiserum. It is not always clear which material (whole kidney, kidney cortex, or purified GBM) was used to produce antiserum to induce disease. Our model is termed NTS (also

sometimes abbreviated as NTN), and we use the kidney cortex to produce anti-mouse antiserum. Here, glomeruli are isolated by sieving followed by lysis of cells. The remaining extract mainly consists of the GBM and is used to produce rabbit anti-mouse antibodies by immunization. Thus, the model might be influenced by purity of isolated glomeruli as well as of the GBM extract, which explains the lack of uniform outcomes reported. Furthermore, experimental research groups using sheep anti-mouse GBM antibodies do not need a preimmunization step of mice, which is needed in our hands to induce robust disease. Again, this difference in disease induction might crucially influence experimental results.

To address this issue, as a starting point for our study, we identified three studies about the role of $CD8^+$ T cells in GN in the existing literature, which used animal models most comparable to our NTS model representing non-autoimmune experimental GN[99–101]. However, all four studies, including our study, differ in several points. First, Kawasaki et al. used a rabbit model system to produce anti-rat antiserum to induce disease in WKY rats, which were then depleted of CD8[99]. Tipping et al. and Li et al. used sheep as model systems for antiserum production. However, Tipping et al. induced disease in CD8 genetic knockout mice, while Li et al. opted to deplete CD8 in C57Bl/6 mice[100,101]. To gather a complete picture of CD8 involvement in NTS, in this study, we induced NTS in both *CD8α*$^{-/-}$ mice and C57Bl/6J mice depleted of CD8α with antiserum of rabbit origin. *CD8α*$^{-/-}$ mice with NTS showed worse disease outcomes, represented by a higher PAS Score, more tubular cast formation, and higher numbers of $CD68^+$ myeloid cells in kidney tissue, representing more inflammation on day 21 of the disease. The numbers of kidney infiltrating $CD4^+$ T cells remained unchanged. These results were accompanied by deteriorating BUN levels starting at day 11 compared to controls and an increase in ACR on day 14 of NTS. These results were strikingly similar to the findings of Tipping et al. in genetic knockout mice[100]. Notably, the data indicate that a lack of $CD8^+$ T cells is associated with increased macrophage influx into the kidney and decline of kidney function, which has also been reported previously[100].

While Kawasaki et al. and Li et al. report lower macrophage numbers in kidney tissue and somewhat beneficial effects due to CD8-depleting therapy, we could not reproduce these findings in our study. While the PAS Score was again higher in mice without CD8, we found no other differences compared to the control group on day 21 of NTS. Interestingly, we found a significant amelioration in kidney function on day 7 of the disease. However, this effect was not sustained. CD8-depletion was highly successful, with only approximately 2% of $CD8^+$ T

cells remaining in kidney tissue. However, these might represent a tissue-resident $CD8^+$ population, which could be crucial in preventing aggravated disease.

This finding highlights two notable limitations of all previous studies, including our study. First, to our knowledge, none of the existing literature discriminates between $CD8^+$ T cells and other cell types expressing CD8, e.g., DCs. This is likely due to the lack of specific CD8 T cell knockouts, which preferentially should be conditional and inducible. However, due to the double positivity of T cells in the thymus, there are no commercially available transgenic CD8 T cell-specific Cre-LoxP-mouse strains. Second, NTS in *CD8α*$^{-/-}$ mice and CD8α-depletion do not allow for studying the effects of $CD8^+$ T cell subsets, which might facilitate different roles in the pathophysiology of GN.

Table 11. An overview of our results on the role of $CD8^+$ T cells in NTS in the context of existing literature.

Study	Disease	Model	Histology	Proteinuria	Kidney function	cell infiltration
Kawasaki et al., *Kidney Int*. 1992	rabbit anti-rat GBM NTS	CD8 depletion in WKY rats	↓ crescent formation	↓	---	↓ macrophages
Tipping et al., *Am J Pathol*. 1998	sheep anti-mouse GBM GN	$CD8^{-/-}$ mice	↑ crescent formation ↑ PAS-positive	=	↑ BUN	= CD4 ↑ macrophages
Li et al., *Clin Exp Immunol*. 2000	sheep anti-mouse GBM GN	CD8 depletion in C57Bl/6 mice	= crescent formation	↓	= creatinine clearance	↓ CD4 ↓ macrophages
Mooslechner et al., unpublished data	rabbit anti-mouse NTS	$CD8α^{-/-}$ mice	↑ PAS-positive ↑ Tubular Casts	↑ d14	↑ BUN	= CD4 ↑ macrophages
		CD8α depletion in C57Bl/6J mice	↑ PAS-positive = Tubular Casts	=	= BUN	= CD4 = macrophages

Taken together, we could not find evidence that overall CD8 depletion might be beneficial in treating GN. This finding contrasts studies conducted in rodent autoimmune models of experimental GN that report the opposite[103,104]. Most interestingly, despite the proposed detrimental roles of $CD8^+$ T cells in GN, our findings suggest a partial protective role in the pathomechanism, with deterioration in a state of complete CD8α absence.

Cytokines pose great potential for immunotherapies. They are potent mediators of immune cell signaling and stimulate diverse immune responses depending on the administered dose. High doses of IL-2, for example, stimulate effector $CD4^+$ T cells, which are successfully used against pathogens and malignancies[145]. On the other hand, $CD4^+$ Tregs have high-affinity IL-2 receptors and are, therefore, more sensitive to lower doses. Low-dose IL-2 therapy has proven effective in treating autoimmune diseases such as systemic lupus erythematosus and type 1 diabetes mellitus[146–148].

IL-2 and IL-15 are pleiotropic cytokines belonging to the α-helix bundle cytokine family. They are closely related, and their receptors share the same Rβ- and Rγ-chains. Therefore, they facilitate some overlapping functions. However, because of their unique Rα-chains, they also play very distinct roles in immune cell signaling. IL-15 significantly promotes $CD8^+$ T cell and NK cell proliferation and cytotoxicity[149]. High-dose IL-15 is used in combination therapies in clinical trials against cancers[128]. Given the success of low-dose IL-2 against autoimmune disease, in this study, we investigated the potential of low-dose IL-15 to treat GN, focusing on $CD8^+$ T cells.

IL-15 and kidney health are closely associated. Transcriptomic datasets generated from kidney biopsies of patients with various nephropathies show that IL-15 expression is uniformly lower than in healthy control kidney tissue[130]. Also, genetic IL-15 knockout mice were more susceptible to NTS[138]. Among other cell types, kidney TECs were found to express all three IL-15 receptor chains, which enables the *trans*-presentation of IL-15 to responding immune cells. Therapeutic use of IL-15 in preclinical experiments found it to counteract renal fibrosis[137] and TEC death[138]. Although IL-15 is known to be the main driver of $CD8^+$ T cell maintenance, these studies have not addressed the role of $CD8^+$ T cells.

Adding to the existing data, we report significant amelioration of disease outcomes in our murine model of NTS, partly by protecting TECs from cell death. Low-dose IL-15 therapy increased TEC survival, reduced tubular cast formation, and improved glomerulosclerosis.

We detected no changes in IgG deposition on the GBM or differences in T cell abundance in kidney tissue, which could explain a better disease phenotype. Injured TECs have been shown to recruit myeloid cells via chemokines[138,150,151]. A recent study found macrophage persistence after TEC injury promoted the infiltration of neutrophils and proinflammatory T cells, further hindering tissue repair[152]. Although we did not find a changed chemokine profile with IL-15 treatment in TEC isolates, we nevertheless found a significant reduction of neutrophil and macrophage infiltration of the kidney. Further studies are needed to unravel how IL-15 alters the recruitment of myeloid cells. Due to the pleiotropic nature of IL-15, we cannot exclude a direct effect of IL-15 on neutrophils and macrophages[153]. The reduction of kidney infiltrating myeloid cells might also explain the improved glomerular phenotype in NTS mice treated with IL-15 compared to vehicle. Neutrophils and macrophages have been shown to play a role in the pathogenesis of NTS[154–156]. Additionally, TIN has been previously found to correlate best with proteinuria and long-term outcome in patients with GN[45], highlighting the close association of TIN and glomerular integrity.

IL-15 is a potent stimulant of $CD8^+$ T cell and NK cell proliferation. To prevent an aggravation of disease by the augmented pro-inflammatory response of these cell types, we used a subproliferation-dose established in previous studies[125,140,141]. NK cells play a minor role in our model[157]. However, iNKT cells are associated with regulatory functions and improve NTS[158]. In our hands, we found no differences in absolute kidney cell numbers of NK, NKT, and iNKT cells in NTS mice treated with IL-15 compared to controls.

IL-15 promotes $CD8^+$ memory T cell survival[141], and we report an increase in activated memory $CD8^+$ T cells in the lymph nodes of NTS mice treated with IL-15. $CD8^+CD44^+CD122^+$ activated memory T cells are critical for immune homeostasis and have been termed $CD8^+$ Tregs. In preclinical studies, adoptive transfer of this cell population reverted autoimmune disease[92,93]. Additionally, we could show an upregulation of the marker Ly49 on activated memory cells in the periphery and the kidney. $Ly49^+CD8^+$ memory T cells have been associated with regulatory functions. Ly49 consists of inhibitory and activating receptors and changes their expression profile upon stimulation[159]. For our characterization, we used an antibody against the C/F/H/I receptors. However, it has been shown that 90% of $Ly49^+CD8^+$ T cells express the F receptor[98,160]. Ly49F is encoded by *Klra6,* and genetic knockout mice showed no difference in viral clearance after challenge. However, 30 days post-infection, knockout mice developed autoimmune nephritis with IgG

deposition in the kidney[98], highlighting the association of $Ly49^+CD8^+$ memory T cells and kidney health.

We found no evidence of increased proliferation in $Ly49^+CD8^+$ memory T cells in the kidney due to IL-15 treatment, which could explain their increase. A thorough characterization of the surface marker profile revealed that $Ly49^+CD8^+$ memory T cells show a central memory phenotype in the periphery. In contrast, the majority of these cells in kidney tissue have either an effector or tissue-resident phenotype. Tissue-resident T cells are classically defined as CD69 and CD103 double positive. However, kidney resident memory T cells are unique and rarely CD103-positive[161,162]. Therefore, no distinct classification between effector or tissue-resident phenotype is possible with our used set of markers. Current literature suggests CD49a as a reliable marker for kidney residency[163]. However, since we found no increase in proliferation, we raise the question of whether these cells might have migrated to the injury site. Further studies are needed to clarify the origin of $Ly49^+CD8^+$ memory T cells in the kidney.

IL-15 is associated with the expression of immune checkpoints[164,165]. However, apart from Ly49, which is primarily an inhibitory receptor[159], we found no difference in the exhaustion profile of $CD8^+$ T cells due to the IL-15 treatment of NTS mice. Interestingly, isolated pan-$CD8^+$ lymphocytes showed a less cytotoxic gene expression profile with a relative decrease of *perforin*, *granzyme B,* and *Ifnγ*. Furthermore, reduced IFNγ production of $CD8^+$ T cells was also found on protein level. Additionally, the transcription factor Helios encoded by *Ikzf2* and prominent in the gene expression profile of $Ly49^+CD8^+$ T cells was increased. Therefore, we claim that IL-15 mediated a shift in $CD8^+$ T cells from a cytotoxic phenotype to an increase in regulatory-associated characteristics, which had beneficial effects on NTS.

$CD4^+$ T cells are central in the pathogenesis of NTS, and IL-15 can facilitate $CD4^+$ T cell proliferation[105] and influence Tregs[166]. However, we found no difference in absolute $CD4^+$ T cell numbers in the kidney or periphery. Additionally, in the kidney of NTS mice treated with IL-15, we found no evidence of $CD4^+$ T cell exhaustion or a shift in $CD4^+$ T cell subsets. In the periphery, Treg frequencies were comparable to controls. However, we detected a signal toward increased Th1 activity that is not typically associated with ameliorating NTS.

IL-15 has been shown to have a direct beneficial effect on TECs *in vitro*[138]. This study shows that *Il-15rα* was upregulated on TECs in NTS mice treated with IL-15, proving an active involvement of TECs in response to the stimulus. Additionally, *IL-15Rα*$^{-/-}$ mice treated with IL-15 showed comparable disease outcomes to vehicle-controlled *IL-15Rα*$^{-/-}$ mice when subjected to NTS. Here, we highlight the importance of the unique IL-15Rα-chain compared to the common β- and γ-chain shared with many cell types in IL-15-mediated amelioration of NTS.

On the other hand, genetic CD8α knockout mice showed an aggravated NTS phenotype with IL-15 treatment compared to vehicle-controlled knockout mice. Here TECs did not upregulate *IL-15rα* and were not protected from cell death. In addition, mice presented with interstitial neutrophil abundance and increased glomerulosclerosis, confirming the association between tubular injury, myeloid cell infiltration, and glomerular integrity. Furthermore, increased tubular cast formation was also seen in wild-type NTS mice depleted of CD8α. Finally, we could reverse the aggravated NTS phenotype in *CD8α*$^{-/-}$ mice with adoptive transfer of CD8^{+} T cells and IL-15 treatment. However, these results were only seen in a delayed manner, raising the question of the involvement of tissue-resident memory CD8^{+} T cells in IL-15-mediated amelioration of NTS.

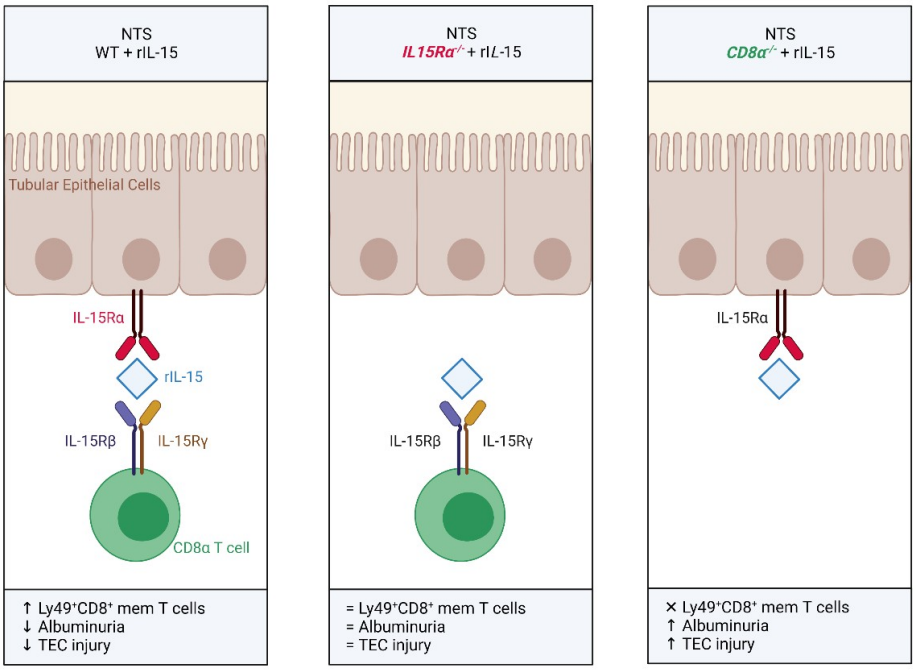

Figure 24. Receptor knockout dependent outcomes of IL-15 therapy in NTS.

Derived from our results generated in two knockout mouse strains, we hypothesize that TECs present soluble IL-15 via the IL-15R in *trans* to $CD8^+$ T cells, facilitating a less cytotoxic phenotype in $CD8^+$ T cells and protects TECs from cell death, which beneficially impacts NTS progression (Figure 22). However, we cannot exclude the involvement of DCs in the presentation process. Therefore, further studies are needed to investigate the potential crosstalk of TECs and $CD8^+$ T cells in NTS.

At last, we were interested in the longevity of the beneficial effects of IL-15 treatment in NTS. However, with our single low-dose therapy, amelioration of the disease was not as pronounced after three weeks of NTS. Since exhaustion was not increased on $CD8^+$ T cells due to IL-15 treatment, we see potential in administering a second dose during the second or third week of NTS.

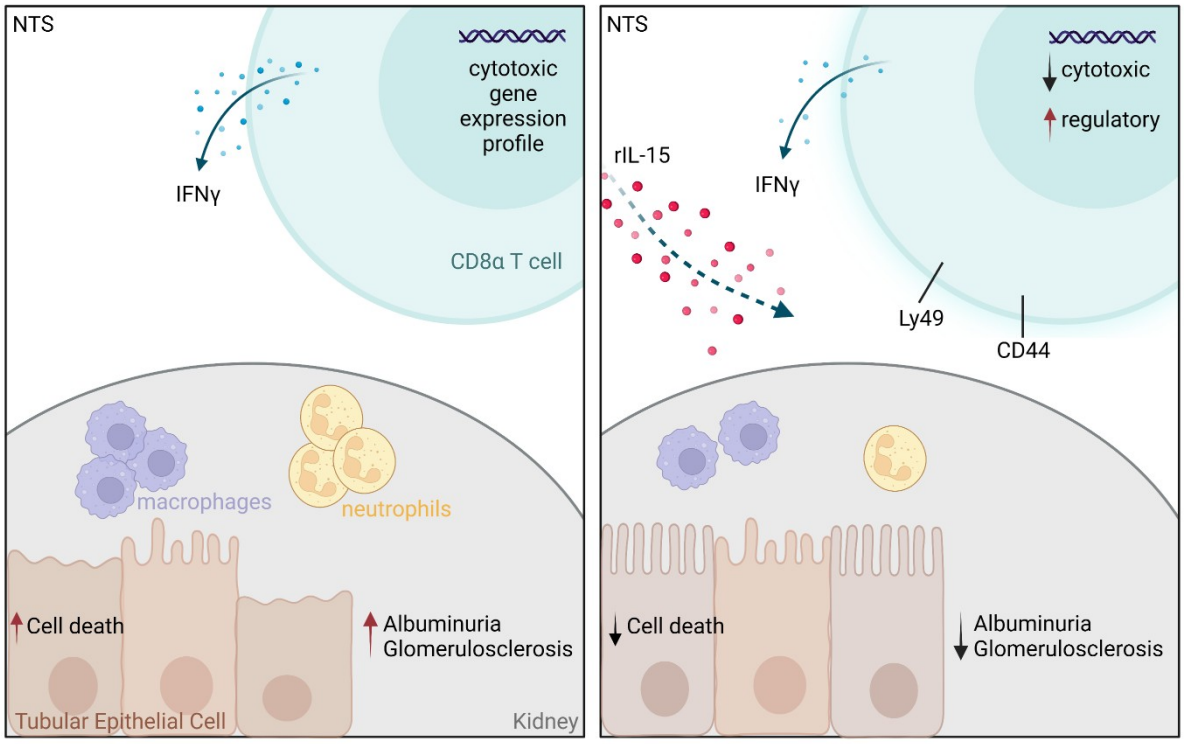

Figure 25. Low-dose IL-15 protects from NTS via $CD8^+$ T cells. Reproduced with modifications from Mooslechner et al. [1] with permission through the MDPI Open Access Policy.

We could collectively demonstrate that IL-15 is potent in ameliorating NTS, in part by protecting TECs from cell death (Figure 23). We show the importance of $CD8^+$ T cells but cannot exclude direct effects of IL-15 on other responding immune cells. We highlight the

finding of increased $Ly49^{+}CD8^{+}$ T cells associated with regulatory functions. $KIR^{+}CD8^{+}$ T cells are the human functional counterpart of $Ly49^{+}CD8^{+}$ T cells and have been found to be active in autoimmune diseases[98]. SLE patients presented with fewer $Helios^{+}CD8^{+}$ T cells[167]. Therefore, we imply a potential role for low-dose IL-15 immunotherapy to treat GN, with a need for further translational studies.

5. References

1. Mooslechner, A.A.; Schuller, M.; Artinger, K.; Kirsch, A.H.; Schabhüttl, C.; Eller, P.; Rosenkranz, A.R.; Eller, K. Low-Dose RIL-15 Protects from Nephrotoxic Serum Nephritis via CD8+ T Cells. *Cells* **2022**, *11*, 3656, doi:10.3390/cells11223656.
2. Lysaght, M.J. Maintenance Dialysis Population Dynamics: Current Trends and Long-Term Implications. *Journal of the American Society of Nephrology* **2002**, *13*, S37–S40, doi:10.1681/ASN.V13SUPPL_1S37.
3. Eknoyan, G.; Lameire, N.; Barsoum, R.; Eckardt, K.U.; Levin, A.; Levin, N.; Locatelli, F.; MacLeod, A.; Vanholder, R.; Walker, R.; et al. The Burden of Kidney Disease: Improving Global Outcomes. *Kidney International* **2004**, *66*, 1310–1314, doi:10.1111/J.1523-1755.2004.00894.X.
4. Levey, A.S.; Levin, A.; Kellum, J.A. Definition and Classification of Kidney Diseases. *American Journal of Kidney Diseases* **2013**, *61*, 686–688, doi:10.1053/J.AJKD.2013.03.003.
5. Kazancioğlu, R. Risk Factors for Chronic Kidney Disease: An Update. *Kidney International Supplements* **2013**, *3*, 368, doi:10.1038/KISUP.2013.79.
6. Pyart, R.; Evans, K.M.; Steenkamp, R.; Casula, A.; Wong, E.; Magadi, W.; Medcalf, J. The 21st UK Renal Registry Annual Report: A Summary of Analyses of Adult Data in 2017. *Nephron* **2020**, *144*, 59–66, doi:10.1159/000504851.
7. Bikbov, B.; Purcell, C.A.; Levey, A.S.; Smith, M.; Abdoli, A.; Abebe, M.; Adebayo, O.M.; Afarideh, M.; Agarwal, S.K.; Agudelo-Botero, M.; et al. Global, Regional, and National Burden of Chronic Kidney Disease, 1990–2017: A Systematic Analysis for the Global Burden of Disease Study 2017. *The Lancet* **2020**, *395*, 709–733, doi:10.1016/S0140-6736(20)30045-3.
8. Preuss, H.G. Basics of Renal Anatomy and Physiology. *Clinics in Laboratory Medicine* **1993**, *13*, 1–11, doi:10.1016/s0272-2712(18)30456-6.
9. Sethi, S.; Haas, M.; Markowitz, G.S.; D'Agati, V.D.; Rennke, H.G.; Jennette, J.C.; Bajema, I.M.; Alpers, C.E.; Chang, A.; Cornell, L.D.; et al. Mayo Clinic/Renal Pathology Society Consensus Report on Pathologic Classification, Diagnosis, and Reporting of GN. *Journal of the American Society of Nephrology : JASN* **2016**, *27*, 1278–1287, doi:10.1681/ASN.2015060612.
10. Sethi, S.; Fervenza, F.C. Standardized Classification and Reporting of Glomerulonephritis. *Nephrology Dialysis Transplantation* **2019**, *34*, 193–199, doi:10.1093/NDT/GFY220.
11. Sethi, S.; D'Agati, V.D.; Nast, C.C.; Fogo, A.B.; De Vriese, A.S.; Markowitz, G.S.; Glassock, R.J.; Fervenza, F.C.; Seshan, S.V.; Rule, A.; et al. A Proposal for Standardized Grading of Chronic Changes in Native Kidney Biopsy Specimens. *Kidney international* **2017**, *91*, 787–789, doi:10.1016/J.KINT.2017.01.002.
12. Rosenkranz, A.R.; Mendrick, D.L.; Cotran, R.S.; Mayadas, T.N. P-Selectin Deficiency Exacerbates Experimental Glomerulonephritis: A Protective Role for Endothelial P-Selectin in Inflammation. *Journal of Clinical Investigation* **1999**, *103*, 649–659, doi:10.1172/JCI5183.

13. Fogo, A.B. Mechanisms of Progression of Chronic Kidney Disease. *Pediatric nephrology (Berlin, Germany)* **2007**, *22*, 2011–2022, doi:10.1007/S00467-007-0524-0.

14. Becker, G.J.; Hewitson, T.D. Animal Models of Chronic Kidney Disease: Useful but Not Perfect. *Nephrology Dialysis Transplantation* **2013**, *28*, 2432–2438, doi:10.1093/NDT/GFT071.

15. Alpers, C.E.; Hudkins, K.L. Mouse Models of Diabetic Nephropathy. *Current opinion in nephrology and hypertension* **2011**, *20*, 278, doi:10.1097/MNH.0B013E3283451901.

16. Sharma, K.; McCue, P.; Dunn, S.R. Diabetic Kidney Disease in the Db/Db Mouse. *American journal of physiology. Renal physiology* **2003**, *284*, doi:10.1152/AJPRENAL.00315.2002.

17. Hewitson, T.D.; Ono, T.; Becker, G.J. Small Animal Models of Kidney Disease: A Review. *Methods in Molecular Biology* **2009**, *466*, 41–57, doi:10.1007/978-1-59745-352-3_4.

18. Dixon, F.J. What Are Sensitized Cells Doing in Glomerulonephritis? *http://dx.doi.org/10.1056/NEJM197009032831011* **2010**, *283*, 536–537, doi:10.1056/NEJM197009032831011.

19. Bolton, W.K.; Innes, D.J.; Sturgill, B.C.; al., et T-Cells and Macrophages in Rapidly Progressive Glomerulonephritis: Clinicopathologic Correlations. *Kidney Int* **1987**, *32*, 869–876.

20. Rocklin, R.E.; Lewis, E.J.; David, J.R. In Vitro Evidence for Cellular Hypersensitivity to Glomerular-Basement-Membrane Antigens in Human Glomerulonephritis. *http://dx.doi.org/10.1056/NEJM197009032831001* **2010**, *283*, 497–501, doi:10.1056/NEJM197009032831001.

21. Bhan, A.K.; Schneeberger, E.E.; Collins, A.B.; McCluskey, R.T. Evidence for a Pathogenic Role of a Cell-Mediated Immune Mechanism in Experimental Glomerulonephritis. *The Journal of Experimental Medicine* **1978**, *148*, 246, doi:10.1084/JEM.148.1.246.

22. Tipping, P.G.; Holdsworth, S.R. T Cells in Crescentic Glomerulonephritis. *Journal of the American Society of Nephrology* **2006**, *17*, 1253–1263, doi:10.1681/ASN.2005091013.

23. Sung, S.S.; Bolton, W.K. T Cells and Dendritic Cells in Glomerular Disease: The New Glomerulotubular Feedback Loop. *Kidney International* **2010**, *77*, 393–399, doi:10.1038/KI.2009.489.

24. Kaissling, B.; Le Hir, M. Characterization and Distribution of Interstitial Cell Types in the Renal Cortex of Rats. *Kidney international* **1994**, *45*, 709–720, doi:10.1038/KI.1994.95.

25. Krüger, T.; Benke, D.; Eitner, F.; Lang, A.; Wirtz, M.; Hamilton-Williams, E.E.; Engel, D.; Giese, B.; Müller-Newen, G.; Floege, J.; et al. Identification and Functional Characterization of Dendritic Cells in the Healthy Murine Kidney and in Experimental Glomerulonephritis. *Journal of the American Society of Nephrology : JASN* **2004**, *15*, 613–621, doi:10.1097/01.ASN.0000114553.36258.91.

26. Woltman, A.M.; De Fijter, J.W.; Zuidwijk, K.; Vlug, A.G.; Bajema, I.M.; Van Der Kooij, S.W.; Van Ham, V.; Van Kooten, C. Quantification of Dendritic Cell Subsets in

Human Renal Tissue under Normal and Pathological Conditions. *Kidney international* **2007**, *71*, 1001–1008, doi:10.1038/SJ.KI.5002187.

27. Krebs, C.F.; Reimers, D.; Zhao, Y.; Paust, H.J.; Bartsch, P.; Nuñez, S.; Rosemblatt, M.V.; Hellmig, M.; Kilian, C.; Borchers, A.; et al. Pathogen-Induced Tissue-Resident Memory T H 17 (T RM 17) Cells Amplify Autoimmune Kidney Disease. *Science immunology* **2020**, *5*, doi:10.1126/SCIIMMUNOL.ABA4163.

28. Devi, S.; Li, A.; Westhorpe, C.L.V.; Lo, C.Y.; Abeynaike, L.D.; Snelgrove, S.L.; Hall, P.; Ooi, J.D.; Sobey, C.G.; Richard Kitching, A.; et al. Multiphoton Imaging Reveals a New Leukocyte Recruitment Paradigm in the Glomerulus. *Nature Medicine 2012 19:1* **2012**, *19*, 107–112, doi:10.1038/nm.3024.

29. Carlin, L.M.; Stamatiades, E.G.; Auffray, C.; Hanna, R.N.; Glover, L.; Vizcay-Barrena, G.; Hedrick, C.C.; Cook, H.T.; Diebold, S.; Geissmann, F. Nr4a1-Dependent Ly6Clow Monocytes Monitor Endothelial Cells and Orchestrate Their Disposal. *Cell* **2013**, *153*, 362–375, doi:10.1016/J.CELL.2013.03.010.

30. Turner, J.E.; Krebs, C.; Tittel, A.P.; Paust, H.J.; Meyer-Schwesinger, C.; Bennstein, S.B.; Steinmetz, O.M.; Prinz, I.; Magnus, T.; Korn, T.; et al. IL-17A Production by Renal Γδ T Cells Promotes Kidney Injury in Crescentic GN. *Journal of the American Society of Nephrology : JASN* **2012**, *23*, 1486–1495, doi:10.1681/ASN.2012010040.

31. Kurts, C.; Panzer, U.; Anders, H.-J.J.; Rees, A.J. The Immune System and Kidney Disease: Basic Concepts and Clinical Implications. *Nature Reviews Immunology* **2013**, *13*, 738–753, doi:10.1038/nri3523.

32. Panzer, U.; Steinmetz, O.M.; Paust, H.J.; Meyer-Schwesinger, C.; Peters, A.; Turner, J.E.; Zahner, G.; Heymann, F.; Kurts, C.; Hopfer, H.; et al. Chemokine Receptor CXCR3 Mediates T Cell Recruitment and Tissue Injury in Nephrotoxic Nephritis in Mice. *Journal of the American Society of Nephrology : JASN* **2007**, *18*, 2071–2084, doi:10.1681/ASN.2006111237.

33. Menke, J.; Zeller, G.C.; Kikawada, E.; Means, T.K.; Huang, X.R.; Lan, H.Y.; Lu, B.; Farber, J.; Luster, A.D.; Kelley, V.R. CXCL9, but Not CXCL10, Promotes CXCR3-Dependent Immune-Mediated Kidney Disease. *Journal of the American Society of Nephrology : JASN* **2008**, *19*, 1177–1189, doi:10.1681/ASN.2007111179.

34. Paust, H.J.; Turner, J.E.; Steinmetz, O.M.; Peters, A.; Heymann, F.; Hölscher, C.; Wolf, G.; Kurts, C.; Mittrücker, H.W.; Stahl, R.A.K.; et al. The IL-23/Th17 Axis Contributes to Renal Injury in Experimental Glomerulonephritis. *Journal of the American Society of Nephrology : JASN* **2009**, *20*, 969–979, doi:10.1681/ASN.2008050556.

35. Rosenkranz, A.R.; Knight, S.; Sethi, S.; Alexander, S.I.; Cotran, R.S.; Mayadas, T.N. Regulatory Interactions of Alphabeta and Gammadelta T Cells in Glomerulonephritis. *Kidney international* **2000**, *58*, 1055–1066, doi:10.1046/J.1523-1755.2000.00263.X.

36. Summers, S.A.; Steinmetz, O.M.; Li, M.; Kausman, J.Y.; Semple, T.; Edgtton, K.L.; Borza, D.-B.; Braley, H.; Holdsworth, S.R.; Kitching, A.R. Th1 and Th17 Cells Induce Proliferative Glomerulonephritis. *Journal of the American Society of Nephrology* **2009**, *20*, 2518–2524, doi:10.1681/ASN.2009030337.

37. Riedel, J.H.; Paust, H.J.; Turner, J.E.; Tittel, A.P.; Krebs, C.; Disteldorf, E.; Wegscheid, C.; Tiegs, G.; Velden, J.; Mittrücker, H.W.; et al. Immature Renal Dendritic Cells Recruit Regulatory CXCR6(+) Invariant Natural Killer T Cells to Attenuate Crescentic GN. *Journal of the American Society of Nephrology : JASN* **2012**, *23*, 1987–2000, doi:10.1681/ASN.2012040394.

38. Kluger, M.A.; Luig, M.; Wegscheid, C.; Goerke, B.; Paust, H.J.; Brix, S.R.; Yan, I.; Mittrücker, H.W.; Hagl, B.; Renner, E.D.; et al. Stat3 Programs Th17-Specific Regulatory T Cells to Control GN. *Journal of the American Society of Nephrology : JASN* **2014**, *25*, 1291–1302, doi:10.1681/ASN.2013080904.

39. Diefenhardt, P.; Nosko, A.; Kluger, M.A.; Richter, J.V.; Wegscheid, C.; Kobayashi, Y.; Tiegs, G.; Huber, S.; Flavell, R.A.; Stahl, R.A.K.; et al. IL-10 Receptor Signaling Empowers Regulatory T Cells to Control Th17 Responses and Protect from GN. *Journal of the American Society of Nephrology* **2018**, *29*, 1825–1837, doi:10.1681/ASN.2017091044.

40. Wolf, D.; Hochegger, K.; Wolf, A.M.; Rumpold, H.F.; Gastl, G.; Tilg, H.; Mayer, G.; Gunsilius, E.; Rosenkranz, A.R. CD4+CD25+ Regulatory T Cells Inhibit Experimental Anti-Glomerular Basement Membrane Glomerulonephritis in Mice. *Journal of the American Society of Nephrology* **2005**, *16*, 1360–1370, doi:10.1681/ASN.2004100837.

41. Paust, H.-J.J.; Ostmann, A.; Erhardt, A.; Turner, J.-E.E.; Velden, J.; Mittrücker, H.W.; Sparwasser, T.; Panzer, U.; Tiegs, G.; Mittrü Cker, H.-W.; et al. Regulatory T Cells Control the Th1 Immune Response in Murine Crescentic Glomerulonephritis. *Kidney International* **2011**, *80*, 154–164.

42. Ostmann, A.; Paust, H.J.; Panzer, U.; Wegscheid, C.; Kapffer, S.; Huber, S.; Flavell, R.A.; Erhardt, A.; Tiegs, G. Regulatory T Cell-Derived IL-10 Ameliorates Crescentic GN. *Journal of the American Society of Nephrology : JASN* **2013**, *24*, 930–942, doi:10.1681/ASN.2012070684.

43. Artinger, K.; Kirsch, A.H.; Aringer, I.; Moschovaki-Filippidou, F.; Eller, P.; Rosenkranz, A.R.; Eller, K. Innate and Adaptive Immunity in Experimental Glomerulonephritis: A Pathfinder Tale. *Pediatric Nephrology (Berlin, Germany)* **2017**, *32*, 943, doi:10.1007/S00467-016-3404-7.

44. Chen, A.; Lee, K.; D'Agati, V.D.; Wei, C.; Fu, J.; Guan, T.-J.; He, J.C.; Schlondorff, D.; Agudo, J. Bowman's Capsule Provides a Protective Niche for Podocytes from Cytotoxic CD8+ T Cells. *Journal of Clinical Investigation* **2018**, *128*, 3413–3424, doi:10.1172/JCI97879.

45. Risdon, R.A.; Sloper, J.C.; De Wardener, H.E. Relationship between Renal Function and Histological Changes Found in Renal-Biopsy Specimens from Patients with Persistent Glomerular Nephritis. *Lancet (London, England)* **1968**, *2*, 363–366, doi:10.1016/S0140-6736(68)90589-8.

46. Macconi, D.; Chiabrando, C.; Schiarea, S.; Aiello, S.; Cassis, L.; Gagliardini, E.; Noris, M.; Buelli, S.; Zoja, C.; Corna, D.; et al. Proteasomal Processing of Albumin by Renal Dendritic Cells Generates Antigenic Peptides. *Journal of the American Society of Nephrology : JASN* **2009**, *20*, 123–130, doi:10.1681/ASN.2007111233.

47. Rees, A. Cross Dendritic Cells Anger T Cells after Kidney Injury. *Journal of the American Society of Nephrology* **2009**, *20*, 3–5, doi:10.1681/ASN.2008111200.

48. Breda, P.C.; Wiech, T.; Meyer-Schwesinger, C.; Grahammer, F.; Huber, T.; Panzer, U.; Tiegs, G.; Neumann, K. Renal Proximal Tubular Epithelial Cells Exert Immunomodulatory Function by Driving Inflammatory CD4+ T Cell Responses. *American Journal of Physiology - Renal Physiology* **2019**, *317*, F77–F89, doi:10.1152/ajprenal.00427.2018.

49. Abbas, A.K.; Lichtman, A.H.; Pillai, S. *Cellular and Molecular Immunology - 10th Edition*; Elsevier Inc. Philadelphia, USA: Philadelphia, USA, 2022; ISBN 978-0-323-75748-5.

50. Butz, E.A.; Bevan, M.J. Massive Expansion of Antigen-Specific CD8+ T Cells during an Acute Virus Infection. *Immunity* **1998**, *8*, 167, doi:10.1016/S1074-7613(00)80469-0.

51. Dieckmann, N.M.G.; Frazer, G.L.; Asano, Y.; Stinchcombe, J.C.; Griffiths, G.M. The Cytotoxic T Lymphocyte Immune Synapse at a Glance. *Journal of cell science* **2016**, *129*, 2881–2886, doi:10.1242/JCS.186205.

52. Voskoboinik, I.; Whisstock, J.C.; Trapani, J.A. Perforin and Granzymes: Function, Dysfunction and Human Pathology. *Nature Reviews Immunology 2015 15:6* **2015**, *15*, 388–400, doi:10.1038/nri3839.

53. Liu, X.; Lieberman, J. Knocking 'em Dead: Pore-Forming Proteins in Immune Defense. *Annual review of immunology* **2020**, *38*, 455–485, doi:10.1146/ANNUREV-IMMUNOL-111319-023800.

54. Barber, D.L.; Wherry, E.J.; Masopust, D.; Zhu, B.; Allison, J.P.; Sharpe, A.H.; Freeman, G.J.; Ahmed, R. Restoring Function in Exhausted CD8 T Cells during Chronic Viral Infection. *Nature* **2006**, *439*, 682–687, doi:10.1038/NATURE04444.

55. Hashimoto, M.; Kamphorst, A.O.; Im, S.J.; Kissick, H.T.; Pillai, R.N.; Ramalingam, S.S.; Araki, K.; Ahmed, R. CD8 T Cell Exhaustion in Chronic Infection and Cancer: Opportunities for Interventions. *Annual review of medicine* **2018**, *69*, 301–318, doi:10.1146/ANNUREV-MED-012017-043208.

56. McLane, L.M.; Abdel-Hakeem, M.S.; Wherry, E.J. CD8 T Cell Exhaustion During Chronic Viral Infection and Cancer. *Annual review of immunology* **2019**, *37*, 457–495, doi:10.1146/ANNUREV-IMMUNOL-041015-055318.

57. Lalvani, A.; Brookes, R.; Hambleton, S.; Britton, W.J.; Hill, A.V.S.; McMichael, A.J. Rapid Effector Function in CD8+ Memory T Cells. *Journal of Experimental Medicine* **1997**, *186*, 859–865, doi:10.1084/JEM.186.6.859.

58. Veiga-Fernandes, H.; Walter, U.; Bourgeois, C.; McLean, A.; Rocha, B. Response of Naïve and Memory CD8+ T Cells to Antigen Stimulation in Vivo. *Nature Immunology 2000 1:1* **2000**, *1*, 47–53, doi:10.1038/76907.

59. Kaech, S.M.; Cui, W. Transcriptional Control of Effector and Memory CD8+ T Cell Differentiation. *Nature Reviews Immunology 2012 12:11* **2012**, *12*, 749–761, doi:10.1038/nri3307.

60. Youngblood, B.; Hale, J.S.; Kissick, H.T.; Ahn, E.; Xu, X.; Wieland, A.; Araki, K.; West, E.E.; Ghoneim, H.E.; Fan, Y.; et al. Effector CD8 T Cells Dedifferentiate into Long-Lived Memory Cells. *Nature 2017 552:7685* **2017**, *552*, 404–409, doi:10.1038/nature25144.

61. Akondy, R.S.; Fitch, M.; Edupuganti, S.; Yang, S.; Kissick, H.T.; Li, K.W.; Youngblood, B.A.; Abdelsamed, H.A.; McGuire, D.J.; Cohen, K.W.; et al. Origin and Differentiation of Human Memory CD8 T Cells after Vaccination. *Nature 2017 552:7685* **2017**, *552*, 362–367, doi:10.1038/nature24633.

62. Sallusto, F.; Lenig, D.; Förster, R.; Lipp, M.; Lanzavecchia, A. Two Subsets of Memory T Lymphocytes with Distinct Homing Potentials and Effector Functions. *Nature 1999 401:6754* **1999**, *401*, 708–712, doi:10.1038/44385.

63. Budd, R.C.; Cerottini, J.C.; Horvath, C.; Bron, C.; Pedrazzini, T.; Howe, R.C.; MacDonald, H.R. Distinction of Virgin and Memory T Lymphocytes. Stable Acquisition of the Pgp-1 Glycoprotein Concomitant with Antigenic Stimulation. *The Journal of Immunology* **1987**, *138*.

64. Masopust, D.; Vezys, V.; Usherwood, E.J.; Cauley, L.S.; Olson, S.; Marzo, A.L.; Ward, R.L.; Woodland, D.L.; Lefrançois, L. Activated Primary and Memory CD8 T Cells Migrate to Nonlymphoid Tissues Regardless of Site of Activation or Tissue of Origin. *The Journal of Immunology* **2004**, *172*, 4875–4882, doi:10.4049/JIMMUNOL.172.8.4875.

65. Rosenblum, M.D.; Way, S.S.; Abbas, A.K. Regulatory T Cell Memory. *Nature Reviews Immunology* **2016**, *16*, 90–101, doi:10.1038/NRI.2015.1.

66. Martin, M.D.; Badovinac, V.P. Defining Memory CD8 T Cell. *Frontiers in Immunology* **2018**, *9*, 2692, doi:10.3389/FIMMU.2018.02692/BIBTEX.

67. Gebhardt, T.; Wakim, L.M.; Eidsmo, L.; Reading, P.C.; Heath, W.R.; Carbone, F.R. Memory T Cells in Nonlymphoid Tissue That Provide Enhanced Local Immunity during Infection with Herpes Simplex Virus. *Nature immunology* **2009**, *10*, 524–530, doi:10.1038/NI.1718.

68. Masopust, D.; Choo, D.; Vezys, V.; Wherry, E.J.; Duraiswamy, J.; Akondy, R.; Wang, J.; Casey, K.A.; Barber, D.L.; Kawamura, K.S.; et al. Dynamic T Cell Migration Program Provides Resident Memory within Intestinal Epithelium. *The Journal of experimental medicine* **2010**, *207*, 553–564, doi:10.1084/JEM.20090858.

69. Schenkel, J.M.; Masopust, D. Tissue-Resident Memory T Cells. *Immunity* **2014**, *41*, 886–897, doi:10.1016/J.IMMUNI.2014.12.007.

70. Masopust, D.; Vezys, V.; Wherry, E.J.; Barber, D.L.; Ahmed, R. Cutting Edge: Gut Microenvironment Promotes Differentiation of a Unique Memory CD8 T Cell Population. *Journal of immunology (Baltimore, Md. : 1950)* **2006**, *176*, 2079–2083, doi:10.4049/JIMMUNOL.176.4.2079.

71. Steinert, E.M.; Schenkel, J.M.; Fraser, K.A.; Beura, L.K.; Manlove, L.S.; Igyártó, B.Z.; Southern, P.J.; Masopust, D. Quantifying Memory CD8 T Cells Reveals Regionalization of Immunosurveillance. *Cell* **2015**, *161*, 737–749, doi:10.1016/j.cell.2015.03.031.

72. Jiang, X.; Clark, R.A.; Liu, L.; Wagers, A.J.; Fuhlbrigge, R.C.; Kupper, T.S. Skin Infection Generates Non-Migratory Memory CD8+ T(RM) Cells Providing Global Skin Immunity. *Nature* **2012**, *483*, 227–231, doi:10.1038/NATURE10851.

73. Mackay, L.K.; Rahimpour, A.; Ma, J.Z.; Collins, N.; Stock, A.T.; Hafon, M.-L.L.; Vega-Ramos, J.; Lauzurica, P.; Mueller, S.N.; Stefanovic, T.; et al. The Developmental

Pathway for CD103+ CD8+ Tissue-Resident Memory T Cells of Skin. *Nature Immunology* **2013**, *14*, 1294–1301, doi:10.1038/ni.2744.

74. Mackay, L.K.; Braun, A.; Macleod, B.L.; Collins, N.; Tebartz, C.; Bedoui, S.; Carbone, F.R.; Gebhardt, T. Cutting Edge: CD69 Interference with Sphingosine-1-Phosphate Receptor Function Regulates Peripheral T Cell Retention. *The Journal of Immunology* **2015**, *194*, 2059–2063, doi:10.4049/JIMMUNOL.1402256/-/DCSUPPLEMENTAL.

75. Schenkel, J.M.; Fraser, K.A.; Beura, L.K.; Pauken, K.E.; Vezys, V.; Masopust, D. Resident Memory CD8 T Cells Trigger Protective Innate and Adaptive Immune Responses. *Science (New York, N.Y.)* **2014**, *346*, 98, doi:10.1126/SCIENCE.1254536.

76. Ariotti, S.; Hogenbirk, M.A.; Dijkgraaf, F.E.; Visser, L.L.; Hoekstra, M.E.; Song, J.Y.; Jacobs, H.; Haanen, J.B.; Schumacher, T.N. T Cell Memory. Skin-Resident Memory $CD8^+$ T Cells Trigger a State of Tissue-Wide Pathogen Alert. *Science (New York, N.Y.)* **2014**, *346*, 101–105, doi:10.1126/SCIENCE.1254803.

77. Jameson, S.C.; Masopust, D. Understanding Subset Diversity in T Cell Memory. *Immunity* **2018**, *48*, 214–226, doi:10.1016/J.IMMUNI.2018.02.010.

78. Haluszczak, C.; Akue, A.D.; Hamilton, S.E.; Johnson, L.D.S.; Pujanauski, L.; Teodorovic, L.; Jameson, S.C.; Kedl, R.M. The Antigen-Specific CD8+ T Cell Repertoire in Unimmunized Mice Includes Memory Phenotype Cells Bearing Markers of Homeostatic Expansion. *The Journal of experimental medicine* **2009**, *206*, 435–448, doi:10.1084/JEM.20081829.

79. White, J.T.; Cross, E.W.; Kedl, R.M. Antigen-Inexperienced Memory CD8+ T Cells: Where They Come from and Why We Need Them. *Nature Reviews Immunology 2017 17:6* **2017**, *17*, 391–400, doi:10.1038/nri.2017.34.

80. Sosinowski, T.; White, J.T.; Cross, E.W.; Haluszczak, C.; Marrack, P.; Gapin, L.; Kedl, R.M. CD8α+ Dendritic Cell Trans Presentation of IL-15 to Naive CD8+ T Cells Produces Antigen-Inexperienced T Cells in the Periphery with Memory Phenotype and Function. *Journal of immunology (Baltimore, Md. : 1950)* **2013**, *190*, 1936–1947, doi:10.4049/JIMMUNOL.1203149.

81. White, J.T.; Cross, E.W.; Burchill, M.A.; Danhorn, T.; McCarter, M.D.; Rosen, H.R.; O'Connor, B.; Kedl, R.M. Virtual Memory T Cells Develop and Mediate Bystander Protective Immunity in an IL-15-Dependent Manner. *Nature Communications* **2016**, *7*, 11291, doi:10.1038/ncomms11291.

82. Akue, A.D.; Lee, J.-Y.; Jameson, S.C. Derivation and Maintenance of Virtual Memory CD8 T Cells. *Journal of immunology (Baltimore, Md. : 1950)* **2012**, *188*, 2516–2523, doi:10.4049/JIMMUNOL.1102213.

83. Jacomet, F.; Cayssials, E.; Basbous, S.; Levescot, A.; Piccirilli, N.; Desmier, D.; Robin, A.; Barra, A.; Giraud, C.; Guilhot, F.; et al. Evidence for Eomesodermin-Expressing Innate-like CD8(+) KIR/NKG2A(+) T Cells in Human Adults and Cord Blood Samples. *European journal of immunology* **2015**, *45*, 1926–1933, doi:10.1002/EJI.201545539.

84. Moran, A.E.; Holzapfel, K.L.; Xing, Y.; Cunningham, N.R.; Maltzman, J.S.; Punt, J.; Hogquist, K.A. T Cell Receptor Signal Strength in Treg and INKT Cell Development

Demonstrated by a Novel Fluorescent Reporter Mouse. *The Journal of experimental medicine* **2011**, *208*, 1279–1289, doi:10.1084/JEM.20110308.

85. Intlekofer, A.M.; Takemoto, N.; Wherry, E.J.; Longworth, S.A.; Northrup, J.T.; Palanivel, V.R.; Mullen, A.C.; Gasink, C.R.; Kaech, S.M.; Miller, J.D.; et al. Effector and Memory CD8+ T Cell Fate Coupled by T-Bet and Eomesodermin. *Nature immunology* **2005**, *6*, 1236–1244, doi:10.1038/NI1268.

86. Hamann, D.; Baars, P.A.; Rep, M.H.G.; Hooibrink, B.; Kerkhof-Garde, S.R.; Klein, M.R.; Van Lier, R.A.W. Phenotypic and Functional Separation of Memory and Effector Human CD8+ T Cells. *The Journal of experimental medicine* **1997**, *186*, 1407–1418, doi:10.1084/JEM.186.9.1407.

87. Else, K.J.; Finkelman, F.D.; Maliszewski, C.R.; Grencis, R.K. Cytokine-Mediated Regulation of Chronic Intestinal Helminth Infection. *The Journal of experimental medicine* **1994**, *179*, 347–351, doi:10.1084/JEM.179.1.347.

88. Gershon, R.K.; Kondo, K. Cell Interactions in the Induction of Tolerance: The Role of Thymic Lymphocytes. *Immunology* **1970**, *18*, 723–737.

89. Sakaguchi, S.; Sakaguchi, N.; Asano, M.; Itoh, M.; Toda, M. Immunologic Self-Tolerance Maintained by Activated T Cells Expressing IL-2 Receptor Alpha-Chains (CD25). Breakdown of a Single Mechanism of Self-Tolerance Causes Various Autoimmune Diseases. *The Journal of Immunology* **1995**, *155*.

90. Fontenot, J.D.; Gavin, M.A.; Rudensky, A.Y. Foxp3 Programs the Development and Function of CD4+CD25+ Regulatory T Cells. *Nat Immunol* **2003**, *4*, 330–336, doi:10.1038/ni904.

91. Niederlova, V.; Tsyklauri, O.; Chadimova, T.; Stepanek, O. CD8+ Tregs Revisited: A Heterogeneous Population with Different Phenotypes and Properties. *European Journal of Immunology* **2021**, *51*, 512–530, doi:10.1002/eji.202048614.

92. Endharti, A.T.; Rifa', M.; Shi, Z.; Fukuoka, Y.; Nakahara, Y.; Kawamoto, Y.; Takeda, K.; Isobe, K. -i.; Suzuki, H. Cutting Edge: CD8+CD122+ Regulatory T Cells Produce IL-10 to Suppress IFN- Production and Proliferation of CD8+ T Cells. *The Journal of Immunology* **2005**, *175*, 7093–7097, doi:10.4049/jimmunol.175.11.7093.

93. Rifa'i, M.; Kawamoto, Y.; Nakashima, I.; Suzuki, H. Essential Roles of CD8+ CD122+ Regulatory T Cells in the Maintenance of T Cell Homeostasis. *The Journal of Experimental Medicine* **2004**, *200*, 1123–1134, doi:10.1084/jem.20040395.

94. Saligrama, N.; Zhao, F.; Sikora, M.J.; Serratelli, W.S.; Fernandes, R.A.; Louis, D.M.; Yao, W.; Ji, X.; Idoyaga, J.; Mahajan, V.B.; et al. Opposing T Cell Responses in Experimental Autoimmune Encephalomyelitis. *Nature* **2019**, doi:10.1038/s41586-019-1467-x.

95. Kim, H.J.; Cantor, H. Regulation of Self-Tolerance by Qa-1-Restricted CD8+regulatory T Cells. *Seminars in Immunology* **2011**, *23*, 446–452, doi:10.1016/j.smim.2011.06.001.

96. Kim, H.-J.; Barnitz, R.A.; Kreslavsky, T.; Brown, F.D.; Moffett, H.; Lemieux, M.E.; Kaygusuz, Y.; Meissner, T.; Holderried, T.A.W.; Chan, S.; et al. Stable Inhibitory Activity of Regulatory T Cells Requires the Transcription Factor Helios. *Science* **2015**, *350*, 334–339, doi:10.1126/science.aad0616.

97. Mishra, S.; Liao, W.; Liu, Y.; Yang, M.; Ma, C.; Wu, H.; Zhao, M.; Zhang, X.; Qiu, Y.; Lu, Q.; et al. TGF-β and Eomes Control the Homeostasis of CD8+ Regulatory T Cells. *Journal of Experimental Medicine* **2020**, *218*, e20200030, doi:10.1084/jem.20200030.

98. Li, J.; Zaslavsky, M.; Su, Y.; Guo, J.; Sikora, M.J.; van Unen, V.; Christophersen, A.; Chiou, S.-H.; Chen, L.; Li, J.; et al. KIR+CD8+ T Cells Suppress Pathogenic T Cells and Are Active in Autoimmune Diseases and COVID-19. *Science* **2022**, doi:10.1126/science.abi9591.

99. Kawasaki, K.; Yaoita, E.; Yamamoto, T.; Kihara, I. Depletion of CD8 Positive Cells in Nephrotoxic Serum Nephritis of WKY Rats. *Kidney International* **1992**, *41*, 1517–1526, doi:10.1038/ki.1992.221.

100. Tipping, P.G.; Huang, X.R.; Qi, M.; Van, G.Y.; Tang, W.W. Crescentic Glomerulonephritis in CD4- and CD8-Deficient Mice. Requirement for CD4 but Not CD8 Cells. *The American journal of pathology* **1998**, *152*, 1541–1548.

101. Li, S.; Holdsworth, S.R.; Tipping, P.G. MHC Class I Pathway Is Not Required for the Development of Crescentic Glomerulonephritis in Mice. *Clinical and Experimental Immunology* **2000**, *122*, 453–458, doi:10.1046/j.1365-2249.2000.01387.x.

102. Mukherjee, R.; Zhang, Z.; Zhong, R.; Yin, Z.Q.; Roopenian, D.C.; Jevnikar, A.M. Lupus Nephritis in the Absence of Renal Major Histocompatibility Complex Class I and Class II Molecules. *J Am Soc Nephrol* **1996**, *7*, 2445–2452, doi:10.1681/ASN.V7112445.

103. Reynolds, J.; Norgan, V.A.; Bhambra, U.; Smith, J.; Cook, H.T.; Pusey, C.D. Anti-CD8 Monoclonal Antibody Therapy Is Effective in the Prevention and Treatment of Experimental Autoimmune Glomerulonephritis. *Journal of the American Society of Nephrology* **2002**, *13*, 359–369, doi:10.1681/asn.v132359.

104. Chang, J.; Eggenhuizen, P.; O'Sullivan, K.M.; Alikhan, M.A.; Holdsworth, S.R.; Ooi, J.D.; Kitching, A.R. CD8+ T Cells Effect Glomerular Injury in Experimental Anti-Myeloperoxidase GN. *Journal of the American Society of Nephrology* **2017**, *28*, 47–55, doi:10.1681/ASN.2015121356.

105. Fehniger, T.A.; Caligiuri, M.A. Interleukin 15: Biology and Relevance to Human Disease. *Blood* **2001**, *97*, 14–32, doi:10.1182/blood.V97.1.14.

106. Grabstein, K.H.; Eisenman, J.; Shanebeck, K.; Rauch, C.; Srinivasan, S.; Fung, V.; Beers, C.; Richardson, J.; Schoenborn, M.A.; Ahdieh, M.; et al. Cloning of a T Cell Growth Factor That Interacts with the β Chain of the Interleukin-2 Receptor. *Science* **1994**, *264*, 965–968, doi:10.1126/SCIENCE.8178155.

107. Bamford, R.N.; Grant, A.J.; Burton, J.D.; Peters, C.; Kurys, G.; Goldman, C.K.; Brennan, J.; Roessler, E.; Waldmann, T.A. The Interleukin (IL) 2 Receptor Beta Chain Is Shared by IL-2 and a Cytokine, Provisionally Designated IL-T, That Stimulates T-Cell Proliferation and the Induction of Lymphokine-Activated Killer Cells. *Proceedings of the National Academy of Sciences of the United States of America* **1994**, *91*, 4940, doi:10.1073/PNAS.91.11.4940.

108. Carson, W.E.; Giri, J.G.; Lindemann, M.J.; Linett, M.L.; Ahdieh, M.; Paxton, R.; Anderson, D.; Eisenmann, J.; Grabstein, K.; Caligiuri, M.A. Interleukin (IL) 15 Is a Novel Cytokine That Activates Human Natural Killer Cells via Components of the IL-2

Receptor. *The Journal of experimental medicine* **1994**, *180*, 1395–1403, doi:10.1084/JEM.180.4.1395.

109. Lodolce, J.P.; Boone, D.L.; Chai, S.; Swain, R.E.; Dassopoulos, T.; Trettin, S.; Ma, A. IL-15 Receptor Maintains Lymphoid Homeostasis by Supporting Lymphocyte Homing and Proliferation. *Immunity* **1998**, *9*, 669–676, doi:10.1016/S1074-7613(00)80664-0.

110. Kennedy, M.K.; Glaccum, M.; Brown, S.N.; Butz, E.A.; Viney, J.L.; Embers, M.; Matsuki, N.; Charrier, K.; Sedger, L.; Willis, C.R.; et al. Reversible Defects in Natural Killer and Memory CD8 T Cell Lineages in Interleukin 15-Deficient Mice. *Journal of Experimental Medicine* **2000**, *191*, 771–780, doi:10.1084/jem.191.5.771.

111. Dubois, S.; Magrangeas, F.; Lehours, P.; Raher, S.; Bernard, J.; Boisteau, O.; Leroy, S.; Minvielle, S.; Godard, A.; Jacques, Y. Natural Splicing of Exon 2 of Human Interleukin-15 Receptor Alpha-Chain MRNA Results in a Shortened Form with a Distinct Pattern of Expression. *The Journal of biological chemistry* **1999**, *274*, 26978–26984, doi:10.1074/JBC.274.38.26978.

112. Miyazaki, T.; Kawahara, A.; Fujii, H.; Nakagawa, Y.; Minami, Y.; Liu, Z.J.; Oishi, I.; Silvennoinen, O.; Witthuhn, B.A.; Ihle, J.N.; et al. Functional Activation of Jak1 and Jak3 by Selective Association with IL-2 Receptor Subunits. *Science (New York, N.Y.)* **1994**, *266*, 1045–1047, doi:10.1126/SCIENCE.7973659.

113. Lin, J.X.; Migone, T.S.; Tseng, M.; Friedmann, M.; Weatherbee, J.A.; Zhou, L.; Yamauchi, A.; Bloom, E.T.; Mietz, J.; John, S.; et al. The Role of Shared Receptor Motifs and Common Stat Proteins in the Generation of Cytokine Pleiotropy and Redundancy by IL-2, IL-4, IL-7, IL-13, and IL-15. *Immunity* **1995**, *2*, 331–339, doi:10.1016/1074-7613(95)90141-8.

114. Miyazaki, T.; Liu, Z.J.; Kawahara, A.; Minami, Y.; Yamada, K.; Tsujimoto, Y.; Barsoumian, E.L.; Perlmutter, R.M.; Taniguchi, T. Three Distinct IL-2 Signaling Pathways Mediated by Bcl-2, c-Myc, and Lck Cooperate in Hematopoietic Cell Proliferation. *Cell* **1995**, *81*, 223–231, doi:10.1016/0092-8674(95)90332-1.

115. Carson, W.E.; Ross, M.E.; Baiocchi, R.A.; Marien, M.J.; Boiani, N.; Grabstein, K.; Caligiuri, M.A. Endogenous Production of Interleukin 15 by Activated Human Monocytes Is Critical for Optimal Production of Interferon-Gamma by Natural Killer Cells in Vitro. *The Journal of clinical investigation* **1995**, *96*, 2578–2582, doi:10.1172/JCI118321.

116. Blauvelt, A.; Asada, H.; Klaus-Kovtun, V.; Altman, D.J.; Lucey, D.R.; Katz, S.I. Interleukin-15 MRNA Is Expressed by Human Keratinocytes Langerhans Cells, and Blood-Derived Dendritic Cells and Is Downregulated by Ultraviolet B Radiation. *The Journal of investigative dermatology* **1996**, *106*, 1047–1052, doi:10.1111/1523-1747.EP12338641.

117. Jonuleit, H.; Wiedemann, K.; Müller, G.; Degwert, J.; Hoppe, U.; Knop, J.; Enk, A.H. Induction of IL-15 Messenger RNA and Protein in Human Blood-Derived Dendritic Cells: A Role for IL-15 in Attraction of T Cells. *The Journal of Immunology* **1997**, *158*.

118. Reinecker, H.C.; MacDermott, R.P.; Mirau, S.; Dignass, A.; Podolsky, D.K. Intestinal Epithelial Cells Both Express and Respond to Interleukin 15. *Gastroenterology* **1996**, *111*, 1706–1713, doi:10.1016/S0016-5085(96)70036-7.

119. Azimi, N.; Brown, K.; Bamford, R.N.; Tagaya, Y.; Siebenlist, U.; Waldmann, T.A. Human T Cell Lymphotropic Virus Type I Tax Protein Trans-Activates Interleukin 15 Gene Transcription through an NF-KappaB Site. *Proceedings of the National Academy of Sciences of the United States of America* **1998**, *95*, 2452–2457, doi:10.1073/PNAS.95.5.2452.

120. Weiler, M.; Rogashev, B.; Einbinder, T.; Hausmann, M.J.; Kaneti, J.; Chaimovitz, C.; Douvdevani, A. Interleukin-15, a Leukocyte Activator and Growth Factor, Is Produced by Cortical Tubular Epithelial Cells. *Journal of the American Society of Nephrology* **1998**, *9*, 1194–1201, doi:10.1681/ASN.V971194.

121. Flamand, L.; Stefanescu, I.; Menezes, J. Human Herpesvirus-6 Enhances Natural Killer Cell Cytotoxicity via IL-15. *The Journal of clinical investigation* **1996**, *97*, 1373–1381, doi:10.1172/JCI118557.

122. Atedzoe, B.N.; Ahmad, A.; Menezes, J. Enhancement of Natural Killer Cell Cytotoxicity by the Human Herpesvirus-7 via IL-15 Induction. *The Journal of Immunology* **1997**, *159*.

123. Wilkinson, P.C.; Liew, F.Y. Chemoattraction of Human Blood T Lymphocytes by Interleukin-15. *The Journal of experimental medicine* **1995**, *181*, 1255–1259, doi:10.1084/JEM.181.3.1255.

124. Kanegane, H.; Tosato, G. Activation of Naive and Memory T Cells by Interleukin-15. *Blood* **1996**, *88*, 230–235, doi:10.1182/blood.v88.1.230.230.

125. Zhang, X.; Sun, S.; Hwang, I.; Tough, D.F.; Sprent, J. Potent and Selective Stimulation of Memory-Phenotype CD8+ T Cells in Vivo by IL-15. *Immunity* **1998**, *8*, 591–599, doi:10.1016/S1074-7613(00)80564-6.

126. Alleva, D.G.; Kaser, S.B.; Monroy, M.A.; Fenton, M.J.; Beller, D.I. IL-15 Functions as a Potent Autocrine Regulator of Macrophage Proinflammatory Cytokine Production: Evidence for Differential Receptor Subunit Utilization Associated with Stimulation or Inhibition. *The Journal of Immunology* **1997**, *159*.

127. Musso, T.; Calosso, L.; Zucca, M.; Millesimo, M.; Ravarino, D.; Giovarelli, M.; Malavasi, F.; Negro Ponzi, A.; Paus, R.; Bulfone-Paus, S. Human Monocytes Constitutively Express Membrane-Bound, Biologically Active, and Interferon-γ–Upregulated Interleukin-15. *Blood* **1999**, *93*, 3531–3539, doi:10.1182/BLOOD.V93.10.3531.410K32_3531_3539.

128. Waldmann, T.A.; Dubois, S.; Miljkovic, M.D.; Conlon, K.C. IL-15 in the Combination Immunotherapy of Cancer. *Frontiers in Immunology* **2020**, *11*, 868, doi:10.3389/FIMMU.2020.00868/BIBTEX.

129. Ruchatz, H.; Leung, B.P.; Wei, X.; McInnes, I.B.; Liew, F.Y. Soluble IL-15 Receptor α-Chain Administration Prevents Murine Collagen-Induced Arthritis: A Role for IL-15 in Development of Antigen-Induced Immunopathology. *The Journal of Immunology* **1998**, *160*.

130. Devocelle, A.; Lecru, L.; François, H.; Desterke, C.; Gallerne, C.; Eid, P.; Estelle, O.; Azzarone, B.; Giron-Michel, J. Inhibition of TGF- β 1 Signaling by IL-15: A Novel Role for IL-15 in the Control of Renal Epithelial-Mesenchymal Transition: IL-15

Counteracts TGF- β 1-Induced EMT in Renal Fibrosis. *International Journal of Cell Biology* **2019**, *2019*, doi:10.1155/2019/9151394.

131. Tejman-Yarden, N.; Zlotnik, M.; Lewis, E.; Etzion, O.; Chaimovitz, C.; Douvdevani, A. Renal Cells Express a Functional Interleukin-15 Receptor. *Nephrology Dialysis Transplantation* **2005**, *20*, 516–523, doi:10.1093/NDT/GFH616.

132. Giron-Michel, J.; Azzi, S.; Khawam, K.; Mortier, E.; Caignard, A.; Devocelle, A.; Ferrini, S.; Croce, M.; François, H.; Lecru, L.; et al. Interleukin-15 Plays a Central Role in Human Kidney Physiology and Cancer through the Γc Signaling Pathway. *PloS one* **2012**, *7*, doi:10.1371/JOURNAL.PONE.0031624.

133. Giron-Michel, J.; Azzi, S.; Khawam, K.; Caignard, A.; Devocelle, A.; Perrier, A.; Chouaib, S.; Eid, P.; Azzarone, B. Interleukin-15 Is a Major Regulator of the Cell-Microenvironment Interactions in Human Renal Cancer. *Bulletin du Cancer* **2011**, *98*, E32–E39, doi:10.1684/bdc.2011.1359.

134. Zhang, B.; Li, H.; Liu, W.; Tian, H.; Li, L.; Gao, C.; Zheng, J. Adoptive Cell Therapy of Patient-Derived Renal Cell Carcinoma Xenograft Model with IL-15-Induced ΓδT Cells. *Medical Oncology* **2021**, *38*, 1–9, doi:10.1007/S12032-021-01474-1/FIGURES/4.

135. Weiler, M.; Kachko, L.; Chaimovitz, C.; Van Kooten, C.; Douvdevani, A. CD40 Ligation Enhances IL-15 Production by Tubular Epithelial Cells. *Journal of the American Society of Nephrology* **2001**, *12*, 80–87, doi:10.1681/ASN.V12.1.80.

136. Eini, H.; Tejman-Yarden, N.; Lewis, E.C.; Chaimovitz, C.; Zlotnik, M.; Douvdevani, A. Association between Renal Injury and Reduced Interleukin-15 and Interleukin-15 Receptor Levels in Acute Kidney Injury. *Journal of Interferon and Cytokine Research* **2010**, *30*, 1–8, doi:10.1089/jir.2009.0005.

137. Devocelle, A.; Lecru, L.; Ferlicot, S.; Bessede, T.; Candelier, J.J.; Giron-michel, J.; François, H. IL-15 Prevents Renal Fibrosis by Inhibiting Collagen Synthesis: A New Pathway in Chronic Kidney Disease? *International Journal of Molecular Sciences 2021, Vol. 22, Page 11698* **2021**, *22*, 11698, doi:10.3390/IJMS222111698.

138. Shinozaki, M.; Hirahashi, J.; Lebedeva, T.; Liew, F.Y.; Salant, D.J.; Maron, R.; Kelley, V.R. IL-15, a Survival Factor for Kidney Epithelial Cells, Counteracts Apoptosis and Inflammation during Nephritis. *The Journal of clinical investigation* **2002**, *109*, 951–960, doi:10.1172/JCI14574.

139. Assmann, K.J.M.; Tangelder, M.M.; Lange, W.P.J.; Tadema, T.M.; Koene, R.A.P. Membranous Glomerulonephritis in the Mouse. *Kidney International Supplements* **1983**, *24*, 303–312, doi:10.1038/ki.1983.159.

140. Lodolce, J.P.; Burkett, P.R.; Boone, D.L.; Chien, M.; Ma, A. T Cell-Independent Interleukin 15Rα Signals Are Required for Bystander Proliferation. *Journal of Experimental Medicine* **2001**, *194*, 1187–1193, doi:10.1084/jem.194.8.1187.

141. Berard, M.; Brandt, K.; Paus, S.B.; Tough, D.F. IL-15 Promotes the Survival of Naive and Memory Phenotype CD8 + T Cells. *The Journal of Immunology* **2003**, *170*, 5018–5026, doi:10.4049/jimmunol.170.10.5018.

142. Kitching, A.R.; Holdsworth, S.R.; Ploplis, V.A.; Plow, E.F.; Collen, D.; Carmeliet, P.; Tipping, P.G. Plasminogen and Plasminogen Activators Protect against Renal Injury in

Crescentic Glomerulonephritis. *Journal of Experimental Medicine* **1997**, *185*, 963–968, doi:10.1084/jem.185.5.963.

143. Armitage, R.J.; Macduff, B.M.; Eisenman, J.; Paxton, R.; Grabstein, K.H. IL-15 Has Stimulatory Activity for the Induction of B Cell Proliferation and Differentiation. *J Immunol* **1995**, *154*, 483–490.

144. Gill, N.; Paltser, G.; Ashkar, A.A. Interleukin-15 Expression Affects Homeostasis and Function of B Cells through NK Cell-Derived Interferon-Gamma. *Cell Immunol* **2009**, *258*, 59–64, doi:10.1016/j.cellimm.2009.03.010.

145. Rosenberg, S.A. IL-2: The First Effective Immunotherapy for Human Cancer. *J Immunol* **2014**, *192*, 5451–5458, doi:10.4049/jimmunol.1490019.

146. Humrich, J.Y.; von Spee-Mayer, C.; Siegert, E.; Alexander, T.; Hiepe, F.; Radbruch, A.; Burmester, G.-R.; Riemekasten, G. Rapid Induction of Clinical Remission by Low-Dose Interleukin-2 in a Patient with Refractory SLE. *Ann Rheum Dis* **2015**, *74*, 791–792, doi:10.1136/annrheumdis-2014-206506.

147. Rosenzwajg, M.; Churlaud, G.; Mallone, R.; Six, A.; Dérian, N.; Chaara, W.; Lorenzon, R.; Long, S.A.; Buckner, J.H.; Afonso, G.; et al. Low-Dose Interleukin-2 Fosters a Dose-Dependent Regulatory T Cell Tuned Milieu in T1D Patients. *Journal of Autoimmunity* **2015**, *58*, 48–58, doi:10.1016/j.jaut.2015.01.001.

148. Long, S.A.; Rieck, M.; Sanda, S.; Bollyky, J.B.; Samuels, P.L.; Goland, R.; Ahmann, A.; Rabinovitch, A.; Aggarwal, S.; Phippard, D.; et al. Rapamycin/IL-2 Combination Therapy in Patients with Type 1 Diabetes Augments Tregs yet Transiently Impairs β-Cell Function. *Diabetes* **2012**, *61*, 2340–2348, doi:10.2337/db12-0049.

149. Waldmann, T.A. The Biology of Interleukin-2 and Interleukin-15: Implications for Cancer Therapy and Vaccine Design. *Nature Reviews Immunology* **2006**, *6*, 595–601, doi:10.1038/nri1901.

150. Aringer, I.; Artinger, K.; Kirsch, A.H.; Schabhüttl, C.; Jandl, K.; Bärnthaler, T.; Mooslechner, A.A.; Herzog, S.A.; Uhlig, M.; Kirsch, A.; et al. Blockade of Prostaglandin E2 Receptor 4 Ameliorates Nephrotoxic Serum Nephritis. *American Journal of Physiology-Renal Physiology* **2018**, *315*, F1869–F1880, doi:10.1152/ajprenal.00113.2018.

151. Wolf, G.; Jocks, T.; Zahner, G.; Panzer, U.; Stahl, R.A.K. Existence of a Regulatory Loop between MCP-1 and TGF-Beta in Glomerular Immune Injury. *Am J Physiol Renal Physiol* **2002**, *283*, F1075-1084, doi:10.1152/ajprenal.00349.2001.

152. Xu, L.; Guo, J.; Moledina, D.G.; Cantley, L.G. Immune-Mediated Tubule Atrophy Promotes Acute Kidney Injury to Chronic Kidney Disease Transition. *Nat Commun* **2022**, *13*, 4892, doi:10.1038/s41467-022-32634-0.

153. Cassatella, M.A.; McDonald, P.P. Interleukin-15 and Its Impact on Neutrophil Function. *Curr Opin Hematol* **2000**, *7*, 174–177, doi:10.1097/00062752-200005000-00008.

154. Ryan, J.; Ma, F.Y.; Han, Y.; Ozols, E.; Kanellis, J.; Tesch, G.H.; Nikolic-Paterson, D.J. Myeloid Cell-Mediated Renal Injury in Rapidly Progressive Glomerulonephritis Depends upon Spleen Tyrosine Kinase. *The Journal of Pathology* **2016**, *238*, 10–20, doi:10.1002/path.4598.

155. Isbel, N.M.; Nikolic-Paterson, D.J.; Hill, P.A.; Dowling, J.; Atkins, R.C. Local Macrophage Proliferation Correlates with Increased Renal M-CSF Expression in Human Glomerulonephritis. *Nephrol Dial Transplant* **2001**, *16*, 1638–1647, doi:10.1093/ndt/16.8.1638.

156. Eardley, K.S.; Zehnder, D.; Quinkler, M.; Lepenies, J.; Bates, R.L.; Savage, C.O.; Howie, A.J.; Adu, D.; Cockwell, P. The Relationship between Albuminuria, MCP-1/CCL2, and Interstitial Macrophages in Chronic Kidney Disease. *Kidney Int* **2006**, *69*, 1189–1197, doi:10.1038/sj.ki.5000212.

157. Rickassel, C.; Gnirck, A.-C.; Shaikh, N.; Adamiak, V.; Waterhölter, A.; Tanriver, Y.; Neumann, K.; Huber, T.B.; Gasteiger, G.; Panzer, U.; et al. Conventional NK Cells and Type 1 Innate Lymphoid Cells Do Not Influence Pathogenesis of Experimental Glomerulonephritis. *J Immunol* **2022**, *208*, 1585–1594, doi:10.4049/jimmunol.2101012.

158. Mesnard, L.; Keller, A.C.; Michel, M.-L.; Vandermeersch, S.; Rafat, C.; Letavernier, E.; Tillet, Y.; Rondeau, E.; Leite-de-Moraes, M.C. Invariant Natural Killer T Cells and TGF-Beta Attenuate Anti-GBM Glomerulonephritis. *J Am Soc Nephrol* **2009**, *20*, 1282–1292, doi:10.1681/ASN.2008040433.

159. Shytikov, D.; Rohila, D.; Li, D.; Wang, P.; Jiang, M.; Zhang, M.; Xu, Q.; Lu, L. Functional Characterization of Ly49+CD8 T-Cells in Both Normal Condition and During Anti-Viral Response. *Frontiers in Immunology* **2021**, *11*, 1–15, doi:10.3389/fimmu.2020.602783.

160. Kim, H.J.; Wang, X.; Radfar, S.; Sproule, T.J.; Roopenian, D.C.; Cantor, H. CD8+ T Regulatory Cells Express the Ly49 Class I MHC Receptor and Are Defective in Autoimmune Prone B6-Yaa Mice. *Proceedings of the National Academy of Sciences of the United States of America* **2011**, *108*, 2010–2015, doi:10.1073/pnas.1018974108.

161. Szabo, P.A.; Miron, M.; Farber, D.L. Location, Location, Location: Tissue Resident Memory T Cells in Mice and Humans. *Sci Immunol* **2019**, *4*, eaas9673, doi:10.1126/sciimmunol.aas9673.

162. Asada, N.; Ginsberg, P.; Gagliani, N.; Mittrücker, H.-W.; Panzer, U. Tissue-Resident Memory T Cells in the Kidney. *Semin Immunopathol* **2022**, *44*, 801–811, doi:10.1007/s00281-022-00927-7.

163. Park, J.-G.; Na, M.; Kim, M.-G.; Park, S.H.; Lee, H.J.; Kim, D.K.; Kwak, C.; Kim, Y.S.; Chang, S.; Moon, K.C.; et al. Immune Cell Composition in Normal Human Kidneys. *Sci Rep* **2020**, *10*, 15678, doi:10.1038/s41598-020-72821-x.

164. Mujib, S.; Jones, R.B.; Lo, C.; Aidarus, N.; Clayton, K.; Sakhdari, A.; Benko, E.; Kovacs, C.; Ostrowski, M.A. Antigen-Independent Induction of Tim-3 Expression on Human T Cells by the Common γ-Chain Cytokines IL-2, IL-7, IL-15, and IL-21 Is Associated with Proliferation and Is Dependent on the Phosphoinositide 3-Kinase Pathway. *J Immunol* **2012**, *188*, 3745–3756, doi:10.4049/jimmunol.1102609.

165. Chew, G.M.; Fujita, T.; Webb, G.M.; Burwitz, B.J.; Wu, H.L.; Reed, J.S.; Hammond, K.B.; Clayton, K.L.; Ishii, N.; Abdel-Mohsen, M.; et al. TIGIT Marks Exhausted T Cells, Correlates with Disease Progression, and Serves as a Target for Immune Restoration in HIV and SIV Infection. *PLoS Pathog* **2016**, *12*, e1005349, doi:10.1371/journal.ppat.1005349.

166. Tosiek, M.J.; Fiette, L.; El Daker, S.; Eberl, G.; Freitas, A.A. IL-15-Dependent Balance between Foxp3 and RORγt Expression Impacts Inflammatory Bowel Disease. *Nat Commun* **2016**, *7*, 10888, doi:10.1038/ncomms10888.
167. Holderried, T.A.; Kruse, M.; Serries, M.; Brossart, P.; Wolf, D.; Wolf, A.M. Helios-Expressing CD8+ T Cells Are Decreased in Patients with Systemic Lupus Erythematosus. *Lupus* **2021**, *30*, 1022–1024, doi:10.1177/0961203321999723.